

# UC Irvine

## UC Irvine Electronic Theses and Dissertations

### Title

Evaluating the role of group 2 innate lymphoid cells in muscular dystrophy

### Permalink

<https://escholarship.org/uc/item/8xx4g0xg>

### Author

Kastenschmidt, Jenna

### Publication Date

2020

Peer reviewed|Thesis/dissertation

UNIVERSITY OF CALIFORNIA,  
IRVINE

Evaluating the role of group 2 innate lymphoid cells in muscular dystrophy

DISSERTATION

submitted in partial satisfaction of the requirements  
for the degree of

DOCTOR OF PHILOSOPHY

in Biomedical Sciences

by

Jenna Marie Kastenschmidt

Dissertation Committee:  
Assistant Professor Armando Villalta Ph.D., Chair  
Professor Craig M. Walsh Ph.D.  
Professor Eric Pearlman Ph.D.

2020



Chapter 1 Components

© 2000 National Academy of Sciences, U.S.A

© 2019 Springer Nature Switzerland AG

© 2015 John Wiley and Sons

© 2014 Elsevier

© 2016 Springer Nature

Chapter 2

© 2019 Kastenschmidt, Ellefsen, Manna, Giebel, Yahia, Ayer, Pham, Rios, Vetrone, Mozaffar and Villalta

All other materials © 2020 Jenna M. Kastenschmidt

## **DEDICATION**

To my greatest achievement yet, my family:  
Jesse, Jamie, Peppers and Bails

# TABLE OF CONTENTS

	Page
LIST OF FIGURES	iv
LIST OF TABLES	vi
ACKNOWLEDGEMENTS	vii
VITA	viii
ABSTRACT OF THE DISSERTATION	xii
CHAPTER 1: Introduction	1
Muscle stem cells and the maintenance of skeletal muscle homeostasis	2
Immune responses following muscle injury	3
Duchenne muscular dystrophy and cellular mechanisms of disease	6
Clinical manifestations and comorbidities during DMD	7
Therapeutic management of DMD	8
Immune responses during Duchenne muscular dystrophy	9
Group 2 innate lymphoid cells (ILC2)	13
Biological functions of ILC2s	14
Introduction to the dissertation - the role of ILC2s in muscle disease	17
CHAPTER 2: QuantiMus: a machine learning-based approach for high precision analysis of skeletal muscle morphology	27
CHAPTER 3: Muscle injury activates group 2 innate lymphoid cells to induce muscle eosinophilia	63
CHAPTER 4: Summary and Conclusions	96
REFERENCES	103

## LIST OF FIGURES

<b><u>CHAPTER 1</u></b>		<b>Page</b>
<b>Figure 1.1</b>	Schematic illustrating the structure of skeletal muscle.	19
<b>Figure 1.2</b>	Myogenic lineage progression.	20
<b>Figure 1.3</b>	Frequencies of immune cell populations in acutely injured muscle.	21
<b>Figure 1.4</b>	The dystrophin–glycoprotein complex.	22
<b>Figure 1.5</b>	Frequencies of immune cell populations in dystrophic muscle.	23
<b>Figure 1.6</b>	The Ying-Yang function of degenerative and regenerative immune cells in muscular dystrophy.	24
<b>Figure 1.7</b>	Activation and functions of ILCs.	25
<b>Figure 1.8</b>	The lineage of ILCs.	26
<b><u>CHAPTER 2</u></b>		
<b>Figure 2.1</b>	QuantiMus application workflow.	52
<b>Figure 2.2</b>	The ‘Fill Myofiber Gaps’ function corrects gaps in myofiber boundaries that hinder single myofiber discrimination.	53
<b>Figure 2.3</b>	Classification of skeletal muscle myofibers.	54
<b>Figure 2.4</b>	Detection of CNFs.	56
<b>Figure 2.5</b>	Measurement of fluorescence intensity in single myofibers.	57
<b>Figure 2.6</b>	Data Export.	58
<b>Figure 2.7</b>	QuantiMus accurately measures myofiber CSA and minimum Feret diameter.	59
<b>Figure 2.8</b>	Defining CNFs.	60
<b>Figure 2.9</b>	Myofiber typing of mouse and human muscle.	61
<b>Figure 2.10</b>	Morphometric analysis of dystrophic pathology in mdx mice.	62

### **CHAPTER 3**

<b>Figure 3.1</b>	Innate lymphoid responses in acutely-injured and mdx skeletal muscle.	88
<b>Figure 3.2</b>	Interleukin-33 is predominantly expressed by fibro/adipogenic progenitors and activates muscle ILC2s.	90
<b>Figure 3.3</b>	ILC2s promote skeletal muscle eosinophilia.	91
<b>Figure 3.4</b>	Eosinophils during muscular dystrophy.	92
<b>SFigure 3.1</b>	Evaluation of ILCs in skeletal muscle.	93
<b>SFigure 3.2</b>	Eosinophils and eosinophilia promoting factors in skeletal muscle.	94
<b>SFigure 3.3</b>	ILC2-mediated regulation of dystrophic muscle macrophages.	95

### **CHAPTER 4**

<b>Figure 4.1</b>	Amphiregulin expression in dystrophic muscle.	101
<b>Figure 4.2</b>	Single-cell RNA sequencing of muscle macrophages.	102

## LIST OF TABLES

<b><u>CHAPTER 2</u></b>		Page
<b>Table 2.1</b>	Antibodies used for histology.	50
<b>Table 2.2</b>	Comparison of imaging processing times of different methods.	51
<b><u>CHAPTER 3</u></b>		
<b>Table 3.1</b>	Antibodies used for flow cytometry analysis.	85
<b>Table 3.2</b>	TaqMan probes used for gene expression analysis in mouse muscle.	86
<b>Table 3.3</b>	Antibodies used for histology.	87

## ACKNOWLEDGEMENTS

I would like to express the most profound appreciation to my mentor Dr. Armando Villalta. Armando's rigor as a scientist and work ethic is inspiring, and I am beyond grateful to have had his training over the last four years. Thank you for always pushing me to strive to be my best.

I would also like to thank my committee members Dr. Eric Pearlman, Dr. Albert Zlotnik, Dr. Craig Walsh, and Dr. Francesco Tombola, for their thoughtful insights on this study and always supporting me both personally and professionally. I am thankful for a number of UCI laboratories that I have collaborated with during my PhD training. They have always been supportive in providing experimental feedback, reagents, and equipment. Thank you to the laboratories of Dr. Eric Pearlman, Dr. Albert Zlotnik, Dr. Craig Walsh, Dr. Devon Lawson, Dr. Kai Kessonbrock, Dr. Xing Dai, and Dr. Selma Masri. I also thank Dr. Tahseen Mozzafar for collaborating with us and providing numerous patient samples for this study. I would especially like to thank Dr. Jennifer Attwood at the UCI Institute of Immunology flow core. I'm grateful for all the knowledge she has instilled upon me and will never forget our friendship and time together.

I would also like to thank my external collaborations, including Dr. Mathew Alexander, at the University of Alabama Birmingham, for including me in his laboratory's study investigating the effects of novel compounds on DMD pathology. Also, I thank Tom Lloyd at John Hopkins University for allowing me to conduct the flow cytometry analysis of their human xenograft mice. Additionally, I want to thank Dr. Steven Moore at the University of Iowa for providing us with numerous human specimens.

Last and most definitely not least, I want to thank my husband Jesse, who, without his continual love and support, I would not have made it this far. And of course, my parents and family back in Wisconsin. They taught me the value of hard work, which makes this all that much sweeter.

# CURRICULUM VITAE

**Jenna M. Kastenschmidt**

Institute for Immunology  
Department of Physiology and Biophysics  
University of California, Irvine

---

## EDUCATION

- University of California, Irvine** **2015-2020**  
Irvine, CA  
Ph.D. Biomedical Sciences, emphasis Immunology  
Advisor: S. Armando Villalta (Physiology and Biophysics)
- University of Wisconsin, Madison** **2010 - 2012**  
Madison, WI  
Doctor of Pharmacy Candidate
- Minnesota State University, Mankato** **2006-2010**  
Mankato, MN  
B.S. Biology, emphasis Human Biology, *Magna Cum Laude*

## RESEARCH EXPERIENCE

- Graduate Research Associate** **2015-2020**  
University of California, Irvine  
Dr. Armando Villalta, Department of Physiology and Biophysics  
Dissertation: "Evaluating the role of group 2 innate lymphoid cells in muscular dystrophy"
- Amgen Summer Scholar** **Summer 2009**  
University of California, San Diego  
Dr. Dwayne Stupack, Department of Pathology  
Moores Cancer Center, La Jolla, CA
- Undergraduate Research Assistant** **2007 - 2010**  
Minnesota State University, Mankato  
Dr. Marilyn Hart, Department of Biological Sciences

## PUBLICATIONS

- Kastenschmidt J.M. et al.** "A fibro/adipogenic progenitor and ILC2 niche promotes eosinophilia in dystrophic muscle." *In preparation*
- Kastenschmidt J.M. et al.** "QuantiMus: a machine learning based software for the automated morphometric analysis of skeletal muscle." *Front Physiol*; 2019. PMID: 31849692
- Hightower R.M., Reid A.L., Gibbs D.E., Wang Y., Widrick J.J., Kunkel L.M., **Kastenschmidt J.M.**, Villalta S.A., Van Groen T., Chang H., Gornisiewicz S., Landesman Y., Tamir S., Alexander M.S. "The SINE Compound KPT-350 Blocks Dystrophic Pathologies in DMD Zebrafish and Mice." *Mol Ther.* 2019. PMID: 31628052
- Kastenschmidt J.M.**, Muñoz K.J., Mannaa A.H., Villalta S.A. "Immune system regulation of muscle injury and disease." *Muscle Gene Therapy (Springer)*; 2018



**Kastenschmidt J.M.**, Avetyan I., Villalta S.A. "Characterization of the Inflammatory Response in Dystrophic Muscle Using Flow Cytometry." *Duchenne Muscular Dystrophy. Methods in Molecular Biology*; 2018. PMID: 29067655

Catalan-Dibene J., Vazquez M.I, Luu V.P, Nuccio S., Karimzadeh A., Inlay M.A, **Kastenschmidt, J.M.** et al. "Identification of Interleukin 40, a novel B cell-associated cytokine." *Journal of Immunology*. 2017. PMID: 28978694

## PRESENTATIONS

### Graduate

- 2019 Immunology 2019, May 2019; Poster
- 2018 UC Irvine Immunology Fair, December, 2018; Poster
- 2018 New Directions in Biology and Disease of Skeletal Muscle Conference, June 2018; Poster
- 2017 Immunology LA - June 2017; Poster
- 2018 Midwinter Conference of Immunologists at Asilomar - January 2018; Poster
- 2017 UC Irvine Immunology Fair, December 2017; Oral presentation
- 2017 La Jolla Immunology Conference – October 2017; Poster
- 2017 Pathways to Cures: Translational Science Research Day (UCI ICTS) - June 2017; Poster
- 2017 Immunology LA - June 2017; Poster
- 2017 UCI Campus-wide Symposium - May 2017; Poster
- 2017 Midwinter Conference of Immunologists at Asilomar - January 2017; Poster

### Undergraduate

Kastenschmidt, J. and Stupack, D. "The localization and Function of Novel Caspase 8 Isoforms"

- 2009 UCSD Summer Research Conference August 13, 2009; Oral presentation

Kastenschmidt, J. and Hart, M.C. "Purification of Isoform specific actin capping protein antibodies and immunofluorescent studies"

- 121st Annual Meeting of the Iowa Academy of Science, April 18, 2009; Oral presentation
- 2008 Minnesota State University Mankato – Undergraduate Research Conference April 28, 2009; Oral presentation

Kastenschmidt, J. and Hart, M.C. "Generation of Rabbit and Chicken Polyclonal Antibodies"

- 2008 Minnesota State University Mankato – Undergraduate Research Conference April 22, 2008; Poster
- 2008 Minnesota Academy of Science; Poster

## FUNDING

- T32 Pre-doctoral fellowship (National Institute of Allergy and Infectious Diseases), 2017-2018/2018-2019
- UCI Center for Complex Biological Systems (CCBS) Opportunity Award, 2018

## HONORS AND AWARDS

### Graduate:

- The AAI Young Investigator Award (The American Association of Immunologists), UCI Institute for Immunology 16<sup>th</sup> Annual Immunology Symposium, 2018
- Stanley Behrens Fellows in Medicine, Honorable Mention, 2018
- Dr. Lorna Carlin Scholar Award, Honorable Mention, 2018
- Physiology and Biophysics Graduate Student Award: “Cahalan Bucks”, 2017
- Best Journal Club Presentation, Physiology and Biophysics Journal Club, Fall 2017
- Ray Owen Poster Award (The American Association of Immunologists), Midwinter Conference of Immunologists, 2017

### Undergraduate:

- Mentored Academic Experience (MAX) Scholarship for Diversity Recipient 2008-2010
- Amgen Summer Scholar, UC San Diego, Summer 2009
- Frank G. Brooks Award (Oral Presentation) Beta Beta Beta National Biological Honor Society, 2009
- Undergraduate Research Conference Foundation Grant, Minnesota State University – Mankato, 2008
- Foundation Research Scholarship, Beta Beta Beta National Biological Honor Society, 2008
- Minnesota State University – Mankato: Biology Department Research Grant, 2007

## MENTORING

2019-Present Mina Nguyen, Undergraduate Researcher

2019-Present Therese Cristal, Undergraduate Researcher

2017-2019 Ali Mannaa, Undergraduate Researcher

2016-2019 Rodolfo Rios, Undergraduate Researcher

2016-2019 Philip Pham, Undergraduate Researcher

2016-2018 Rachel Ayer, Undergraduate Researcher

2016-2018 Rayan Yahia, Undergraduate Researcher

2015-2017 Ileen Avetyan, Undergraduate Researcher

## TECHNICAL SKILLS

**Immunology:** Multi-parameter flow cytometry (10+ Colors) utilizing 5 laser systems, fluorescence activated cell sorting, designing complex flow cytometry panels for the integration of rare populations, surface and intracellular staining, magnetic cellular purification, primary cell isolation and culture, *in vitro* T cell activation and expansion.

**Histology and microscopy:** Preparation of fresh-frozen and fixed tissue for histological analysis, immunohistochemistry and immunofluorescence staining of mouse and human

tissues, multi-color fluorescence microscopy, image analysis and high-throughput quantification.

**Molecular biology:** RNA isolation from cells and tissue, PCR, qPCR, droplet-based single cell RNAseq

**Human Sample Processing:** Isolation and preparation of human muscle xenografts, blood processing, extraction of blood mononuclear cells.

**Computational:** Bioinformatic analysis and data mining of single cell sequencing data, software development, competent in Python and R.

**Animal Models:** Extensive murine husbandry including breeding strategies, induction and clinical scoring of EAE mice, chronic (mdx mouse) and acute muscle injury models (Cardiotoxin, Barium Chloride), isolation and preparation of single cell suspensions from muscle, lung, intestine, spleen, CNS and lymph nodes.

**Software:** MacOS, Windows operating systems, Adobe Illustrator, BD FACS DIVA, FlowJo, GraphPad PRISM, Image J, MS Office and Excel.

## **ABSTRACT OF THE DISSERTATION**

Evaluating the role of group 2 innate lymphoid cells in muscular dystrophy

by

Jenna Marie Kastenschmidt

Doctor of Philosophy in Biomedical Sciences

University of California, Irvine, 2020

Armando Villalta, Chair

Duchenne muscular dystrophy (DMD) is a lethal, x-linked genetic neuromuscular disorder caused by mutations in the dystrophin gene. The resulting non-functional dystrophin protein renders muscle myofibers susceptible to contraction-induced injury, and normal ambulation leads to muscle degeneration and eventual death. Further contributing to disease is the activation of chronic immune responses caused by asynchronous and continuous bouts of injury. This disrupts the homeostasis-promoting balance of immune responses, further causing exacerbated muscle degeneration and impaired regeneration. Importantly, different facets of the immune system, such as type I or type II immunity, are implicated as being injury-promoting or pro-regenerative, respectively. In acute injury settings, type II immune responses such as the activation of M2-like macrophages and eosinophils are critical for efficient muscle regeneration. It is suspected that a similar type II immune response is activated in dystrophic muscle, but its role in promoting regeneration is disrupted by competing pro-inflammatory responses. However, the regulation of type II immunity in dystrophic muscle is largely unknown.

Intriguingly, a recently identified subset of immune cells, group 2 innate lymphoid cells (ILC2), have been shown to be potent regulators of type II immunity and promote repair in other diseases. The focus of this dissertation is aimed at understanding the role of ILC2s in regulating skeletal muscle type II immune responses during chronic muscle disorders such as DMD

(**Chapter 3**). We found that mdx muscle ILC2s were increased in number and expressed higher levels of type II cytokines interleukin-5 and interleukin-13 compared to wildtype controls, indicating that muscle degeneration activates ILC2s. We also sought to identify how muscle ILC2s are activated and found that fibro/adipogenic progenitors were the primary source of IL-33, an alarmin known to activate ILC2s. We found that muscle ILC2s are activated by exogenous cytokines, including IL-2/anti-IL-2 complex (IL-2c) and IL-33, which we also used to induce the expansion of ILC2s *in vivo*. Using additional mouse models in which ILC2s are genetically depleted, we found that ILC2s are potent regulators of skeletal muscle eosinophilia. As ILC2s have also been shown to activate M2-like macrophages in other tissues, we also evaluated this interaction in dystrophic skeletal muscle. To our surprise, ILC2s did not regulate macrophage numbers or phenotype in mdx muscle during this study.

In addition to investigating the role of ILC2s in muscle dystrophy, another aim of this work was focused on the development of software that evaluates the morphological features of skeletal muscle (**Chapter 2**). Muscle function is commonly assessed by evaluating and quantifying histological features of muscle cross-sections. This includes evaluating myofiber size, the expression of markers for injury and regeneration, as well as measuring centrally-located myofiber nuclei. Historically, the time-consuming and tedious nature of manually quantifying muscle samples hindered accurate evaluation, as many analyses were limited to the sampling of parts of the entire cross-section. Furthermore, morphological features are much more complex in diseased muscle compared to healthy, which further inhibited the ability to use software to automatically evaluate the tissue in a high-throughput manner. To address these issues in the field, and provide a tool that we could use to evaluate how perturbations to the immune system effect muscle pathology, we developed QuantiMus. QuantiMus is a machine learning-based software that allows the accurate detection of muscle myofibers as well as the location of nuclei (i.e., centrally-located) and intra-myofiber presence of investigator-chosen proteins stained by immunofluorescence in entire muscle cross-sections. To date, we have successfully used

QuantiMus to measure myofiber regeneration, myofiber injury, centrally-nucleated fibers, and to determine the myofiber type distribution of entire muscle cross-sections. The ability to measure full cross-sections is an advancement in the field that allows investigators to avoid random sampling of tissue sections and prevents bias in the data.

All together, this study defines a role for ILC2s in regulating skeletal muscle eosinophilia during muscular dystrophy. We also developed software that allows us to evaluate muscle morphology in a high-throughput manner. Future directions will be aimed at understating what, in addition to regulating muscle eosinophilia, role ILC2s play in regulating DMD pathogenesis. In part, these future studies will encompass the power of QuantiMus to histologically evaluate how perturbations to ILC2s and eosinophils regulate pathology.

# **CHAPTER 1**

## **Introduction**

Incorporates components from the published article:

Kastenschmidt J.M., Manna A.H., Muñoz K.J., Villalta S.A. Immune System Regulation of Muscle Injury and Disease. Muscle Gene Therapy. 2019 Springer

## **Muscle stem cells and the maintenance of skeletal muscle homeostasis**

Skeletal muscle is a highly resilient and regenerative tissue that maintains homeostasis despite dynamic changes in activity, mechanical load, and stress. Nonetheless, acute trauma or genetic and environmental factors that exceed this homeostatic threshold of resilience, cause muscle injury and loss of function. Post-natal growth and regeneration of muscle are dependent (Lepper et al., 2011; McCarthy et al., 2011; Murphy et al., 2011) on paired box 7 (Pax7) expressing myogenic precursors (Seale et al., 2000), known as muscle satellite cells (mSC), which reside the basal lamina and myofiber plasma membrane (i.e., sarcolemma) (Katz, 1961; Mauro, 1961) (**Figure 1.1**).

In mice, these post-mitotic cells express characteristic markers including, vascular cell adhesion molecule 1, integrin alpha-7, and integrin beta-1 (Maesner et al., 2016). In response to injury, mSCs become activated and enter a well-characterized transcriptional program that gives rise to new or repaired myofibers (**Figure 1.2**). Upon activation, mSCs migrate towards sites of injury and differentiate into proliferating myoblasts. This process is associated with the upregulation of myogenic factor 5 (Myf5) and myogenic differentiation 1 (MyoD) (Cornelison and Wold, 1997; Hawke and Garry, 2001). Following proliferation, myoblasts terminally differentiate to form myocytes (i.e., muscle cells), which is accompanied by decreases in Pax7 and Myf5 expression and an upregulation of myogenin (MyoG) and myogenic regulatory factor 4 (MRF4). Finally, myocytes fuse to form new multinucleated myofibers or fuse with injured fibers to promote repair. Of note, mSCs undergo asymmetric cell division, where a subpopulation of activated mSCs (Pax7<sup>+</sup>, Myf5<sup>-</sup> cells) (Kuang et al., 2007) returns to a quiescent state to maintain the myogenic progenitor pool (**Figure 1.2**). Altogether, these stem-cell mediated responses following skeletal muscle insult lead to the restoration of homeostasis. In the following sections, the immune system-mediated regulation of this regenerative response will be discussed.



## Immune responses following muscle injury

Muscle injury activates multiple immune system pathways that cooperatively regulate the spatiotemporal dynamics of immune cell subpopulations (e.g., macrophages and T cells) recruited to injured muscle (**Figure 1.3**). These events are characterized by an early innate immune response, running in parallel with T cell responses that together enhance the regeneration of damaged myofibers by promoting satellite cell proliferation and/or differentiation. These carefully controlled series of immunological events ensure the effective and complete recovery of acutely injured muscle.

Muscle fiber necrosis results in the release of damage-associated molecular patterns (DAMPs) that activate innate immunity (Rayavarapu et al., 2013). Ly6G<sup>+</sup> neutrophils are the first immune cells to infiltrate the site of injury (Haiyan Lu et al., 2011), causing secondary damage by secreting free radicals (Nguyen and Tidball, 2003) and pro-inflammatory cytokines, the latter of which promotes the homing of bone marrow-derived monocytes (Pizza et al., 2005; Swirski et al., 2010; Tidball, 2005). A recent study revealed that CD18 (integrin beta 2) is required for the extravasation of neutrophils into the acutely injured muscle, and mice deficient in CD18 exhibited enhanced signs of muscle repair, suggesting that neutrophils have a detrimental role in the repair process (Hammers et al., 2015). Following the neutrophil response, CD11b<sup>+</sup>Ly6C<sup>hi</sup>CX3CR1<sup>lo</sup> monocytes enter the damaged tissue and differentiate into pro-inflammatory M1-like macrophages (Geissmann et al., 2003). M1 macrophages secrete the inflammatory cytokines, interleukin-1 $\beta$  (IL-1 $\beta$ ) and tumor necrosis factor- $\alpha$  (TNF $\alpha$ ) and phagocytose necrotic debris, suggesting that they participate in the repair process by clearing dead muscle (Geissmann et al., 2003). A requirement for M1-like macrophages in muscle repair is further supported by *in vitro* studies showing that they promote myoblast proliferation while having no effect on differentiation (Geissmann et al., 2003). Although previous studies have shown that M1-like macrophages promote the cytolysis of muscle cells *in vitro*, it is not clear whether they promote myofiber injury *in vivo* during acute injury (Nguyen and Tidball, 2002).

CD11b<sup>+</sup>Ly6C<sup>lo</sup>F4/80<sup>hi</sup>, anti-inflammatory M2 macrophages infiltrate injured muscle as M1 macrophages begin to resolve (Arnold et al., 2007). M2-like macrophages can be further divided into distinct M2a, M2b, and M2c populations (Liu et al., 2014; Rigamonti et al., 2014; Wermuth and Jimenez). In skeletal muscle, M2a macrophages are characterized as F4/80<sup>high</sup>Ly6C<sup>low</sup>Arg1<sup>high</sup> (Capote et al., 2016) macrophages that may have a pro-fibrotic function (Song et al., 2000). Alternately, M2c macrophages are F4/80<sup>high</sup>Ly6C<sup>low</sup>CD163<sup>high</sup>CD206<sup>high</sup>Arg1<sup>low</sup> and have been shown to deactivate M1-like macrophages and have a pro-regenerative phenotype, as they promote mSC proliferation *in vitro* (Villalta et al., 2009). The transition from M1 to M2 macrophages is necessary for efficient regeneration of injured muscle. Although the mechanisms that regulate this process are not completely understood, recent studies highlighted regulatory T cells (Tregs) and IL-10 as having important roles in this transition; the ablation of either impeded on the M1 to M2 transition during acute injury (Burzyn et al., 2013; Deng et al., 2012). The importance of this transition is demonstrated by an increase in myofiber injury and altered regeneration in this setting (Burzyn et al., 2013; Deng et al., 2012).

The central role of M2-like macrophages in muscle repair is supported by several studies showing that depletion or the inability to induce M2 activation impedes muscle regeneration (Mounier et al., 2013; Tidball and Wehling-Henricks, 2007). The depletion of F4/80<sup>+</sup> macrophages during the time when M2-like macrophages infiltrate muscle impairs regeneration (Tidball and Wehling-Henricks, 2007). Moreover, the deficiency of AMPK $\alpha$ 1 in macrophages, which prevented M2 activation, also resulted in an impairment in muscle regeneration following cardiotoxin-induced muscle injury (Mounier et al., 2013). Recent studies also showed that the adoptive transfer of CD11b<sup>+</sup>Ly6C<sup>lo</sup>F4/80<sup>hi</sup> macrophages into mouse skeletal muscle increased the regeneration and functional recovery of skeletal muscle in an ischemia-reperfusion model of injury (Hammers et al., 2015).

Although the role of M2-like macrophages in muscle regeneration is well accepted, we are only recently beginning to uncover the molecular basis of M2 macrophage-mediated regeneration.

Recent studies show that M2-like macrophages promote regeneration, in part, by secreting factors that regulate inflammation and regeneration. For example, they secrete the anti-inflammatory cytokines transforming growth factor beta (TGF- $\beta$ ) and IL-10 that modulate the inflammatory response to establish an environment favorable for muscle regeneration (Martinez et al., 2009). Reparative macrophages also express growth differentiation factor 3 (Varga et al., 2016) and insulin growth factor 1 that promote regeneration by enhancing satellite cell fusion and differentiation (H Lu et al., 2011; Musarò et al., 2004; Tonkin et al., 2015).

Recruitment of macrophage populations to damaged muscle is an additional layer of regulation controlling the macrophage-specific contributions to muscle regeneration. A recent study by Brigitte and colleagues demonstrated that following acute injury, muscle resident macrophages (CD11b<sup>+</sup>F4/80<sup>+</sup>CD11c<sup>-</sup>Ly6C<sup>-</sup>CX3CR1<sup>-</sup>) orchestrate early immune responses through the production of chemoattractants that recruit neutrophils and monocytes (Brigitte et al., 2010). The CCL2:CCR2 chemotactic axis is required for macrophage recruitment to injured muscle, and preferentially recruits inflammatory monocytes that are Ly6C<sup>hi</sup>CCR2<sup>hi</sup> (H Lu et al., 2011; Haiyan Lu et al., 2011). In contrast, the chemokine receptor CX3CR1 is not required for macrophage recruitment to injured muscle but is important for regulating macrophage phagocytosis (Zhao et al., 2016). Macrophages also promote chemotaxis of immune cells through their intrinsic production of chemokines. For example, macrophages expressing CCL5 (RANTES) recruit CD8<sup>+</sup> T cells following cardiotoxin-induced injury (Kohno et al., 2011) and other immune cells, including eosinophils (Alam et al., 1993; Ying et al., 2016). Recent studies showed that eosinophils are required for efficient muscle regeneration, and their accumulation in injured muscle paralleled an increase in CCL5 (Heredia et al., 2013). Given that macrophages are known to express CCL5, a potent eosinophil chemoattractant, these studies collectively suggest that macrophages recruit eosinophils, and both cooperatively promote regeneration.

Although myeloid cells dominate the immune cell infiltrate following injury, lymphocytes are also recruited and regulate muscle regeneration. Recent investigations showed that following

cardiotoxin injury, forkhead box P3 (FoxP3)<sup>+</sup>CD25<sup>+</sup>CD4<sup>+</sup> Tregs were recruited to skeletal muscle at the time when the M1 to M2 macrophage transition occurs (Burzyn et al., 2013; Castiglioni et al., 2015). The functional importance of Tregs in acute muscle injury was shown by loss- or gain-of-function experiments where muscle regeneration was hindered or enhanced, respectively (Burzyn et al., 2013). Although muscle Tregs in acutely injured muscle expressed high levels of amphiregulin (Areg), and intramuscular and intraperitoneal injections of Areg in injured mice enhanced a transcriptional signature associated with muscle regeneration, it remains to be defined whether Treg-derived amphiregulin directly promotes muscle regeneration *in vivo* (Burzyn et al., 2013). Burzyn and colleagues showed that Areg treatment enhanced satellite cell proliferation and differentiation, further supporting a regenerative function for Areg in acutely-injured muscle. Further corroborating these findings, Castiglioni and colleagues independently demonstrated that muscle Tregs promoted regeneration by increasing satellite cell proliferation but inhibited differentiation (Castiglioni et al., 2015). In their studies, Castiglioni et al. cocultured Tregs with satellite cells, in contrast to the Burzyn et al. study, where satellite cells were treated with recombinant Areg (Burzyn et al., 2013; Castiglioni et al., 2015). Thus, the contradicting results on satellite cell differentiation in these two studies may be attributed to differences in the experimental assays used. Collectively, these studies highlight a critical role for macrophages and T regs in muscle regeneration following acute injury.

### **Duchenne muscular dystrophy and cellular mechanisms of disease**

Duchenne muscular dystrophy (DMD) is a fatal X-linked childhood disease caused by dystrophin gene mutations (Hoffman et al., 1987; Koenig et al., 1987) that arise in approximately 1:5000 males (Mendell et al., 2012; Moat et al., 2013). The dystrophin protein resides at the myofiber sarcolemmal surface and interacts with membrane proteins known as the dystrophin-glycoprotein complex (DGC) to form an interaction between the intracellular cytoskeleton and extracellular matrix (**Figure 1.4**). Together, dystrophin and its interactions (i.e., the DGC)

mechanically stabilize and protect the sarcolemma from longitudinal and radial forces generated during muscle contraction (Lapidos et al., 2004; Petrof et al., 1993). Importantly, dystrophin also plays a role in regulating intracellular calcium homeostasis and the production of reactive oxygen species (ROS) (Khairallah et al., 2012) and nitric oxide (NO) (Garbincius and Michele, 2015).

During DMD, gene mutation(s) lead to the translation of nonfunctional dystrophin protein, which subsequently disrupts the DGC and its homeostatic functions. This loss of structural support renders the sarcolemma susceptible to contraction-induced injury (Petrof et al., 1993) and normal ambulation induces myofiber injury, inflammation, and progressive degeneration (Lapidos et al., 2004). Dystrophin deficiency also leads to increased intra-myofiber calcium and ROS, which further exacerbate myofiber degeneration (Mariol and Ségalat, 2001; Rando et al., 1998). Additionally, the loss of dystrophin disrupts normal muscle NO signaling, causing functional ischemia and exaggerated muscle fatigue (Brenman et al., 1995; Garbincius and Michele, 2015) which further exacerbates disease.

### **Clinical manifestations and comorbidities during DMD**

DMD patients appear normal at birth, but clinical symptoms arise at 3-5 years of age. A diagnosis of DMD can be made with physical examination, and is confirmed by a muscle biopsy or genetic testing (Bushby et al., 2010). Early physical symptoms begin with proximal muscle weakness, followed by distal weakness (Mercuri and Muntoni, 2013) that leads to abnormal gait and eventually, frequent falls (Wood and Straub, 2018). Symptoms progressively worsen, and on average, patients lose ambulation by their preteens (Allsop and Ziter, 1981; Desilva et al., 1987; Gardner-Medwin, 1980). Pathological features of the disease are also observed histologically (Bell and Conen, 1968). These include regions of muscle necrosis and degeneration, inflammation, myofiber regeneration as indicated by centrally-located nuclei, and in later stages of disease, fibrosis (Kharraz et al., 2014).

Other comorbidities include orthopedic complications (e.g., bone fractures (Khoury and Szalay, 2007; Larson and Henderson, 1981) and progressive scoliosis (Hsu and Quinlivan, 2013)) and mental defects including lower IQ (Rasic et al., 2014). Similar to skeletal muscle, the lack of functional dystrophin affects cardiomyocytes, causing cardiac muscle wasting that hinders cardiac function (e.g., decreased systolic function (Spurney, 2011) and resting sinus tachycardia (Thomas et al., 2012)). As a result of weakened respiratory muscles and scoliosis, respiratory function is compromised in DMD, and patients often experience hypoventilation, and in later stages of disease, respiratory failure (Lo Mauro et al., 2015). It is the combination of respiratory and cardiac comorbidities that are the main causes of mortality in DMD, usually occurring around the second to third decade of life (Passamano et al., 2012).

### **Therapeutic management of DMD**

There is no cure for DMD and therapies are mostly aimed at optimizing muscle growth and development, while delaying disease progression and preventing or alleviating comorbidities. However, substantial progress in the research areas of cellular and gene therapy have provided new therapeutic approaches for DMD treatment. Gene therapies (Pachavant 2011), which aim to restore functional dystrophin gene expression and subsequent restoration of muscle function, have shown great promise. For example, the recent FDA approval of Eteplirsen, an antisense oligo nucleotide that leads to the “skipping” of mutated exons, is a major therapeutic milestone that could be effective in a wide spectrum of DMD patients who harbor mutations in “hotspot” exons (i.e., Exons 45-63), nearly 13% of all DMD cases (Charleston et al., 2018; Lim et al., 2017). Even though strides to find a cure and new management strategies for DMD are actively being pursued, most current therapies are palliative and usually include long-term glucocorticosteroid (GC) treatment.

Standard GC treatment includes daily dosing based on a patient’s body weight. Studies show steroid treatment increases muscle mass (Rifai et al., 1995) and function (Mendell et al.,

1989), improves pulmonary function (Brooke et al., 1987) and cardiac performance (Duboc et al., 2005; Silversides et al., 2003), prolongs ambulation (Desilva et al., 1987) and increases the overall length of survival (McDonald et al., 2018; Passamano et al., 2012). Although not well understood, GCs are thought to elicit these beneficial effects through several mechanisms. The immunosuppressive actions of GCs (Coutinho and Chapman, 2011) lead to decreased infiltration of many immune subsets in DMD that may prevent further muscle injury by inhibiting certain inflammatory subsets (as discussed below). GCs also help to preserve muscle mass by inhibiting proteolysis and skeletal muscle breakdown (Rifai et al., 1995). Furthermore, certain GCs induce the transcriptional repression of genes that negatively affect myocyte viability, providing another mechanism by which these agents regulate disease progression (St.-Pierre et al., 2004).

GCs slow disease progression but are accompanied by significant side effects that can be poorly tolerated in DMD patients. Long-term GC use is associated with weight gain that can further hinder ambulation (Mendell 1989, Angelini 2012), a reduction in bone density which may or (Picado 1996) may not (McDonald 2002) increase the risk for fractures, and cataract development (Rice 2018). Additionally, the broad immunosuppressive actions of these drugs hinder both the injury-promoting and pro-regenerative inflammatory responses activated following skeletal muscle insult that exacerbate disease and prevent degeneration, respectively. Indeed, future therapeutic targets would ideally preserve pro-regenerative responses while suppressing pathogenic ones.

### **Immune responses during Duchenne muscular dystrophy**

The current understanding of the immune system's role in regulating dystrophic muscle pathology has largely been uncovered using the mdx mouse model of DMD. The mdx mouse lacks functional dystrophin caused by a spontaneous mutation on exon 23 of the dystrophin gene, yielding a premature stop codon and a truncated, nonfunctional protein (Bulfield et al., 1984; Ng et al., 2012). Although both mdx mice and human DMD patients lack dystrophin, mdx mice display

lessened disease severity and delayed progression compared to their human counterparts. For example, mdx mice maintain a relatively normal life span, rarely lose ambulation, and display minimal clinical symptoms. In mdx mice, severe dystrophic phenotypes such as muscle wasting, scoliosis, and heart failure are not observed until after 15 months of age (McGreevy et al., 2015). Even though the pathology of mdx mice differs in human patients, chronic inflammatory responses to muscle injury are conserved and provide an experimental system to evaluate the immune-mediated regulation of DMD.

The critical function of inflammatory immune cells in muscle regeneration during acute injury is dysregulated in DMD, consequently promoting muscle degeneration. Persistent myofiber injury triggers a chronic muscle inflammatory response that contributes to the development and progression of DMD (Spencer and Tidball, 2001). Muscle injury during DMD induces an oscillating pattern of chronic muscle inflammation that mirrors the asynchronous and cyclic nature of injury (**Figure 1.5**). This dysregulated inflammatory response subsequently promotes fibrosis and failure of regeneration (Spencer and Tidball, 2001). The increased immune cell numbers and expression of genes related to immune cell function in DMD muscle further support the immune system's contribution to the pathogenesis of muscular dystrophy (Haslett et al., 2002; Lundberg et al., 1995; McDouall et al., 1990; Pescatori et al., 2007). Moreover, the immunosuppressive activity of glucocorticoids (Coutinho and Chapman, 2011), and their known role in promoting muscle atrophy (Schakman et al., 2013), suggests that the incremental delay in disease progression is mediated by inhibition of the immune system. This argument is supported by studies performed in mdx mice, which demonstrated that glucocorticoid treatment reduces the expression of adhesion molecules required for immune cell extravasation and the number of immune cells present in dystrophic muscle (Wehling-Henricks et al., 2004). More specific methods of immune cell ablation in mdx mice have demonstrated that the depletion of eosinophils, macrophages or T cells in muscle causes a 60-80% decrease in muscle pathology (Cai et al., 2000; Spencer et al., 2001; Wehling et al., 2001). These early studies aided in establishing



inflammation as a secondary disease process contributing to the severity of muscular dystrophy, and are the basis for much of the research aimed at uncovering the cellular and molecular basis of immune-mediated pathology in DMD.

In addition to promoting muscle injury, the immune system is also critical in mediating muscle regeneration during muscular dystrophy (De Paepe and De Bleecker, 2013; Madaro et al., 2014; Rosenberg et al., 2015; Tidball, 2017; Villalta et al., 2015). This dichotomy can be partly explained by a division in functional facets of the immune system, in which distinct immune cell populations are responsible for causing injury or promoting regeneration (**Figure 1.6**). This process is exemplified by the accumulation of macrophages with distinct polarized states of M1- or M2-like activation that are known to promote either injury or repair, respectively. M1 and M2 macrophages reflect polar extremes of activation. However, macrophages present in dystrophic muscle likely exist as a broad continuum in which cells transition from one state of activation to another according to changes in the pro- and anti-inflammatory environment (Gordon, 2003; Mosser and Edwards, 2008). Although the epigenetic regulation of gene expression may influence macrophage function in this setting (Hoeksema and De Winther, 2016), the presence of different cytokines elicits distinct macrophage responses. Pro-inflammatory cytokines such as IFN $\gamma$  and TNF $\alpha$  promote the classical activation of M1 macrophage that induces myofiber injury through an iNOS-dependent mechanism (Villalta et al., 2009). In contrast, cytokines such as IL-4, IL-13, and IL-10 induce M2 activation of macrophages that antagonize the action of M1-like macrophages via arginase-dependent mechanisms (Villalta et al., 2009). Recent studies have begun to identify the cell types that orchestrate changes in the inflamed environment of dystrophic muscle. Tregs, for example, have been implicated as critical regulators of muscle inflammation and regeneration due to their capacity to shift the balance between M1 and M2 macrophages in favor of M2 activation.

As discussed above, Tregs are elevated in regenerating muscle and promote muscle regeneration by regulating macrophage activation and enhancing myogenesis through Areg-

dependent mechanisms. Comparably, studies in the mdx mouse and in patients with chronic muscle disorders indicate that muscle Tregs are also increased (Antiga et al., 2010; Vercoulen et al., 2014; Vetrone et al., 2009; Villalta et al., 2014). Tregs in mdx muscle were elevated in number and expressed high levels of IL-10, and inhibited M1 macrophage activation and reduced myofiber injury (Villalta et al., 2014). Similarly, Tregs and IL-10 were elevated in human dystrophic muscle (Villalta et al., 2014), supporting the view that the Treg-mediated suppression of muscle inflammation is mediated by IL-10. Additionally, *in vitro* studies have shown that human Tregs express IL-10 and induce M2 macrophages (Tiemessen et al., 2007). Although the Treg-specific role of IL-10 in suppressing muscle inflammation has not been tested, its importance is supported by studies showing that IL-10 deficiency in mdx mice exacerbates dystrophinopathy (Nitahara-Kasahara et al., 2014; Villalta et al., 2011). However, the mechanism of Treg-mediated suppression of immunity in other tissues is multifaceted, involving the inhibition of antigen-presenting cells (i.e., dendritic cells), cytolysis of conventional T cells and the production of anti-inflammatory cytokines IL-10 and IL-35 (Tang and Bluestone, 2008; Vignali et al., 2008). Moreover, recent studies indicate that tissue Tregs also harness specialized functions adapted to their environment. Thus, in addition to suppressive activity, Tregs in dystrophic muscle are likely involved in the promotion of regeneration through Areg, and/or other growth factors, as seen during acute injury (Burzyn et al., 2013).

The role of eosinophils in DMD pathology has also been investigated. Although Heredia and colleagues demonstrated that eosinophils enhance muscle regeneration following acute injury (Heredia et al., 2013), their role in chronic muscle diseases such as DMD is not completely understood. Several studies suggest that eosinophils have a pathogenic role in DMD, and skeletal muscle eosinophilia is observed in a number of myopathies (Baumeister et al., 2009; Cantarini et al., 2009; Schröder et al., 2013; Weinstock et al., 1997). Studies have also shown that eosinophil derived factors promote myofiber degradation (Sugihara et al., 2001) and myofiber lysis (Wehling-Henricks et al., 2008) in dystrophin-deficient mice. In contrast, more recent studies demonstrated

that eosinophils do not drive pathology in the mdx mouse (Sek et al., 2019). Interestingly, eosinophil-derived granule proteins (Aceves, 2014; Noguchi et al., 1992) have been shown to promote fibrosis in a variety of chronic diseases. Although fibrosis is a secondary pathogenic feature found in DMD patients (Kharraz et al., 2014), the role of eosinophils in these pro-fibrotic processes has yet to be elucidated. Finally, although effector T cells promote dystrophic muscle eosinophilia in a perforin-dependent manner (Cai et al., 2000), the mechanism of regulation of skeletal muscle eosinophils has yet to be fully elucidated. In contrast, the regulation of eosinophils in other tissues like the lung and adipose tissues, are regulated by group 2 innate lymphoid cells (Molofsky et al., 2015; Nussbaum et al., 2013). However, this axis has not been studied in skeletal muscle and additional investigation as to the role and regulation of eosinophils in this setting is warranted.

### **Group 2 innate lymphoid cells (ILC2)**

Innate lymphoid cells are a subset of lymphocytes that include three distinct subsets, ILC1, ILC2, and ILC3, which mirror the transcriptional profiles and effector functions of T helper cells 1, 2 and 17 cells, respectively (**Figure 1.7**) (Eberl et al., 2015). These cells share a common lineage with other lymphocytes, such as B and T cells, and are progeny of the common lymphoid progenitor (CLP). The upregulation of transcription factors such as inhibitor of DNA binding 2 (Id2) induces the differentiation into common helper-like ILC progenitors (CHILP) that give rise to ILC1, ILC2 and ILC3 (**Figure 1.8**) (Diefenbach et al., 2014). ILC2s are largely tissue-resident and are enriched in parenchymal tissues. Recent parabiosis studies demonstrated that ILCs rarely undergo replenishment from the bone marrow under steady-state conditions (Gasteiger et al., 2015; Moro et al., 2016; Peng et al., 2013). Distinct from other lymphocytes such as B and T cells, ILC2s lack antigen-specific receptors (Cella et al., 2014; Spits and Cupedo, 2012). Alternatively, ILC2s are activated to elicit their effector functions (i.e., cytokines production) in an antigen-

independent manner through activating signals in the local environment, hence their classification as “innate-like” cells.

Group 2 innate lymphoid cells (ILC2s) (Spits et al., 2013), previously known as natural helper cells (Moro et al., 2010), nuocytes (Neill et al., 2010), and type 2 innate helper cells (April E Price et al., 2010), are dependent on the expression of transcription factors ROR $\alpha$  and GATA3 (Furusawa et al., 2013; Hoyler et al., 2012; Walker and McKenzie, 2013) and can be distinguished by their surface expression of KLRG1, CD25, CD127(IL-7 $\alpha$ ), Sca1, ICOS. Furthermore, ILC2s are also characterized by their expression of ST2 (IL-33 receptor), TSLP, and IL-25 receptor. ILC2s are activated by tissue alarmins, including IL-25, IL-33, and TSLP, which are induced following tissue trauma. Upon activation, ILC2s produce type II cytokines (Herbert et al., 2019). Importantly, ILC2s are widely disseminated cells that are present in the respiratory airways (Mjösberg et al., 2011) and lung (Chang et al., 2011; Halim et al., 2012; Monticelli et al., 2011), intestinal lamina propria (Hoyler et al., 2012), liver (Mchedlidze et al., 2013) and skin (Roediger et al., 2013).

## **Biological functions of ILC2s**

### Regulation of type II immunity

Type II immunity was first shown to be associated with responses against helminth infections that is characterized by an increase in cytokines, including IL-4, IL-5, and IL-13 and eosinophil recruitment and/or the activation of M2 macrophages (Lloyd and Snelgrove, 2018). Type II immunity also plays a role in wound healing and the return to homeostasis following insult, however, when dysregulated, this response can lead to asthma, rhinitis, and dermatitis. Importantly, ILC2s have been implicated as key mediators of type II immune responses and are potent secretors of the canonical type II cytokines IL-5 and IL-13 (Molofsky et al., 2013; Moro et al., 2010; Neill et al., 2010; April E Price et al., 2010; Pulendran and Artis, 2012) and in some settings IL-4 (Pelly et al., 2016). ILC2-derived IL-5 is required for the maintenance of eosinophil

homeostasis (Nussbaum et al., 2013) and ILC2s promote eosinophilia in several tissues, including lung (Halim et al., 2012; Monticelli et al., 2011) and visceral adipose tissue (VAT) (Molofsky et al., 2013). Additionally, ILC2s have been implicated in promoting the activation of M2-like macrophages in both visceral adipose tissue (Molofsky et al., 2013) and in mouse models of cerebral malaria (Besnard et al., 2015). Recent *in vitro* coculture experiments have also demonstrated that ILC2s decrease the bone marrow-derived macrophage-production of IL-1 $\beta$ , a pro-inflammatory cytokine produced by canonical M1 macrophages (Omata et al., 2018). Together these studies show an important role for ILC2 in regulating type II immune cells such as macrophages and eosinophils in multiple biological settings.

#### Protection against helminth infections

ILC2s have a critical role in the innate protection and clearance of helminth infection (Omata et al., 2018). Some of the earliest studies identifying ILC2s described these IL-25 responsive cells were involved in the rapid expulsion of the parasitic nematode *Nippostrongylus brasiliensis* (NB) in a T and B cell-independent manner (Fallon et al., 2006; April E Price et al., 2010). More recent studies have shown that the ILC2-derived IL-5 and IL-13 are critical for effective pathogen protection (Neill et al., 2010; April E Price et al., 2010). Furthermore, the absence of IL-25 and IL-33 signaling leads to impaired worm expulsion, but the adoptive transfer of ILC2s can restore efficient pathogen protection and clearance (Neill et al., 2010).

#### Allergic diseases

Recent studies demonstrate that ILC2s are critical for the initiation and progression of allergic disease in skin and lung. During allergic airway inflammation, the ILC2-mediated secretion of type II cytokines (Barlow et al., 2012) promotes the recruitment of eosinophils (Gold et al., 2014). Importantly, eosinophilia is a hallmark of allergic inflammation and has been implicated in promoting airway hyperresponsiveness and tissue remodeling (Humbles et al., 2004) which

contributes to pathology. ILC2s promote eosinophilia in the lung, in part, through the secretion of IL-5 (Van Gool et al., 2014). An additional proposed mechanism is through the secretion of IL-13, which induces epithelial cell secretion of eosinophil chemoattractants (Li et al., 1999; Nussbaum et al., 2013; Pope et al., 2001). It has also been suggested that ILC2s play a pathogenic role in asthma, as increased numbers of type II cytokine-secreting ILC2s are found in the blood and sputum of patients with severe asthma compared to those with a more mild phenotype (Smith et al., 2016). This is further supported by evidence from clinical trials showing that antibody-mediated blockade of TSLP, an activating signal for ILC2s, reduced asthma symptoms in humans (Gauvreau et al., 2014). Similar to asthma patients, ILC2s are present in human nasal polyps and are enriched in patients with chronic rhinosinusitis (Miljkovic et al., 2014; Mjösberg et al., 2011; Poposki et al., 2017) implicating that ILC2s also have a disease-exacerbating role in this setting.

ILC2s have also been implicated in the health and disease of skin. ILC2s are found in healthy skin of mice and humans, and in during the inflammatory skin disease atopic dermatitis (AD), type II cytokines are considered the main contributors to pathogenesis. Recent studies have shown that ILC2-derived IL-5 and IL-13 are necessary for inflammation in AD mouse models (Kim et al., 2013; Roediger et al., 2013). ILC2s are also enriched in human AD lesions, suggesting a similar pathogenic role.

### ILC2 cells and Metabolism

In obese individuals, chronic type 1 inflammation in visceral adipose tissue (VAT) promotes insulin resistance and metabolic dysregulation, including type II diabetes (Chawla et al., 2011; Hotamisligil, 2006). However, in normal lean VAT, type II immune responses promote insulin sensitivity and metabolic homeostasis. Recent studies have shown that VAT resident ILC2s are critical regulators of type II immunity and the main sources of IL-5 and IL-13, which promote the accumulation of eosinophils and macrophages, respectively (Molofsky et al., 2013). Tissue adipose M2 macrophages are required for the maintenance of glucose homeostasis, and

Wu and colleagues demonstrated that eosinophils are a major source of IL-4, which sustains these cells (Wu et al., 2011). Together these studies show that ILC2s regulate metabolic homeostasis and promote glucose tolerance through multiple mechanisms, including the maintenance of VAT eosinophils and by directly and indirectly promoting the activation of M2 macrophages.

### Tissue repair and homeostasis

ILC2s also promote tissue repair and the return to homeostasis by producing the epidermal growth factor, amphiregulin (Areg) (Monticelli et al., 2011). Following *Nippostrongylus* infection, ILC2s produce Areg and promote lung tissue repair (Turner et al., 2013). Similarly, ILC2-derived Areg is critical for the repair of lung epithelium following influenza infection (Monticelli et al., 2011). ILC2s and Areg are also involved in epithelium repair following inflammation in the intestine (Monticelli et al., 2015) and the skin (Iordanov et al., 2005; Salimi et al., 2013).

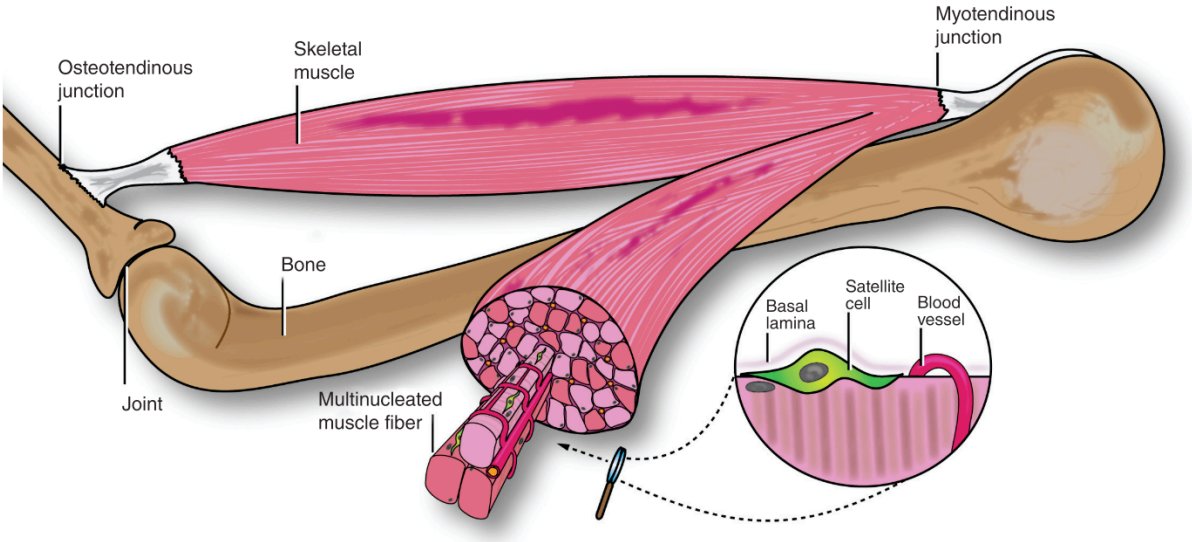
### **Introduction to the dissertation - the role of ILC2s in muscle disease**

Type II immune responses characterized by the infiltration of eosinophils and M2-like macrophages have been demonstrated to be important for muscle repair and regeneration. The presence and activation of M2-like macrophages are critical for the resolution of muscle insult and the return to homeostasis following both acute injury and during disease (e.g., DMD). Similarly, eosinophils play a pro-regenerative role in acute injury. Contradicting studies on the role of eosinophils in dystrophic muscle leaves a gap in our understanding as to their function in this setting. Further, the regulation of eosinophils has yet to be fully elucidated, which provides a barrier to completely understanding eosinophil function in muscular dystrophy. One aim of this dissertation was to evaluate the role of ILC2s, which are potent regulators of type II immunity in other settings, in regulating macrophage and eosinophil responses in muscle. We also aimed to understand the functional role that ILC2s play in regulating DMD pathology. One method of

evaluating pathology includes the histological assessment of skeletal muscle tissues. However, previous methods relied on time-consuming, manual methods that were prone to bias. To circumvent this limitation and allow us to fully evaluate the role of ILC2s in dystrophic muscle, we first generated a new analysis software that allows for the high throughput and objective analysis of skeletal muscle. This body of work first describes the development and validation of a new histological tool, known as QuantiMus, to quantify metamorphic features of skeletal muscle (Chapter 2). Chapter 3 describes a study investigating the role of ILC2s in regulating type II immunity in muscular dystrophy. We found that indeed, ILC2s are potent regulators of skeletal muscle eosinophilia. The role of these cells in regulating macrophage function as well as DMD pathology are ongoing and future studies that are further discussed in Chapter 4.

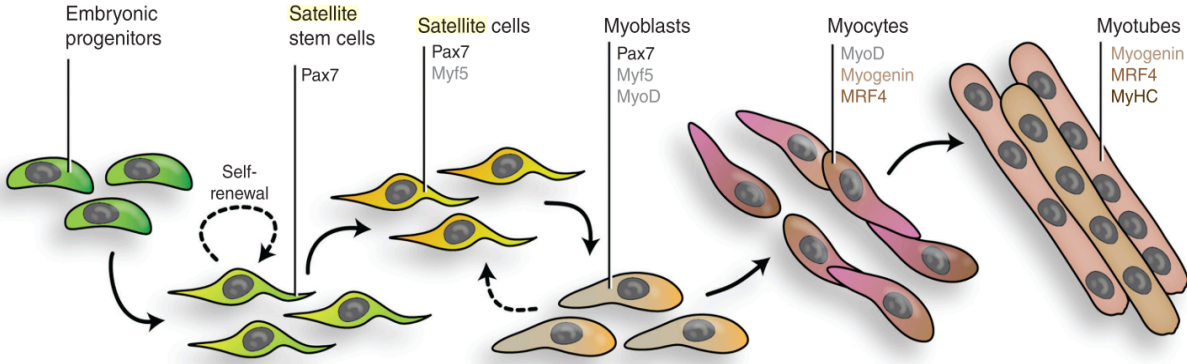


**Figure 1.1. Schematic illustrating the structure of skeletal muscle.** Pax7+ cells reside near the myofiber sarcolemma, beneath the basal lamina. Adapted from (Dumont et al., 2015).

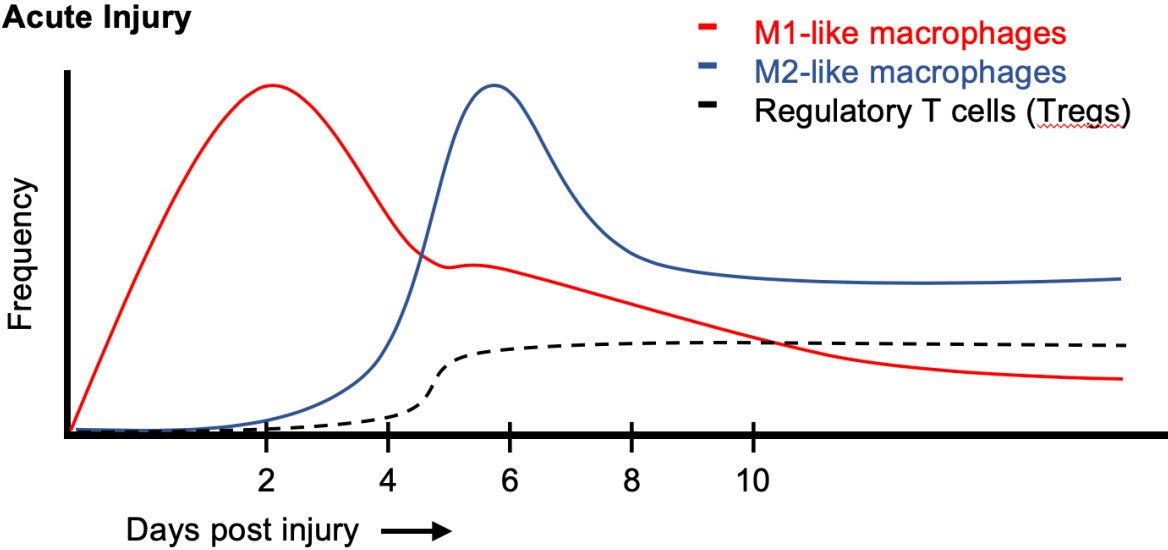


**Figure 1.2. Myogenic lineage progression.**

Following muscle injury quiescent satellite cells (Pax7+ and Myf5+/-) are activated and differentiate to myoblasts (Pax7+, Myf5+, and MyoD+). After several rounds of proliferation, myoblasts exit the cell cycle and become myocytes (Pax7-, MyoD+, myogenin+, and MRF4+). Myocytes can undergo a fusion process to form multinucleated myotubes (myogenin+, MRF4+, and MyHC+) that eventually mature into myofibers. The satellite stem cell subpopulation (Pax7+ and Myf5-) can also self-renew to replenish the satellite cell pool. Adapted from (Dumont et al., 2015).

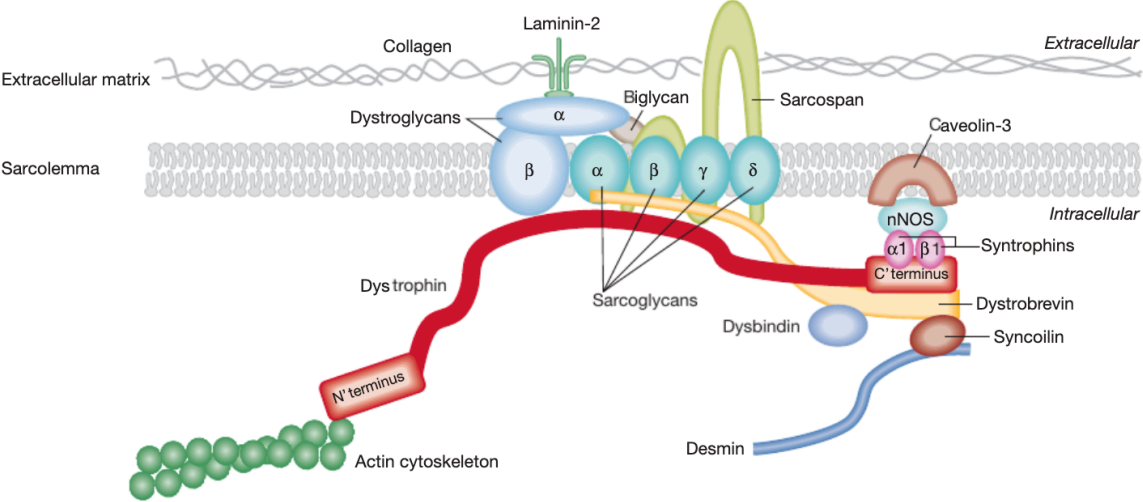


**Figure 1.3. Frequencies of immune cell populations in acutely injured muscle.** Postulated macrophage and Treg frequencies during acute muscle injury. Red, blue, and dashed black lines represent frequencies of M1-like macrophages, M2-like macrophages, and Tregs, respectively. Adapted from (Kastenschmidt et al., 2019b).

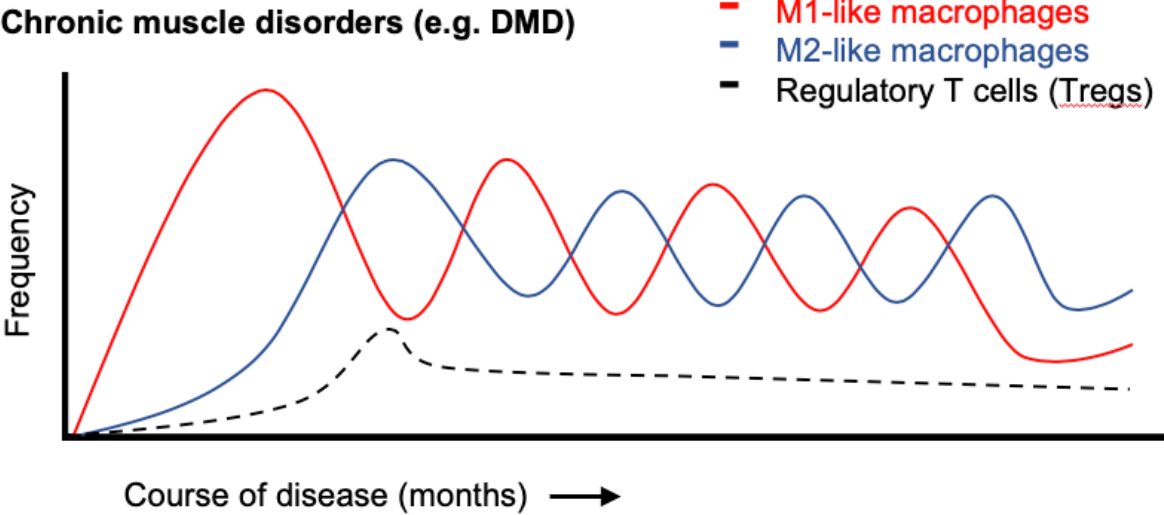


**Figure 1.4. The dystrophin–glycoprotein complex.**

Dystrophin interacts with other transmembrane proteins in the sarcolemma, serving as a bridge to connect the actin cytoskeleton and extracellular matrix. Incorporated from (Nowak and Davies, 2004).



**Figure 1.5. Frequencies of immune cell populations in dystrophic muscle.**  
Postulated macrophage and Treg frequencies during muscular dystrophy. Red, blue, and dashed black lines represent frequencies of M1-like macrophages, M2-like macrophages, and Tregs, respectively. Adapted from (Kastenschmidt et al., 2019b).







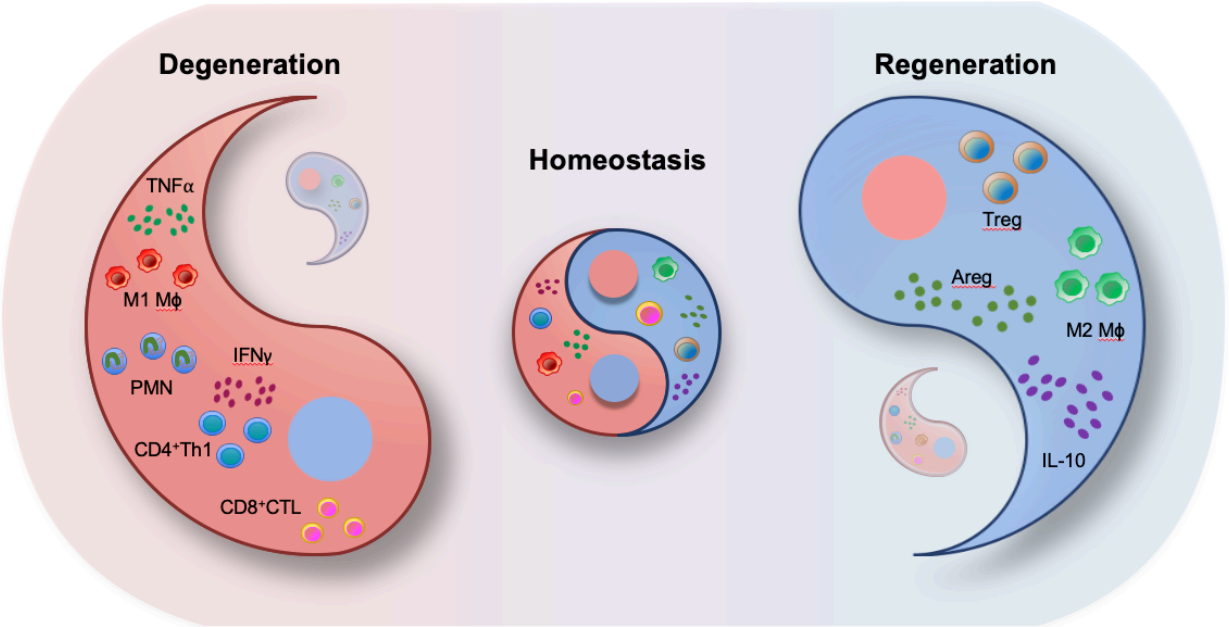






**Figure 1.6. The Ying-Yang function of degenerative and regenerative immune cells in muscular dystrophy.**

In healthy muscle degenerative and regenerative immune cell populations are balanced, maintaining homeostasis (center). During muscular dystrophy, shifts in this balance either promote degeneration (left) or regeneration (right). A degenerative type 1 inflammatory response is characterized by increased expression of pro-inflammatory cytokines such as  $\text{IFN}\gamma$  and  $\text{TNF}\alpha$  and the presence of polymorphonuclear neutrophils (PMN), M1-like macrophages (M1 M $\phi$ ),  $\text{CD4}^+$  Th1 cells, and  $\text{CD8}^+$  cytotoxic T lymphocytes (CTL). Regenerative responses are characterized by the presence of Tregs and M2-like macrophages (M2 M $\phi$ ) that express amphiregulin (Areg) and IL-10. Eosinophils are not depicted because they are suspected to play a role in degeneration and regeneration. Adapted from (Kastenschmidt et al., 2019b).



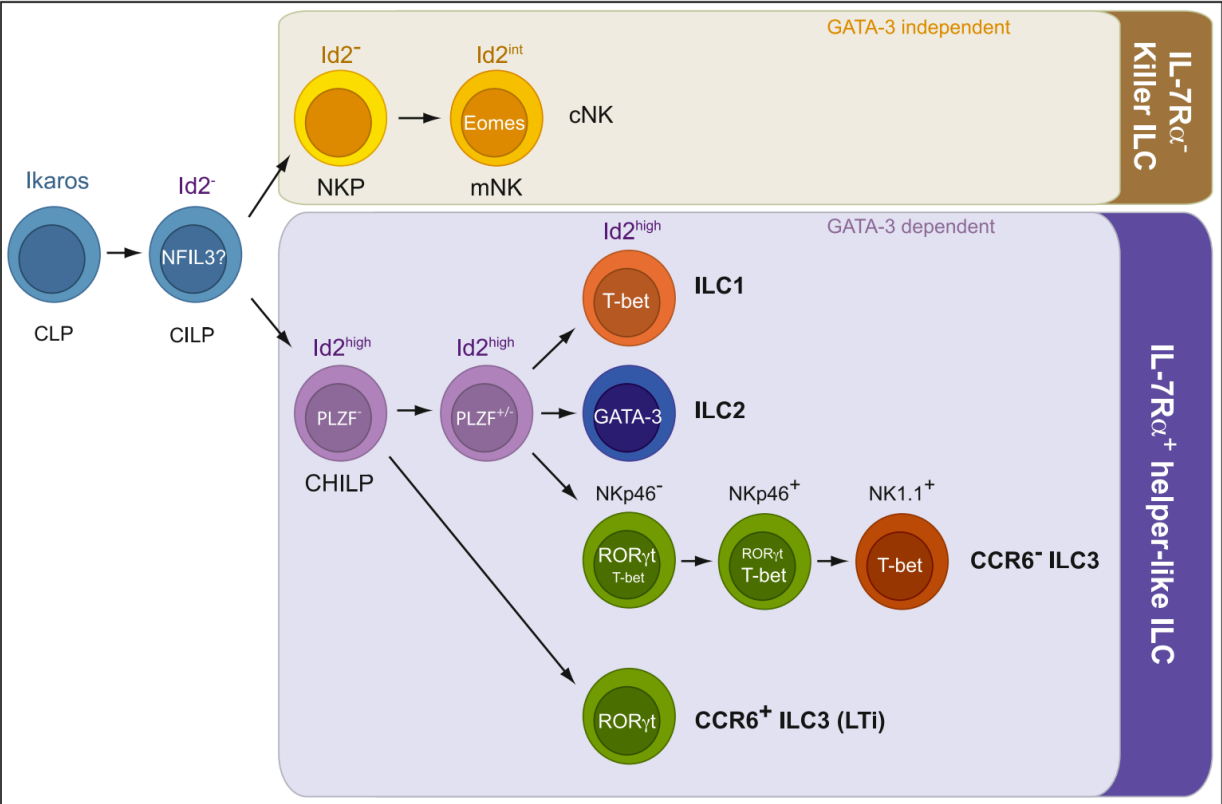
**Figure 1.7 Activation and functions of ILCs.**

The tissue signals that expand and activate ILC1s, ILC2s, and ILC3s, and the effector functions of ILCs, mirror the activation and functions of Tcells. In this figure ILC1s, ILC2s, and ILC3s could be replaced by T helper 1, T helper 2, and T helper 17 cells, respectively. Incorporated from (Forkel and Mjösberg, 2016).

ILC Group	Stimulation	Subtypes	Production	Function
<b>Group 1 ILC</b>  	IL-15 IL-12 IL-18	NK  CD127 <sup>-</sup> ILC1  CD127 <sup>+</sup> ILC1 	IFN $\gamma$ Perforin Granzymes   IFN $\gamma$	<b>Homeostasis</b> Anti-tumor immunity  Immune response to intracellular pathogens  <b>Pathogenesis</b> Intestinal inflammation
<b>Group 2 ILC</b>  	IL-33 IL-25 TSLP PGD <sub>2</sub> ICOSL TCR NKp30L TL1A	ILC2 	IL-13 IL-5 IL-4 IL-9 Amphiregulin	<b>Homeostasis</b> Helminth expulsion  Wound healing  <b>Pathogenesis</b> Allergy  Asthma
<b>Group 3 ILC</b>  	IL-23 IL-1 $\beta$ TL1A PGE <sub>2</sub> AHR ligand	LTi  NKp44 <sup>+</sup> ILC3  NKp44 <sup>-</sup> ILC3 	LT $\beta$ TNF $\alpha$ IL-17 IL-22  IL-22  IL-22 IL-17	<b>Homeostasis</b> Immune responses to extracellular pathogens and rotavirus  Intestinal barrier function  <b>Pathogenesis</b> Intestinal inflammation

**Figure 1.8. The lineage of ILCs.**

ILCs share a common progenitor with other lymphoid cells, the CLP. ID2 expression induce the differentiation of the CHILP that give rise to ILC1, ILC2, and ILC3s. CLP, common lymphoid progenitor; CILP, common ILC progenitor; CHILP, common helper-like ILC progenitor; NKP, cNK- restricted progenitor. Adapted from (Diefenbach et al., 2014).





## **CHAPTER 2**

### **QuantiMus: a machine learning-based approach for high precision analysis of skeletal muscle morphology**

Jenna M. Kastenschmidt, Kyle L. Ellefsen, Ali H. Manna, Jesse J. Giebel, Rayan Yahia, Rachel E. Ayer, Phillip Pham, Rodolfo Rios, Sylvia A. Vetrone, Tahseen Mozaffar, S. Armando Villalta. *Frontiers in Physiology* 2019.

## ABSTRACT

Skeletal muscle injury provokes a regenerative response, characterized by the *de novo* generation of myofibers that are distinguished by central nucleation and re-expression of developmentally-restricted genes. In addition to these characteristics, myofiber cross-sectional area (CSA) is widely used to evaluate muscle hypertrophic and regenerative responses. Here we introduce QuantiMus, a free software program that uses machine learning algorithms to quantify muscle morphology and molecular features with high precision and quick processing-time. The ability of QuantiMus to define and measure myofibers was compared to manual measurement or other automated software programs. QuantiMus rapidly and accurately defined total myofibers and measured CSA with comparable performance, but quantified the CSA of centrally-nucleated fibers (CNFs) with greater precision compared to other software. It additionally quantified the fluorescence intensity of individual myofibers of human and mouse muscle, which was used to assess the distribution of myofiber type, based on the myosin heavy chain isoform that was expressed. Furthermore, analysis of entire quadriceps cross-sections of healthy and mdx mice showed that dystrophic muscle had an increased frequency of Evans blue dye<sup>+</sup> injured myofibers. QuantiMus also revealed that the proportion of centrally-nucleated, regenerating myofibers that express embryonic myosin heavy chain (eMyHC) or neural cell adhesion molecule (NCAM) were increased in dystrophic mice. Our findings reveal that QuantiMus has several advantages over existing software. The unique self-learning capacity of the machine learning algorithms provides superior accuracy and the ability to rapidly interrogate the complete muscle section. These qualities increase rigor and reproducibility by avoiding methods that rely on the sampling of representative areas of a section. This is of particular importance for the analysis of dystrophic muscle given the 'patchy' distribution of muscle pathology. QuantiMus is an open source tool, allowing customization to meet investigator-specific needs and provides novel analytical approaches for quantifying muscle morphology.

## INTRODUCTION

Acute trauma, prolonged periods of mechanical unloading or genetic mutations can all independently cause skeletal muscle cell death, atrophy and changes in myofiber cross-sectional area (CSA). The resilience of skeletal muscle to overcome these environmental and genetic insults is partly attributed to its highly adaptive and regenerative capacity (Dumont et al., 2015). Although mechanical load influences myofiber CSA, muscle injury and regeneration provokes a larger variance in CSA because of the *de novo* formation of growing myofibers (McDonald et al., 2015; Torres and Duchon, 1987). In addition to their variance in CSA, developing myofibers express embryonic myosin heavy chain (eMyHC) and neural cell adhesion molecule (NCAM) during regeneration (Capkovic et al., 2008; Dubois et al., 1994; Dumont et al., 2015; Rochlin et al., 2010; Schiaffino et al., 1986; Tedesco et al., 2010). Thus, measuring the frequency or expression of regeneration markers and CSA is frequently used to quantitatively assess muscle regeneration (Capkovic et al., 2008; Charlton et al., 2000; Covault and Sanes, 1985; Dubach-Powell, 2011; Dubois et al., 1994; Illa et al., 1992; Schiaffino et al., 1986).

The manual quantification of myofiber type, CSA and centrally-nucleated fibers (CNF) by histological methods is time-consuming and prone to user bias, negatively affecting the quality of data. Further, quantifying protein expression by microscopy methods is difficult because several factors (sensitivity and dynamic range of the imaging system; specificity of the antibodies; technical anomalies; inappropriately performing image post-processing prior to image analysis) can comprise the proportional relationship between protein expression and fluorescence intensity. Recently, multiple groups have successfully developed software that address the above limitations for the semi-automated, morphometric analysis of healthy skeletal muscle. For example, the Semi-automatic Muscle Analysis using Segmentation of Histology (SMASH) method was developed as an open source MATLAB application that measures myofiber properties such as size (CSA and minimum Feret diameter), CNFs and myofiber type in immunofluorescence-labeled images (Smith and Barton, 2014). More recently, MyoVision was developed to evaluate

CSA, myofiber type and myonuclear number (Wen et al., 2017). Although MyoVision does not have the function to quantify CNFs, the software expands the automated potential of these aforementioned histological analyses by using algorithms that decrease the amount of user supervision.

Current software packages reliably assess the morphology of healthy muscle, in which morphometric features are uniform. However, the performance of a subset of these packages has not been validated in more complex model systems that vary greatly in morphology. Accurate assessment of diseased muscle (e.g. dystrophic muscle of the mdx mouse model of Duchenne muscular dystrophy (DMD)) is challenged by muscle necrosis and inflammation, and constant tissue remodeling that contributes to large variance in myofiber size and increased interstitial tissue (McDonald et al., 2015; Torres and Duchon, 1987). We found that these complex disease features hinder the ability of existing software from discerning a true myofiber from artifact. To circumvent this limitation, we developed QuantiMus, a machine learning-based tool that uses a support vector machine (SVM) algorithm (Artan, 2011) to define myofibers with high fidelity. QuantiMus can be downloaded at <https://quantimus.github.io>. QuantiMus was developed as a plugin for the software program Flika (Ellefsen et al., 2014) which can be downloaded at <https://flika-org.github.io>.

QuantiMus integrates the analytical features of previous morphometric software programs, such as measurement of CSA and CNFs (Smith and Barton, 2014; Wen et al., 2017), with the capability to measure myofiber fluorescence intensity. Together, these features provide a single tool to simultaneously quantify fluorescence intensity, CNFs and CSA, and the use of machine learning algorithms reduces processing time and computing power. We compared the performance of QuantiMus to other semi-automated methods and validated that this tool accurately determined myofiber CSA and CNFs in healthy and diseased skeletal muscle. QuantiMus rapidly determined the proportion of type I and II myofibers in healthy mouse and human skeletal muscle, and the CSA of each myofiber type. QuantiMus also quantified the

frequency of Evans blue dye (EBD), NCAM or eMyHC positive myofibers in dystrophic muscle, and measured their fluorescence intensity. Collectively, we demonstrate the utility of QuantiMus as a tool for the rapid and rigorous quantification of multiple molecular and morphological features of skeletal muscle during homeostasis and disease.

## **MATERIALS**

### **Ethical approval**

Deidentified frozen, muscle cross-sections from archived human muscle biopsies were provided by UCI pathology laboratory, and their identity remained confidential throughout the study. Prior to biopsy collection, participants were informed about the requirements and potential risks of the procedures before providing their written informed consent. Biopsies were collected from patients because a suspected inflammatory myopathy, which after pathological assessment revealed no skeletal muscle involvement. The experimental procedures adhered to the standards in the latest revision of the *Declaration of Helsinki* and were approved by the Institutional Review Board at the University of California, Irvine (HS#2016-3191).

### **Animal models**

In compliance with federal regulations, the use of mice in our study was approved by the University of California Irvine Institutional Animal Care and Use Committee. Mice were housed in a temperature-controlled facility under a standard 12 hour light-12 hour dark cycle with food and water provided *ad libitum*. C57BL/10 wildtype and C57BL/10ScSn-Dmd<sup>mdx</sup>/J (mdx) mice were originally obtained from Jackson laboratory (Bar Harbour, ME) and breeding colonies were maintained in-house. Mice were euthanized at 4 weeks of age with carbon dioxide using a gradual fill method per American Veterinary Medical Association guidelines, followed by cervical dislocation. For Evans blue dye (EBD) injected mice, animals were interperitoneally injected with a 1% EBD solution at a dose of 50 mg/kg, 16 hours before euthanasia.

## **Mouse tissue preparation**

Quadriceps were isolated from 4-wk-old WT and mdx mice. Quadriceps were embedded in optimal cutting temperature (O.C.T) compound (Sakaura Fine Tech, 25608-930), frozen in liquid nitrogen-cooled isopentane for 1 minute and stored at -80°C. Eight-micron cross-sections were prepared on a Leica CM1950 cryostat, mounted on positively-charged microscope slides and stored at -80°C until the time of staining. Although most section thicknesses can be accommodated, we choose 8  $\mu\text{m}$  as the optimal thickness for image quantification in this study; sections below 8  $\mu\text{m}$  resulted in a larger occurrence of gaps in laminin labeling, whereas sections greater than 8  $\mu\text{m}$  yielded artifactual laminin labeling that obscured the myofiber perimeter.

## **Immunofluorescence labeling and imaging**

All immunofluorescent labeling procedures were performed with routine and validated protocols (Capkovic et al., 2008; Illa et al., 1992; Schiaffino et al., 1986; Wen et al., 2017). Sections were all labeled on the same day to eliminate inter-experimental variation. Images were acquired in a manner to ensure that fluorescence signals were not saturated, and specificity of the stain was ensured by comparison to control sections in which the primary antibody was omitted. Fluorescently-labeled sections were protected from light through the staining procedure and image acquisition. Further the measurement of fluorescence intensity was done on unaltered images (i.e. native brightness and contrast settings were never manipulated). A RGB image was converted to its single channel components and saved as an 8-bit TIFF file for compatibility with the QuantiMus pipeline.

*Myofiber Regeneration and laminin:* to quantify the frequency and CSA of regenerating myofibers, frozen cross-sections of mouse quadriceps were labeled with anti-laminin, anti-NCAM and anti-eMyHC antibodies (Table 2.1). Briefly, cross-sections were fixed with 2%

paraformaldehyde for 5 minutes and endogenous biotin was blocked with an avidin/biotin blocking kit (Vector Laboratories, SP-2001) per manufacturer instructions. Following washes with 1X PBS, endogenous mouse IgG was blocked with Mouse-on-Mouse blocking reagent (Vector laboratories, MKB-2213) for 1 hour at RT. Muscle sections were washed in 1X PBS and incubated for 5 min at RT in blocking buffer comprised of 1X Tris-buffered saline with 2.5% normal donkey serum. Primary antibodies against laminin, NCAM and eMyHC were diluted in blocking buffer at concentrations described in Table 2.1 and were incubated with sections for 1 hour at RT. Primary antibodies were detected by indirect immunofluorescence staining with Alexa 488- and Alexa 647-conjugated secondary antibodies (**Table 2.1**) for 1 hour at RT, protected from light. For the detection of eMyHC labeling, sections were incubated with biotinylated anti-mouse antibodies for 10 min followed by staining with Alexa 594-conjugated streptavidin for 5 minutes. Sections were counter-stained with 4',6-Diamidino-2-Phenylindole, Dihydrochloride (DAPI, Sigma, 10236276001, 1.2 nM in 1X PBS) for 10 minutes to visualize nuclei. For the staining of laminin in human muscle, sections were fixed as described above, and were blocked with 5% normal donkey serum, 3% BSA and 0.05% Tween-20 in 1X Tris-buffered saline for 1 hour. Blocking solution was removed and sections were stained with anti-laminin antibody for 1 hour at RT. Sections were washed and stained with secondary antibodies and DAPI as described above.

*Myofiber typing:* The immunofluorescent detection of myofiber expression of myosin heavy chain isoforms was performed as previously described (Wen et al., 2017). Briefly, mouse quadriceps cross-sections were air-dried for 10 minutes, rehydrated with 1X PBS and were blocked with Mouse-On-Mouse blocking reagent (Vector laboratories, MKB-2213) for 1 hour at RT. Cross-sections were stained with type 1, IIa, IIb MyHC-specific antibodies and anti-laminin (**Table 2.1**) for 1.5 hours. For human samples, antibodies against myofiber type IIx were used instead of type IIb (**Table 2.1**). To detect myofiber types and laminin, sections were stained with secondary antibodies Dylight 405 goat anti-mouse IgG2b, Cy2 goat anti-mouse IgG1, Dylight 594 goat anti-mouse IgM and anti-rabbit Alexa 647 (**Table 2.1**) to detect type I, IIa, IIb/x MyHC and

laminin staining, respectively. Sections were washed with 1X PBS and mounted for imaging. All tissue sections were imaged with a Keyence BZ-X700 inverted fluorescence microscope with a 10x (human) or 20x (mouse) objective and were stitched using BZ-X Analyzer software (Keyence).

### **FIJI analysis**

To define muscle myofibers, images of laminin-stained cross-sections were first imported into FIJI and converted to binary images using the 'make binary' function. The FIJI 'wand tool' (Legacy mode, Tolerance= 0) was used to define the edge of operator-selected myofibers. The area ( $\mu\text{m}^2$ ) and minimum Feret diameter ( $\mu\text{m}$ ) of these operator-selected myofibers were measured using the FIJI 'measure' function. To manually define CNFs, DAPI-stained images were binarized and overlaid onto corresponding binarized images of laminin-stained sections. Operators used the FIJI 'wand tool' (Legacy mode, Tolerance= 0) to manually select CNFs. The CSA of CNFs was measured using the FIJI 'measure' function.

### **SMASH Analysis**

Because SMASH (Version 5) requires RGB files for analysis, we used FIJI to convert acquired 8-bit greyscale images to a RGB format. As previously described (Smith and Barton, 2014), the detection of myofibers and CNFs using SMASH was performed using the following parameters: pixel size ( $\mu\text{m}/\text{pixel}$ )= 1.216 (mouse) or 1.780 (human); segmentation filter= 8 (mouse) or 25 (human); minimum fiber area= 12 (mouse) or 1000  $\mu\text{m}^2$  (human); maximum fiber area= 5000 (mouse) or 20000  $\mu\text{m}^2$  (human). For the determination of CNFs the following settings were used: distance from edge= 1.5  $\mu\text{m}$ ; nuclear size= 5  $\mu\text{m}^2$ ; nuclear smoothing= 5.

### **MyoVision Analysis**



Images of laminin-stained sections were analyzed using MyoVision Basic (Version 1) as previously described (Wen et al., 2017). Various settings were tested, and the optimal following values were used: Min Area= 10, Maximum Area= 5000 (mouse) or 50000 (human), Pixel/ $\mu\text{m}$ = 1. Myofiber size was manually converted to  $\mu\text{m}$  after export.

### **Determination of accuracy and variance**

As previously described, accuracy for the number of defined myofibers, average CSA and number of CNFs was determined by Eq. 1, where test software is defined as QuantiMus, MyoVision or SMASH and manual measurement are values obtained by FIJI analysis (Wen et al., 2017).

$$\text{Eq. 1: Accuracy} = \left(1 - \frac{|\text{Test Software Value} - \text{Manual Measurement}|}{\text{Manual Measurement}}\right) \times 100\%$$

Coefficient of variation (CV) is defined by Eq. 2.

$$\text{Eq. 2: CV} = \left(\frac{\text{Standard Deviation}}{\text{Average}}\right) \times 100$$

Data are expressed as the average  $\pm$  standard error of the mean (SEM) or individual replicate values where indicated.

### **Statistics**

All statistical analyses were performed using GraphPad Prism Version 7.0 (GraphPad Software, Inc.). A two-way repeated measures ANOVA with a multiple comparison test (main column effect) was performed for fiber counting, CNF detection and CSA accuracy measurements. A paired two-tailed t-test was performed for the analysis of the accuracy of CNF

number and average area of CNFs. Statistical analysis for comparisons of WT and mdx measurements was performed using an unpaired two-tailed t-test with Welch's correction.

## **METHODS**

### **Overview of the QuantiMus pipeline**

The QuantiMus analysis pipeline is composed of 5 steps. Laminin-stained images of muscle cross-sections are first imported into the QuantiMus software. The 'Fill Myofiber Gaps' function (**Figure 2.1**, Step 1) ensures accurate boundary definition by filling-in discontinuous regions of the laminin stain, which is used to define the myofiber perimeter and generate a binary image used in the myofiber detection function. The 'Myofiber Detection' function accurately classifies regions of interest (ROI) as myofibers (**Figure 2.1**, Step 2), generating a classified image used in downstream functions. The 'Centrally-Nucleated Fibers' function (**Figure 2.1**, Step 3) defines myofibers with centrally-located nuclei by overlaying binarized images of laminin-corresponding DAPI-stained images onto the classified image. The 'Measure Fluorescence' function of the QuantiMus pipeline (**Figure 2.1**, Step 4) allows users to measure myofiber fluorescence intensity emanating from immunofluorescence-labeled proteins. The 'Save and Export Data' function is used to export processed data as an Excel sheet for further analysis and statistical testing (**Figure 2.1**, Step 5).

### **Segmentation of Myofibers**

Image segmentation assists the automation of image analysis by partitioning pixels of similar characteristics to define the boundary of an object (Liu and Structures, 2009; Zaitoun and Aqel, 2015). However, structural deformities in the tissue or technical artifacts in the staining procedure that result in discontinuous boundaries, prevents current segmentation methods to accurately determine the myofiber perimeter (Kostrominova et al., 2013). To circumvent this

limitation, we developed an algorithm to fill discontinuous myofiber boundaries (i.e. 'gaps') by coupling thresholding techniques with novel methods we developed and describe below.

The 'Fill Myofiber Gaps' function is executed within the 'Fill Myofiber Gaps' tab of the QuantiMus user interface (**Figure 2.2A**). TIFF images of laminin-stained sections (**Figure 2.2B,C**) are first imported and the user defines the myofiber boundary by manipulating the 'Blue Threshold' and 'White Threshold' sliders within the 'Fill Myofiber Gaps' tab, such that the blue indicates the thickest possible boundary and white indicates the thinnest (**Figure 2.2A,D**). These slider settings are used to generate an evenly spaced list of thresholding values that are sequentially applied to the original image to form a series of binary images. Contiguous pixels from the binary image resulting from the lowest threshold value are grouped together into regions that become seeds for segmented regions. Each region of pixels is compared to the corresponding region from the binary image generated with the next higher threshold value. If the area of a respective region exceeds a defined size and increases by more than 20%, the region is considered to have exceeded the boundaries of the candidate myofiber and is erroneously 'expanded'. In this case, a 'white filler' (**Figure 2.2E**, yellow arrows) is inserted at the intersection of the original and 'expanded' regions. These two steps – evaluating increases in candidate myofiber area and building borders when the increase is too large – are repeated for every region in each binary image of the series. Contiguous regions of pixels remaining at the end of this process are considered segmented regions and are fed into the next step of the QuantiMus pipeline. Binarization alone fails to resolve gaps within the myofiber perimeter, leading to the misclassification of adjacent myofibers as one combined region. An example of this is illustrated in Figure 2F, where each colored region demonstrates the incorrect clustering of multiple fibers. The 'Fill Myofiber Gaps' methodology fills in breaks within the myofiber boundary to generate a binarized image (**Figure 2.2G**) with 'corrected' myofiber detection. Although breaks in non-myofiber regions may also be filled in, these erroneously segmented regions are not classified as true myofibers during the "define myofibers" step (**Figure 1**, Step 3).

## Binary classification of myofibers and interstitial space

The 'Fill Myofiber Gaps' function yields a binary segmented image that contains contiguous regions of pixels that are converted to unique regions of interest (ROIs) in the 'Define Myofibers' tab (**Figure 2.3A**). We used a machine learning algorithm, a support vector machine (SVM), to accurately classify ROIs as myofibers. Initially, binary images are selected (**Figure 2.3B**) in the 'Define Myofibers' tab, and the user manually classifies ROIs into two categories. As shown in Figure 2.3C, user-selected green ROIs are categorized as myofibers, whereas, red ROIs are categorized as non-myofiber features (i.e. interstitial space or artifact). Four properties are determined for each ROI using functions from the open source scikit-image toolbox: area, eccentricity, convexity, circularity (Van Der Walt et al., 2014). Area is defined as the number of pixels within each ROI (**Figure 2.3D**, grey area). Eccentricity describes the ellipticity of a region and is defined as the focal distance (**Figure 2.3E**, green line) divided by the major axis length (**Figure 3E**, red line). Convexity is defined as the ratio between the area (**Figure 2.3F**, hatched area) and the convex area of a region (**Figure 2.3F**, blue area) which is the area of the smallest convex polygon that encloses the region. Circularity (**Figure 2.3G**) describes the roundness of a region and is calculated as in Eq. 3.

$$\text{Eq. 3: Circularity} = \frac{4\pi \cdot \text{Area}}{\text{Perimeter}^2}$$

These properties are then used to train a SVM with a radial bias function as the kernel, which is implemented from the open source scikit-learn library for machine learning in Python (Pedregosa et al., 2012). The trained SVM can then be applied to classify ROIs of the remaining image (**Figure 2.3H**). Training data can also be saved and later used to classify ROIs in binarized images of multiple muscle samples, reducing analysis time. Furthermore, the 'Correction Filter' feature

within the 'Define Myofibers' tab provides a degree of flexibility that allows users to remove incorrectly classified myofibers (**Figure 2.3A**).

### Defining CNFs

In the 'CNF' tab of QuantiMus (**Figure 2.4A**), a classified image from the 'Myofiber Detection' function (**Figure 2.4B**) is selected and a corresponding binarized DAPI-stained image of the same area (**Figure 2.4C**) is overlaid (**Figure 2.4D**). Using functions from the scikit-image toolbox (Van Der Walt et al., 2014), the area of myofibers (green ROIs) are eroded (**Figure 2.4E**, yellow regions) to exclude peripheral nuclei during the classification of CNFs. The degree of erosion is determined by a user-defined value from 0-99, where 99 is equal to approximately 99 percent myofiber erosion; 80 is used as the default (**Figure 2.4A**). If there is colocalization of the eroded myofiber ROI (**Figure 2.4E**, yellow regions) and DAPI signal, then a myofiber is classified as centrally nucleated. CNFs are then recolored to purple (**Figure 2.4F**) and myofiber CNF status is saved for later data export.

### Measuring myofiber fluorescence

The 'Measure Fluorescence' function, selected in the 'Measure Fluorescence' tab (**Figure 2.5A**), was used to measure the frequency of regenerating myofibers based on their expression of eMyHC, a marker of regeneration (Schiaffino et al., 1986). Classified images (**Figure 2.5B**) are superimposed with fluorescently-labeled eMyHC images (**Figure 2.5C**) to yield an overlay (**Figure 2.5D**). Scikit-image functions are used to measure the NCAM and eMyHC mean fluorescence intensity (MFI), defined as the average fluorescence intensity of all pixels within a given myofiber (Van Der Walt et al., 2014). The 'Determine Positive Fibers' feature (**Figure 2.5A**), is used to manually select a subset of myofibers in the overlay image (**Figure 2.5D**) with the lowest positive fluorescence signal (**Figure 2.5E**, yellow myofibers). These user-defined positive myofibers serve as a threshold to classify eMyHC positive myofibers in the entire cross-section; myofibers with an

MFI equal to or greater than the threshold value are considered positive. After the algorithm completes the classification, positive myofibers are relabeled blue (**Figure 2.5F**). The MFI of all myofibers and the classification status (i.e. positive or not) is then saved for downstream analysis and data export.

### **Data Export**

All measurements generated in earlier steps are saved for final data export. When applicable, the pixel/micron ratio is entered in the 'Print Data' tab of QuantiMus (**Figure 2.6A**). It is important to note that when analyzing stitched images, pixel/micron ratios are distinct for each image and should be recorded during acquisition. In the BZ-X Analyzer software (Keyence) used to acquire images in this study, this value is found in the pop-up window that is displayed when inserting a scale bar. Alternatively, the 'Set Scale' function in FIJI can be used to determine the pixel/micron ratio for images that contain scale bars inserted during acquisition. ROI number, myofiber area ( $\mu\text{m}^2$ ), minimum Feret diameter ( $\mu\text{m}$ ), CNF classification, MFI and regenerating myofiber classification are exported as an Excel (XLS) file by clicking on 'Print Data'.

## **RESULTS**

### **Image processing time using multiple methods**

Assessing morphometric features of entire muscle cross-sections removes potential biases inherent to random-sampling techniques and is recommended by the TREAT-NMD (Nagaraju and Willmann, 2009). The manual assessment of an entire muscle cross-section is time consuming, and the requirement for high computational processing power by some analysis software makes these tools inaccessible to some users (Kostrominova et al., 2013; Wen et al., 2017). QuantiMus was developed for the accurate evaluation of entire muscle cross-sections without requiring large computational resources. A laptop computer containing 12.0 gigabytes of random access memory and a 2.50 gigahertz central processing unit (i7-6500U) was used to

evaluate the processing time of an entire muscle cross-section using FIJI, SMASH, MyoVision or QuantiMus. 108 .TIFF images of 4-week-old mdx mouse quadriceps taken with a 20x objective (1920x1440 pixels each) were stitched together with BZ-X Analyzer software to reconstruct the entire muscle cross-section. Our analysis showed that SMASH and QuantiMus had similar processing times, but QuantiMus classified myofibers and measured size with higher precision (**Table 2.2**). Using TIFF images, MyoVision was unable to complete image segmentation and myofiber measurement within a four-hour analysis time; this software could not process the image beyond the “Separated Seeds Step 10” step. It is important to note that MyoVision was able to process a lower resolution .PNG image of a full cross-section, however this analysis resulted in inaccurate myofiber detection and CSA measurements (Data not shown). Together our analysis shows QuantiMus’ ability to rapidly assess morphology in a high content image of an entire muscle section

### **Accuracy of myofiber classification and CSA measurement**

We next tested the accuracy of QuantiMus in classifying myofibers and measuring CSA. QuantiMus was compared to SMASH, MyoVision and manual detection with FIJI, which was used to establish the ground truth. Due to the inability of MyoVision to completely process a stitched .TIFF image of the entire muscle cross-section, we used a single image of a representative field taken at 20x for further analysis. We found that all methods were accurate and detected a similar number of myofibers, although MyoVision overestimated the number of myofibers in WT mice (**Figure 2.7A,B**). We also found that QuantiMus, MyoVision and FIJI performed with similar accuracy when measuring the average myofiber CSA in WT mice, but was overestimated by SMASH (**Figure 2.7C,D**). This observation is likely due to SMASH’s method of image segmentation where measured myofibers include some of the extracellular region leading to larger CSAs for each fiber (Smith and Barton, 2014). In mdx quadriceps, our analysis showed that the average size of myofibers defined by QuantiMus was similar to those measured with FIJI,

but MyoVision grossly underestimated myofiber CSA (**Figure 2.7C**). We anticipate this finding to be a result of more ROIs of smaller size being inappropriately classified as true myofibers. As a result of over and underestimated CSA measurements, MyoVision and SMASH accuracies are variably influenced by different muscle conditions (i.e. healthy versus diseased muscle, **Figure 2.7D**). Taken together, although each program detected a similar number of myofibers, QuantiMus most accurately measured area across different muscle conditions.

We also assessed the ability of QuantiMus to accurately detect myofibers and measure myofiber CSA in de-identified tissue sections of archived human skeletal muscle. Biopsies were collected from patients with a suspected inflammatory myopathy, which after pathological assessment revealed no skeletal muscle involvement. We found that QuantiMus detected a similar number of myofibers compared to FIJI (**Figure 2.7E**) and was more accurate than MyoVision (**Figure 2.7F**), which detected fewer fibers (**Figure 2.7E**). We also evaluated CSA in cross-sections of human muscle. Although QuantiMus measured a similar average CSA compared to manual measurement using FIJI, SMASH and MyoVision measured an artificially larger CSA, thus reducing their accuracy (**Figure 2.7G,H**). Collectively, these results validate QuantiMus as an accurate and reliable tool for the rapid and accurate assessment of CSA in mouse and human skeletal muscle.

### **Accuracy of CNF classification and CSA**

We also compared the ability of QuantiMus and SMASH to accurately determine and measure CNFs. MyoVision was not included in the comparison, as this analytical feature is not available in its current version. All methods measured CNF number in 4-week-old mdx quadriceps with similar accuracy (**Figure 2.8A,B**). We next determined the lower threshold of CNF size detection. Our analysis showed that the lowest CSA determined by FIJI and QuantiMus was on average  $51.16 \pm 8.61$  and  $50.32 \pm 7.47 \mu\text{m}^2$ , respectively. SMASH was unable to define CNFs smaller than on average  $258.09 \pm 22.48 \mu\text{m}^2$ , likely explaining the overestimation of CSA (**Figure**



**2.8C**). Furthermore, this overestimation of CNF CSA by SMASH resulted in decreased accuracy (**Figure 2.8D**). The lower threshold of detection for CNF size led QuantiMus to reliably measure the CSA of CNFs (**Figure 2.8D**).

### **Myofiber Typing of full muscle cross-sections**

Skeletal muscle is composed of multiple myofiber types that differ in their metabolic profiles and contractile properties, and can be classified based on their expression of specific myosin heavy chain isoforms. We tested the ability of QuantiMus to assess the myofiber expression and distribution of specific myosin heavy chain isoforms to define the proportion of type I, IIa, IIb, and IIx myofibers in entire cross-sections of WT mouse quadriceps (**Figure 2.9A**). As previously shown (Rederstorff et al., 2011), this analysis revealed that the majority of myofibers in quadriceps are type IIb fibers (70.3%), followed by type IIx (19.7%), type IIa (6.0%) and type I (1.1%) (**Figure 2.9B**). A small proportion of 'Hybrid' myofibers that express more than one myosin heavy chain isoform were also detected (**Figure 2.9B**) (Matsuura et al., 2007). The quantification of myofiber type-specific CSA revealed that Type IIb are the largest in mouse quadriceps (**Figure 2.9C**). The accumulation of endogenous IgG in injured myofibers, despite blocking with commercially available mouse-on-mouse blocking reagents, precluded the ability to accurately type myofibers in mdx mice (data not shown). We also tested the ability of this tool to perform myofiber typing of various human muscles (**Figure 2.9D**). Our analysis showed the majority of myofibers in an entire muscle cross-section of biceps brachii from patient 1 were type I fibers (49.9%) followed by type IIa (22.4%) and IIx (18.2%) fibers (**Figure 2.9E**). The gastrocnemius of the second patient was primarily comprised of type I fibers (34.5%) followed by type IIx (31.2%) and IIa (28.1%) fibers (**Figure 2.9F**). Additionally, hybrid myofibers that expressed more than one myosin heavy chain isoform were also detected (**Figure 2.9E,F**). The average CSA of each myofiber type was also measured in the biceps (**Figure 2.9G**) and gastrocnemius (**Figure 2.9H**). Together, this analysis shows the capacity of QuantiMus to measure myofiber type distribution

and their myofiber type-specific CSA in entire skeletal muscle cross-sections of mouse and human.

### **Morphometric analysis of dystrophic muscle using QuantiMus**

We also evaluated the ability of QuantiMus to assess the morphological features of dystrophic muscle, which contains more complex structural features (i.e. injured myofibers, varying myofiber size, increased interstitial space). Evaluating myofiber injury provides a histological index of the severity of muscular dystrophy and is routinely evaluated by measuring the accumulation of Evans blue dye (EBD) in injured myofibers (Hamer et al., 2002; Straub et al., 1997). We tested the ability of QuantiMus to measure muscle injury in EBD-injected WT and mdx mice by assessing the frequency of EBD positive fibers and their fluorescence intensity within the entire quadriceps cross-section. As shown previously (Straub et al., 1997), these studies revealed an increased proportion of injured fibers in mdx muscle compared to healthy controls (**Figure 2.10A**). Furthermore, we measured the EBD fluorescence intensity of individual myofibers with the 'Measure Fluorescence' function. Notably, we found a broad range in the fluorescence intensity of EBD+ myofibers, which was absent in WT muscle (**Figure 2.10B**, inset).

QuantiMus was also used to histologically assess regeneration in healthy and dystrophic mouse muscle (**Figure 2.10C**). Using CNFs as an indicator of regeneration, we found the proportion of regenerating myofibers was elevated in mdx quadriceps and nearly absent in WT controls (**Figure 2.10D**) (McDonald et al., 2015; Torres and Duchon, 1987). Nascent myotubes and regenerating myofibers can also be distinguished by their expression of developmental genes like eMyHC (DiMario et al., 1991) or NCAM (Capkovic et al., 2008). We, therefore, used QuantiMus to quantify the frequency of eMyHC<sup>+</sup> and NCAM<sup>+</sup> regenerating myofibers. Our analysis showed that the proportion of both eMyHC<sup>+</sup> and NCAM<sup>+</sup> myofibers was elevated in dystrophic muscle (**Figure 2.10E,F**), consistent with the increased proportion of CNFs. Moreover, the individual myofiber MFI of eMyHC and NCAM was higher in mdx mice compared to WT,

suggesting a relative increased expression of these markers in mdx quadriceps (**Figure 2.10G,H**). The use of mean or median fluorescence intensity as an indirect measure of protein expression is a common technique used in variety of semi-quantitative and quantitative platforms to report relative changes in protein or gene expression (Banks et al., 2014; Cirak et al., 2012; Gonçalves et al., 2011; Guirado et al., 2018; Guiraud et al., 2019; McCabe et al., 2005; Omairi et al., 2017; Van Battum et al., 2014). We next evaluated the relationship between CSA and eMyHC (**Figure 2.10I,J**) or NCAM (**Figure 2.10K,L**) MFI and found no correlation in WT mice (**Figure 2.10I,K**). However, eMyHC and NCAM MFI and CSA were negatively correlated in mdx mice, with the smallest myofibers having the highest MFI for these markers (**Figure 2.10J,L**). We also noted that there was a larger proportion of large NCAM<sup>+</sup> myofibers (>1000  $\mu\text{m}^2$ ) that did not express eMyHC (**compare Figure 2.10L-J**), suggesting that the loss of eMyHC precedes the loss of NCAM as regenerating myofiber differentiate and grow. This observation also likely accounts for the increased proportion of NCAM<sup>+</sup> myofibers compared to eMyHC<sup>+</sup> myofibers in mdx mice (**compare Figure 2.10F to 2.10E**). The ability of QuantiMus to simultaneously measure CSA and MFI provided a novel analytic approach using linear regression analysis to quantify small myofibers expressing high levels of NCAM or eMyHC in regenerating muscle (**Figure 2.10I-L**).

## DISCUSSION

The histomorphological and molecular assessment of injured or diseased skeletal muscle historically required time-consuming, manual methods. More recently, the histological evaluation of muscle tissue has been significantly accelerated by the development of semi-automated tools (Kostrominova et al., 2013; Reyes-Fernandez et al., 2019; Smith and Barton, 2014; Wen et al., 2017). These methods are able to successfully measure uniform myofibers of healthy muscle. However, these methods are not readily adaptable to the highly variable terrain of diseased muscle. Here we introduce QuantiMus, a machine learning-based software that addresses this and accelerates the histological evaluation of skeletal muscle. Benchmark comparisons validate

this tool for the high-throughput and semi-automated determination of CSA, CNFs, fluorescence intensity and myofiber type of entire skeletal muscle cross-sections.

The implementation of unique segmentation and SVM-based classification algorithms advances current morphometric methods by enhancing the ability to define individual myofibers and assess muscle pathology of entire muscle cross-sections. SVMs have been previously utilized to segment images (Wang et al., 2012, 2011) and classify objects (Adamiak et al., 2016) by using descriptors in a trained image as inputs for its supervised learning methods (Nayak et al., 2015). In the histological assessment of skeletal muscle, the SVM generates a complex nonlinear decision boundary between myofibers and other structural features, thereby removing the reliance on rigid user-defined parameters used by other methods that may lead to ROI misclassification. The novel development and implementation of the 'Fill Myofiber Gaps' function also enhances accurate myofiber classification by 'filling' artifactual gaps in the laminin-stained image used to define the myofiber perimeter. A binarized image with more precise boundaries is generated, consequently increasing the SVM's ability to accurately classify ROIs as myofibers. An additional layer of accuracy has been added by implementing a semi-automated "Correction Filter" and a point-and-click user interface that allows investigators to manually change ROI status. These features allow the removal of myofibers at the edge of the muscle cross-section or in areas with poor sectional integrity. Further, the point-and-click feature allows the addition of true myofibers that were missed during classification. Together these features integrate to form an accurate and user-friendly method for segmenting skeletal muscle images and classifying myofibers for downstream analysis.

We also implemented a novel myofiber eroding feature that facilitates the accurate classification of regenerating, CNFs ranging widely in size. We used an open-source algorithm (Pedregosa et al., 2012) to erode each myofiber by a percent area that scales with changing CSA size. In contrast, the use of hard-set parameters prevents the accurate discernment of small CNFs. As a result, SMASH failed to detect CNFs smaller than  $258.09 \pm 22.48 \mu\text{m}^2$ , which are

prevalent in regenerating regions of dystrophic muscle (Torres and Duchen, 1987). We attributed the increased CNF detection accuracy of QuantiMus to the erosion method, which is not adversely affected by heterogeneous myofiber populations. Currently, the difficulty to resolve single nuclei in areas of high cellular density and overlapping nuclei limit our tool to detecting centrally-located nuclei. These limitations especially arise in settings of muscle inflammation, where infiltrating immune cells juxtaposed with myofibers make it difficult to discern infiltrating nuclei from peripheral myofiber nuclei. However, the ability to quantify peripheral nuclei in healthy muscle that lack densely compacted nuclei has been successfully performed (Wen et al., 2017).

We coupled machine learning-based classification and fluorescence intensity measurement methods to evaluate muscle function by simultaneously assessing the morphology and molecular features of a myofiber. We took rigorous measures, including labeling all sections on the same day; fluorescence signals were not saturated during image acquisition; specificity of the antibodies was validated (i.e. we used biological samples –mdx vs WT– known to have increased expression of eMyHC and NCAM; fluorescently-labeled sections were protected from light; measurement of fluorescence intensity was done on unaltered images, to preserve a proportional relationship between MFI and protein expression. Combining these functions provided the capability to ascertain a relationship between myofiber size and eMyHC or NCAM fluorescence intensity at single-myofiber resolution. This becomes a critical analytical quality given that eMyHC<sup>+</sup> and NCAM<sup>+</sup> regenerating myofibers represent a minor fraction of total myofibers. Thus, small, but physiologically impactful changes in size or protein expression in this population may be missed because of their low prevalence. Although previous studies characterized NCAM expression in regenerating muscle, they did not measure CSA (Dubois et al., 1994; Illa et al., 1992). Here, measuring CSA and NCAM expression permitted a linear regression analysis that revealed a negative correlation between NCAM expression and myofiber size, which was also true for eMyHC<sup>+</sup> myofibers. The reduction of eMyHC and NCAM expression with increasing myofiber size in mdx mice is consistent with other studies showing that these

markers of regeneration are down-regulated with myofiber differentiation and/or growth (Agbulut et al., 2003; Covault and Sanes, 1986; Dubois et al., 1994; Schiaffino et al., 2015). Further, QuantiMus reliably identified a subset of very small myofibers expressing high levels of eMyHC and NCAM protein (**Figure 2.10I-L** green box), likely representing nascent myotubes present in mdx muscle (Charlton et al., 2000). Our study demonstrates that QuantiMus measures protein expression over a high dynamic range and accurately classifies small regenerating myotubes, to assess muscle regeneration with unprecedented sensitivity and accuracy.

QuantiMus was designed to segment and classify images for myofiber determination and measuring their fluorescence intensity. This design does not allow QuantiMus to measure unsegmented areas, preventing the quantification of injured or fibrotic areas over the entire cross section. However, the 'Measure Fluorescence' feature can be used to quantify the frequency of necrotic myofibers and their uptake of Evans Blue dye by measuring the MFI (Hamer et al., 2002; Straub et al., 1997). Similar approaches have been used to measure muscle membrane injury following acute injury detected with procion orange (Tidball and Wehling-Henricks, 2007). As expected, QuantiMus revealed a greater than 15-fold increase in EBD<sup>+</sup> injured myofibers in mdx mice compared to WT mice. Further, measuring the MFI of EBD of all myofibers in a cross-section revealed a broad range in the fluorescence intensity of EBD in dystrophic muscle. We attribute this broad distribution to an increase in the number and/or size of lesions in the sarcolemma of a single myofiber that causes a larger and variable influx and accumulation of EBD. Measuring the MFI of EBD consequently becomes useful to measure injury when the frequency of injured myofibers is not different between experimental conditions, but the number of lesions per myofiber or size are significantly altered.

QuantiMus is an open-source software plug-in written in the Python programming language and is available at no cost. Python has a large open-source community that actively maintains a rich set of software libraries and packages that can be used to customize the functionality of QuantiMus for investigator-specific needs. The algorithms designed for QuantiMus

were written to rapidly process high-content images and must be launched through the computer terminal, which may require some guidance to operate. To circumvent this limitation for novice users, we have provided extensive instructions for installation and program start-up of QuantiMus at <https://quantimus.github.io>.

Through extensive benchmarking, we validated QuantiMus as a novel machine learning-based tool for quantitative skeletal muscle morphometry. QuantiMus quantified the frequency of centrally-nucleated, injured and regenerating myofibers in whole cross-sections with high precision. Further, QuantiMus rapidly typed myofibers based on the expression of MyHC isoforms. The capability to simultaneously measure fluorescence intensity and cross-sectional area provided a novel analytical approach for quantifying myofiber injury and regeneration. In summary, QuantiMus operates with equal and for many parameters exceeds the performance of existing software in quantifying histological and molecular features of muscle disease in human and mouse.

## **ACKNOWLEDGEMENTS**

We thank Dr. Albert Zlotnik and Suhas Sureshchandra for their insightful input and critical assessment of the manuscript. We also thank the UCI Center for Statistical Counseling for their suggestions regarding statistical analyses used.

**Table 2.1. Antibodies used for histology.**

<b>Antibody/labeling reagents</b>	<b>Vender</b>	<b>Clone</b>	<b>Dilution</b>	<b>Final (ug/ml)</b>
eMyHC	DSHB	F.1652	30	0.6
NCAM	SCBT	H28-123	200	0.5
Rabbit anti-Laminin	Sigma	Polyclonal	200	2.5
Biotin Anti-Mouse IgG	Jackson Immuno	Polyclonal	80	15
MyHC Type I	DSHB	BA-D5	200	1.4
MyHC Type IIa	DSHB	SC-71	200	1.9
MyHC Type IIb	DSHB	BF-F3	200	2
MyHC Type IIx	DSHB	6H1	20	1.1
Streptavidin Alexa Fluor 594	Invitrogen	Polyclonal	80	25.0
Anti-Rat Alexa Flour 488	Invitrogen	Polyclonal	200	10
Anti-Rabbit Alexa Flour 647	Invitrogen	Polyclonal	200	10
Anti-Mouse IgG 2b DyLight 405	Jackson Immuno	Polyclonal	400	4.3
Anti-Mouse IgG1 Cy2	Jackson Immuno	Polyclonal	400	4
Anti-Mouse IgM DyLight 594	Jackson Immuno	Polyclonal	400/1500 <sup>a</sup>	3.8/1

<sup>a</sup> Final dilution of 1:400 was used for mouse sections. 1:1500 was used for human.



**Table 2.2. Comparison of imaging processing times of different methods.**

<b>Method</b>	<b>Time (min)<sup>a</sup></b>	<b>Fibers/cross section</b>	<b>CSA (<math>\mu\text{m}^2</math>)<sup>b</sup></b>	<b>Min Feret (<math>\mu\text{m}</math>)<sup>c</sup></b>
FIJI	133 $\pm$ 21	6699 $\pm$ 153	745.53 $\pm$ 12.69	24.49 $\pm$ 0.88
QuantiMus	7 $\pm$ 1	7638 $\pm$ 5	710.73 $\pm$ 0.38	23.10 $\pm$ 0.00
SMASH	5 $\pm$ 0.5	8630 $\pm$ 0	813.86 $\pm$ 0.00	26.51 $\pm$ 0.00
MyoVision	Failed <sup>d</sup>	N.D.	N.D.	N.D.

*Data is the average  $\pm$  standard error of the mean of three independent analyses of one entire muscle cross-section*

*<sup>a</sup> Processing time (minutes) required to analyze myofiber size in full quadriceps cross-section image*

*<sup>b</sup> Average cross-sectional area (CSA)*

*<sup>c</sup> Average minimum Feret diameter*

*<sup>d</sup> Analysis did not complete within a four-hour period*

*N.D. not determined*

**Figure 2.1. QuantiMus application workflow.**

The QuantiMus analysis pipeline is composed of 5 steps: 1) the 'Fill Myofiber Gaps' function; 2) 'Myofiber Detection' function; 3) 'Centrally-Nucleated Fibers' function; 4) 'Measure Fluorescence' function; and 5) 'Save and Export Data' function.

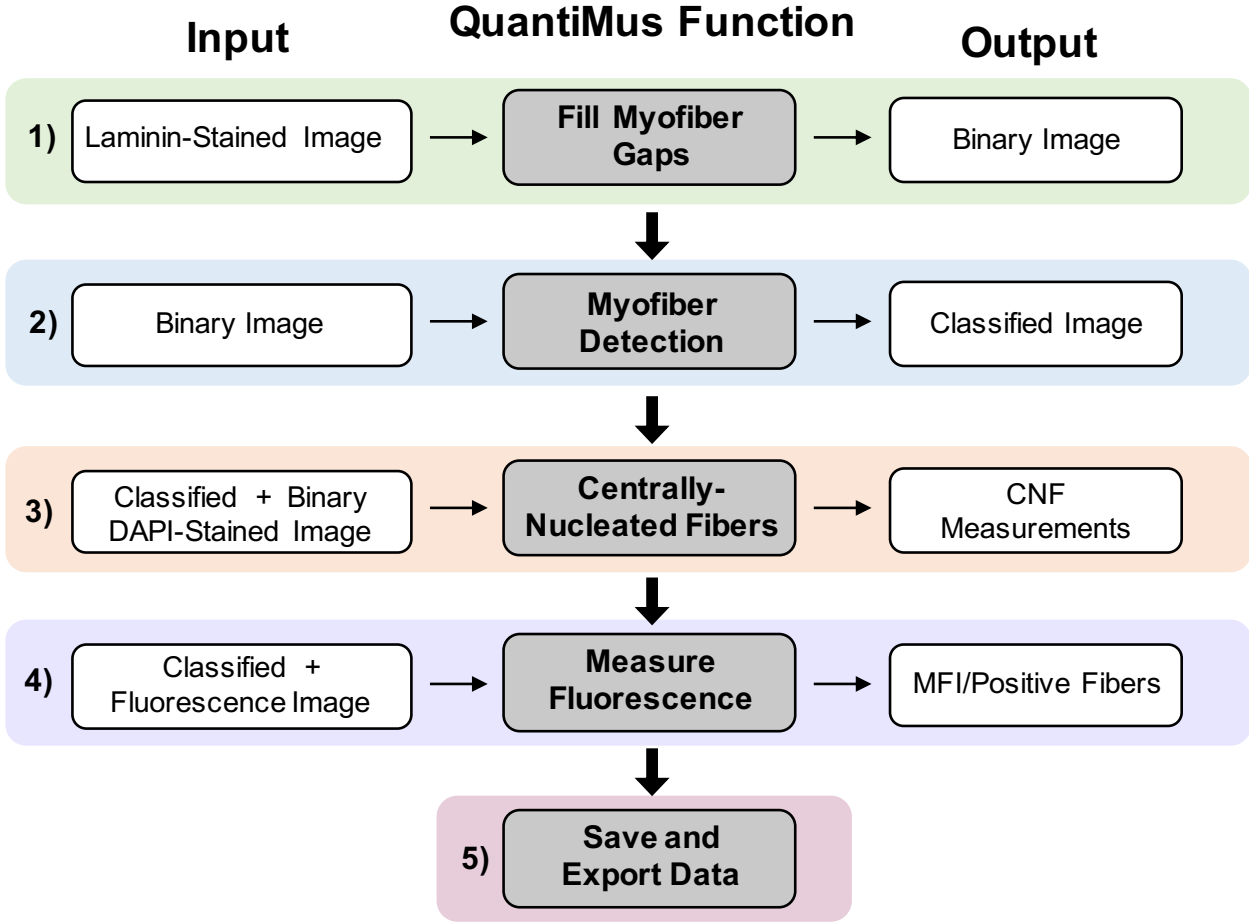


**Figure 2.2. The 'Fill Myofiber Gaps' function corrects gaps in myofiber boundaries that hinder single myofiber discrimination.**

A) Screenshot of the QuantiMus user interface used for the 'Fill Myofiber Gaps' function. B) Representative image of a cross-section of 4-week-old mdx quadriceps, stained with anti-laminin antibody (white). C) Zoomed in region of the cross-section in B (yellow box). D) Interactive display showing thresholds set by the user with sliders in the Fill Myofiber Gaps tab. E) Myofiber gaps detected and filled by the algorithm (white regions highlighted by yellow arrows). F) Binary image generated from the cross-section in C that was not corrected with the 'Fill Myofiber Gaps' function; colored regions indicate grouped ROIs incorrectly detected as one myofiber. G) Binary image generated from the cross-section in C that was corrected using the 'Fill Myofiber Gaps' function. Scale bar= 200  $\mu$ m.

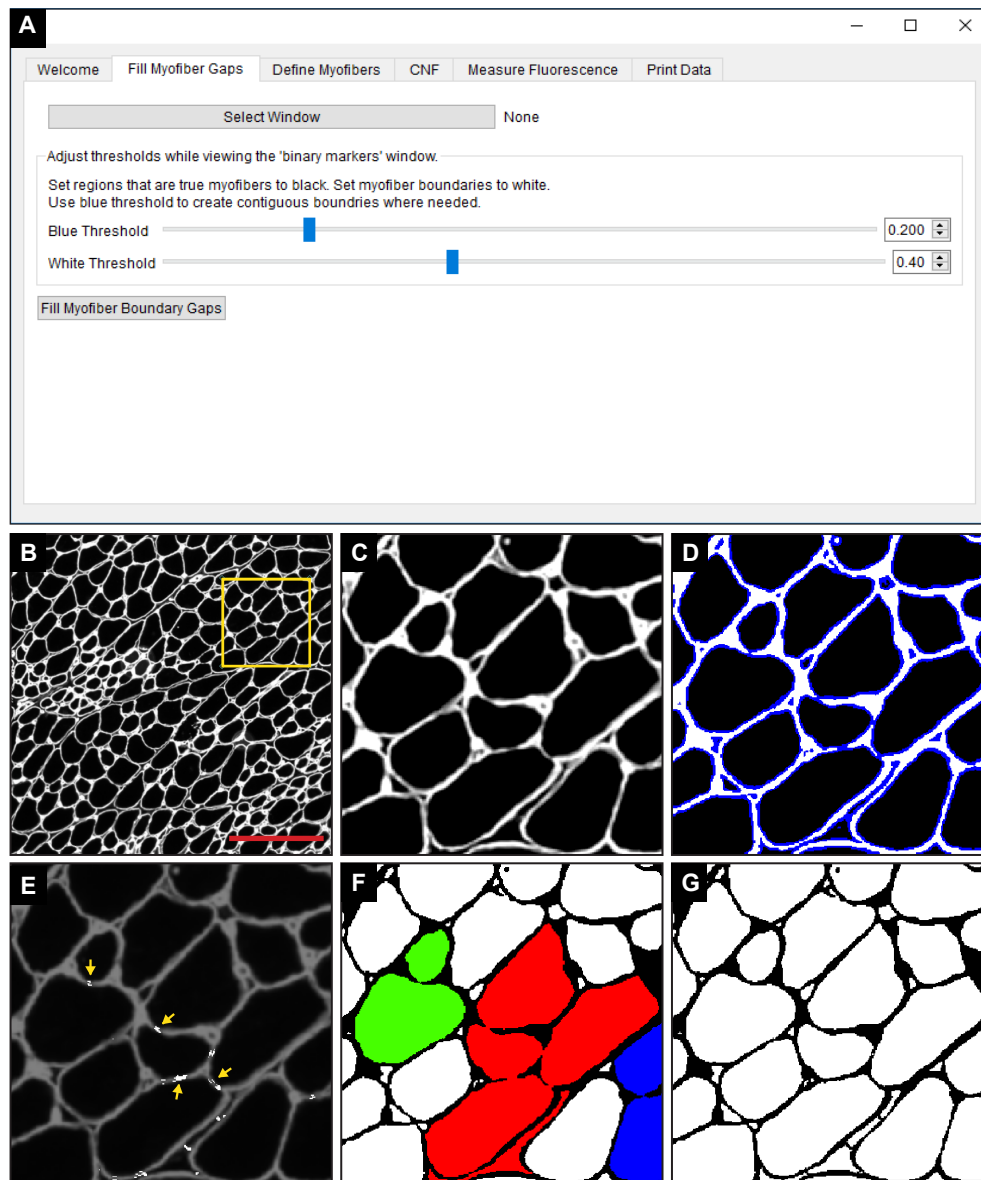
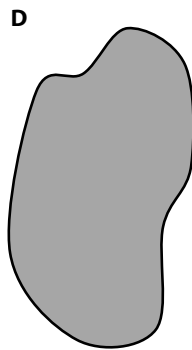
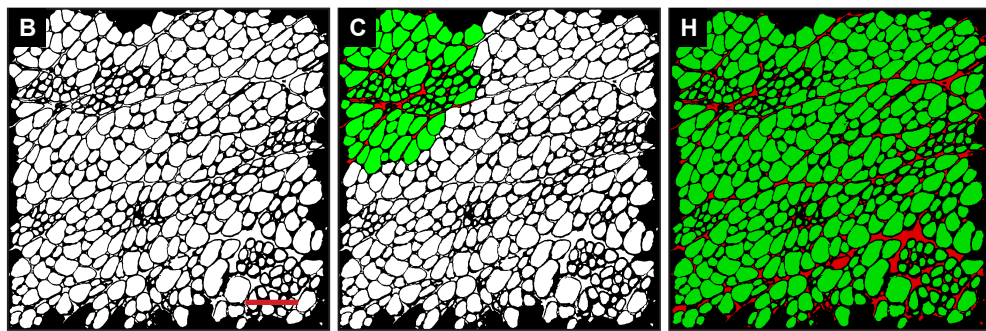
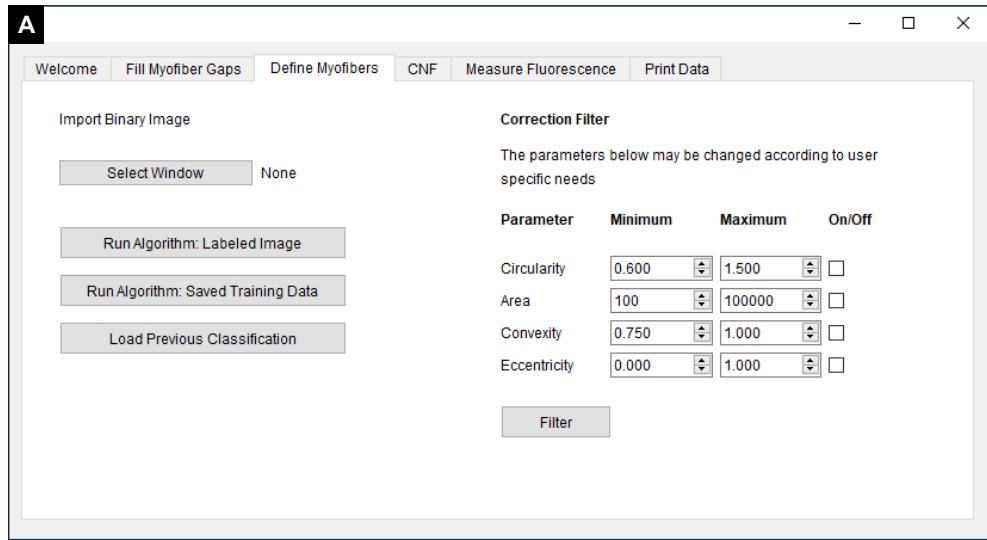
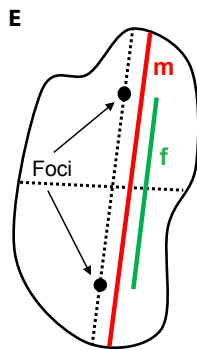


**Figure 2.3. Classification of skeletal muscle myofibers.**

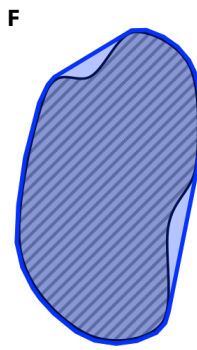
A) Image of the QuantiMus user interface used to classify myofibers. B) Binary image of quadriceps from 4-week-old mdx mice generated during the 'Fill Myofiber Gaps' function. C) Binary image highlighting user-classified ROIs (an ROI is defined as any contiguous region of pixels) used to train the machine learning algorithm for subsequent automated ROI classification. Green ROIs= myofibers, red ROIs= interstitial space and artifacts. D-G) Properties used to classify regions as myofibers. D) Area (grey) is the total number of pixels in the region. E) Eccentricity is calculated by dividing the focal distance (f, green line) by the major axis length (m, red line). Focal distance is defined as the length between the foci and the major axis length is the longest diameter of a region. F) Convexity of an ROI is calculated by dividing the area (hatched area) by the convex area (blue area). The convex area is defined as the area within the smallest convex polygon that can be drawn around a region. G) Circularity is determined using Eq. 3 as shown. Area= grey region, Perimeter= red boundary. H) A representative final image rendered by automated classification subsequently used for myofiber quantification and downstream analysis. Scale bar= 200  $\mu\text{m}$ .



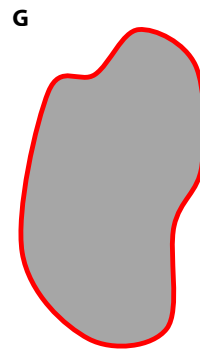
Area



Eccentricity =  $\frac{f}{m}$



Convexity



Circularity =  $\frac{4\pi \cdot \text{Area}}{\text{Perimeter}^2}$

## Figure 2.4. Detection of CNFs.

A) The QuantiMus user interface that is utilized for the detection of CNFs. B) Representative cross-section of 4-week-old mdx mouse quadriceps previously classified using the 'Myofiber Detection' function. C) The corresponding DAPI image of the cross-section in B. D) The overlay of classified and DAPI images. E) Eroded myofibers (yellow) generated during the "Centrally-Nucleated Fibers" function. F) The 'Centrally-Nucleated Fibers' function end-product provides an image with CNFs labeled purple. Scale bar= 200  $\mu$ m.

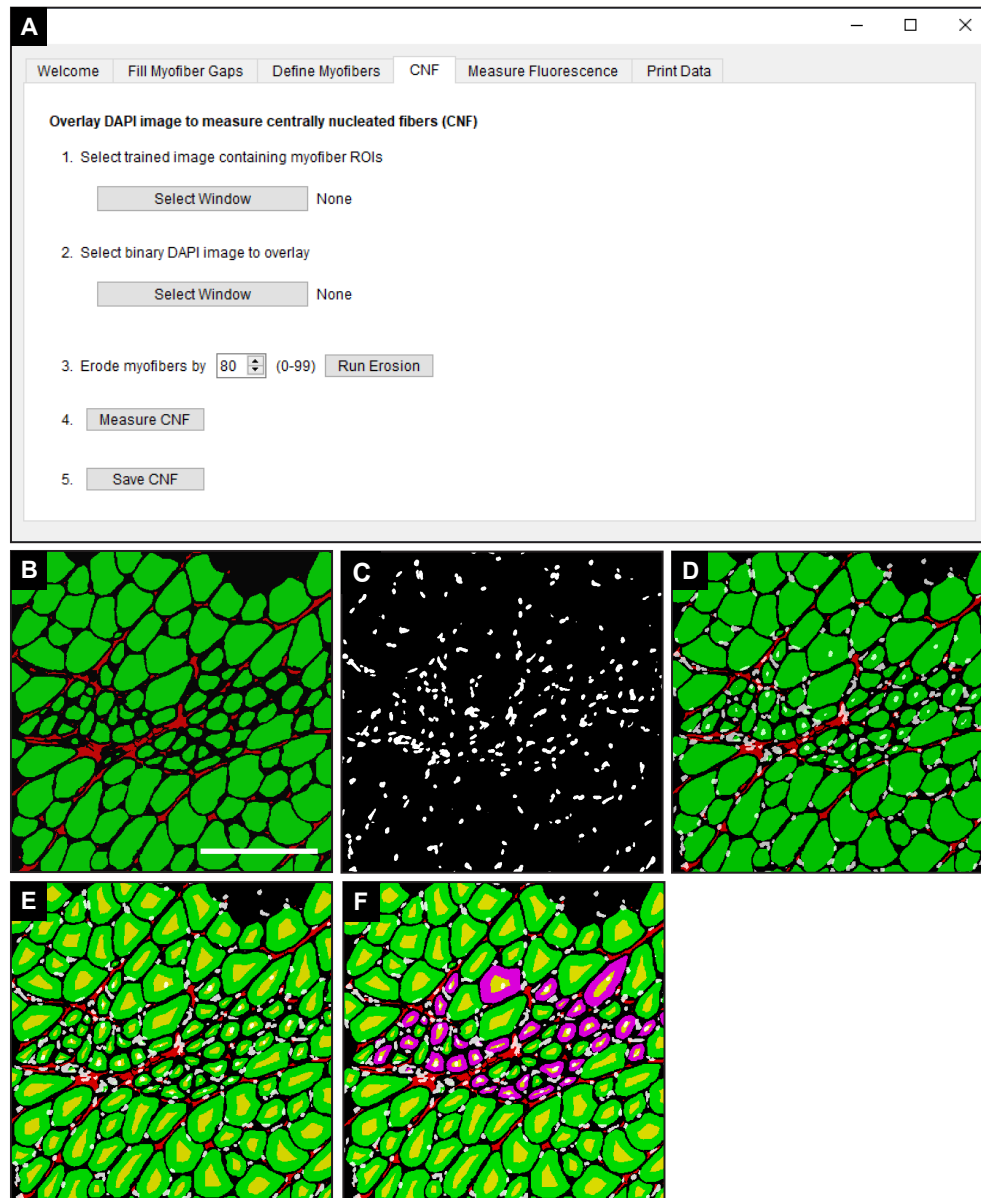


### Figure 2.5. Measurement of fluorescence intensity in single myofibers.

A) QuantiMus user interface that is utilized for measuring the myofiber mean fluorescence intensity (MFI) of an overlaid fluorescence image. B) Classified image generated by the 'Myofiber Detection' function. C) Fluorescence image of anti-eMyHC antibody-stained quadriceps. D) Image in C is overlaid onto the corresponding classified image in B. E) User-defined eMyHC<sup>+</sup> myofibers (yellow) are used as a threshold for the automated determination of remaining eMyHC<sup>+</sup> myofibers. F) eMyHC<sup>+</sup> myofibers are relabeled blue following the "Determine Positive Fibers" step. Scale bar= 100  $\mu$ m.

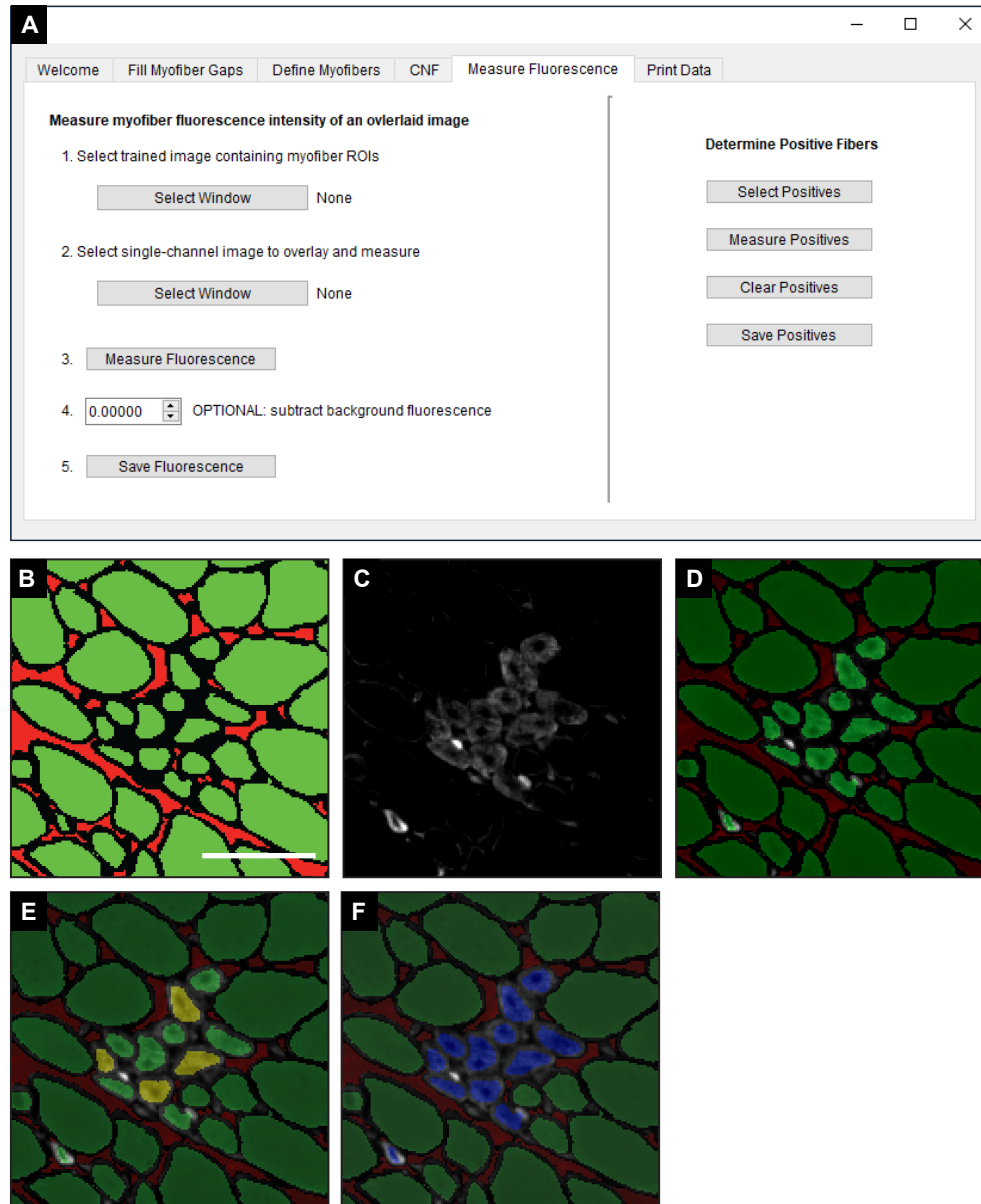


**Figure 2.6. Data export.** QuantiMus user interface utilized for the export of saved data.

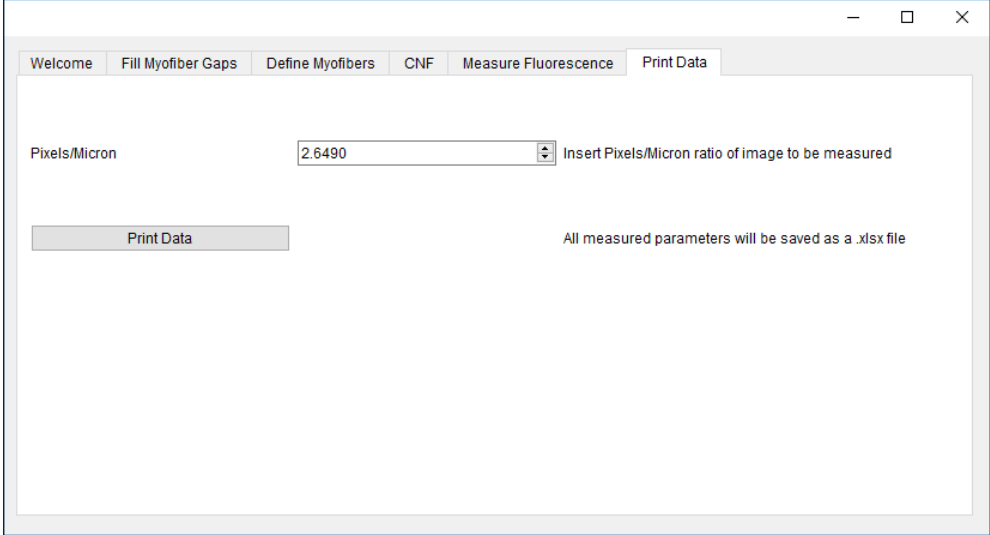




**Figure 2.7. QuantiMus accurately measures myofiber CSA and minimum Feret diameter.**

A) The number of myofibers detected using FIJI, QuantiMus (QM), MyoVision (MV) and SMASH in 4-week-old WT and mdx quadriceps. B) The percent accuracy of the number of myofibers detected by each method. C) The average (Avg) CSA ( $\mu\text{m}^2$ ) of myofibers in A. D) The percent accuracy of average myofiber CSA for each method. Greater than 2000 fibers from 5 representative fields, taken from two mice were used for each group. E) The number of myofibers detected in human muscle. F) The percent accuracy of myofiber classification for each method in E. G) The Avg CSA ( $\mu\text{m}^2$ ) detected by each method in E. H) The percent accuracy of average myofiber CSA for each method in G. Over 2400 myofibers from 6 representative fields, taken from 2 patients were measured. Connected data points are indicative of a single image analyzed by each method. \*  $p < 0.05$ , \*\*  $p < 0.01$  \*\*\*  $p < 0.001$  and \*\*\*\*  $p < 0.0001$  using a two-way repeated measures ANOVA with a multiple comparison test (main column effect). Statistics are compared to FIJI (A,C,E,G) or QM (B,D,F,H).

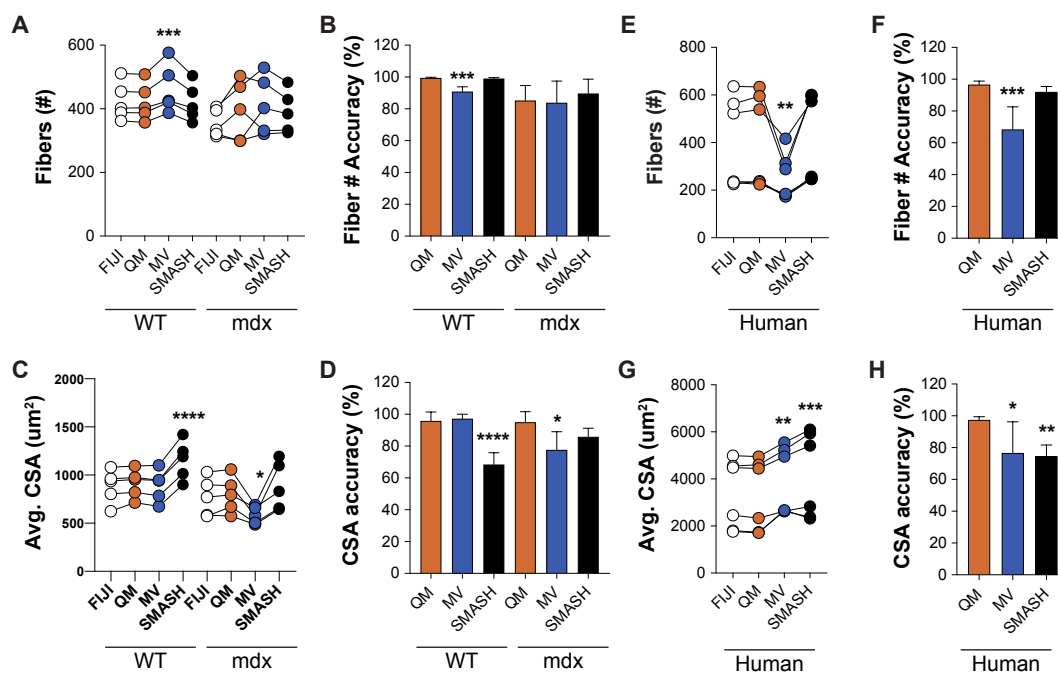


### Figure 2.8. Defining CNFs.

A) The number of CNFs detected using manual measurement (FIJI), QuantiMus (QM), and SMASH in 4-week-old mdx quadriceps. B) The percent accuracy of QuantiMus and SMASH to detect CNFs in A. C) The average CSA ( $\mu\text{m}^2$ ) of CNFs detected by manual measurement (FIJI), QuantiMus, or SMASH. D) The percent accuracy of QuantiMus and SMASH in measuring the CSA of detected CNFs compared to FIJI. Connected data points are indicative of a single image analyzed by each method. 5 representative fields taken from 2 mice were used for analysis. \*\*  $p < 0.01$  using a two-way repeated measures ANOVA with a multiple comparison test (main column effect) (A,C) or an paired two-tailed t-test (B,D). Statistics are compared to FIJI.

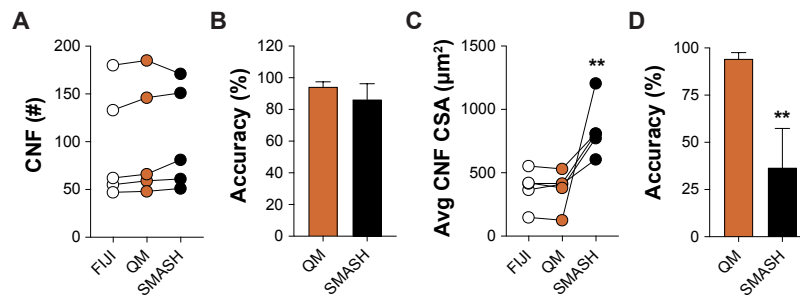


**Figure 2.9. Myofiber typing of mouse and human muscle.**

A) Representative image of WT mouse quadriceps cross-sections stained with antibodies against myosin heavy chain-specific isoforms. Blue= Type 1, Green= Type IIa, Red= Type IIb. Fibers with no isoform present are defined as type IIx. B) The proportion of each myofiber type. C) The average (Avg) cross-sectional area (CSA) of each fiber type. Data is displayed as the average  $\pm$  SEM from full section measurements of 4 WT mice. A total of 25,757 fibers were measured. D) Representative image of human cross-sections stained with antibodies against myosin heavy chain-specific isoforms. Blue= Type 1, Green= Type IIa, Red= Type IIx. E-F) The proportion of each fiber type in human biceps brachii or gastrocnemius. G-H) The Avg CSA of each fiber type in both muscle groups. Data is measured from full cross-sections and is displayed as the average  $\pm$  SEM CSA of each patient sample (G,H). 1,488 (Biceps) and 2036 (Gastroc) fibers were measured. Scale bars= 100 (A) or 200 (D)  $\mu$ m.

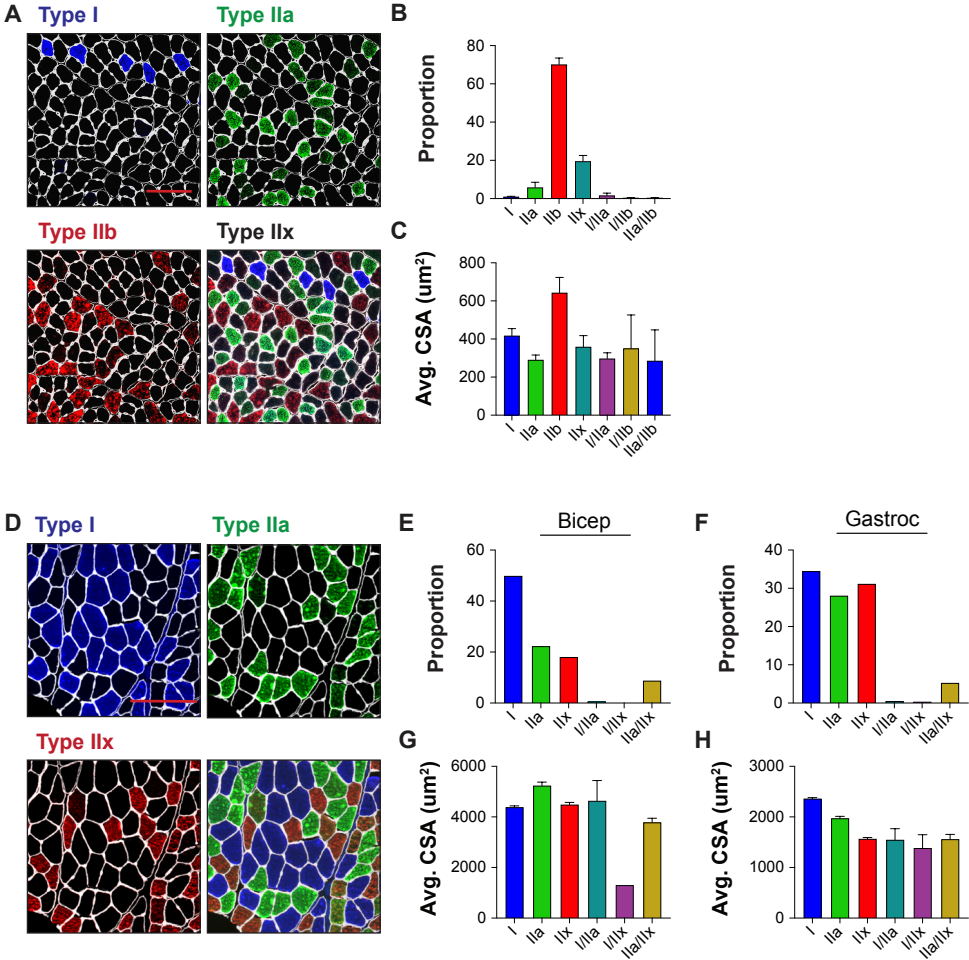
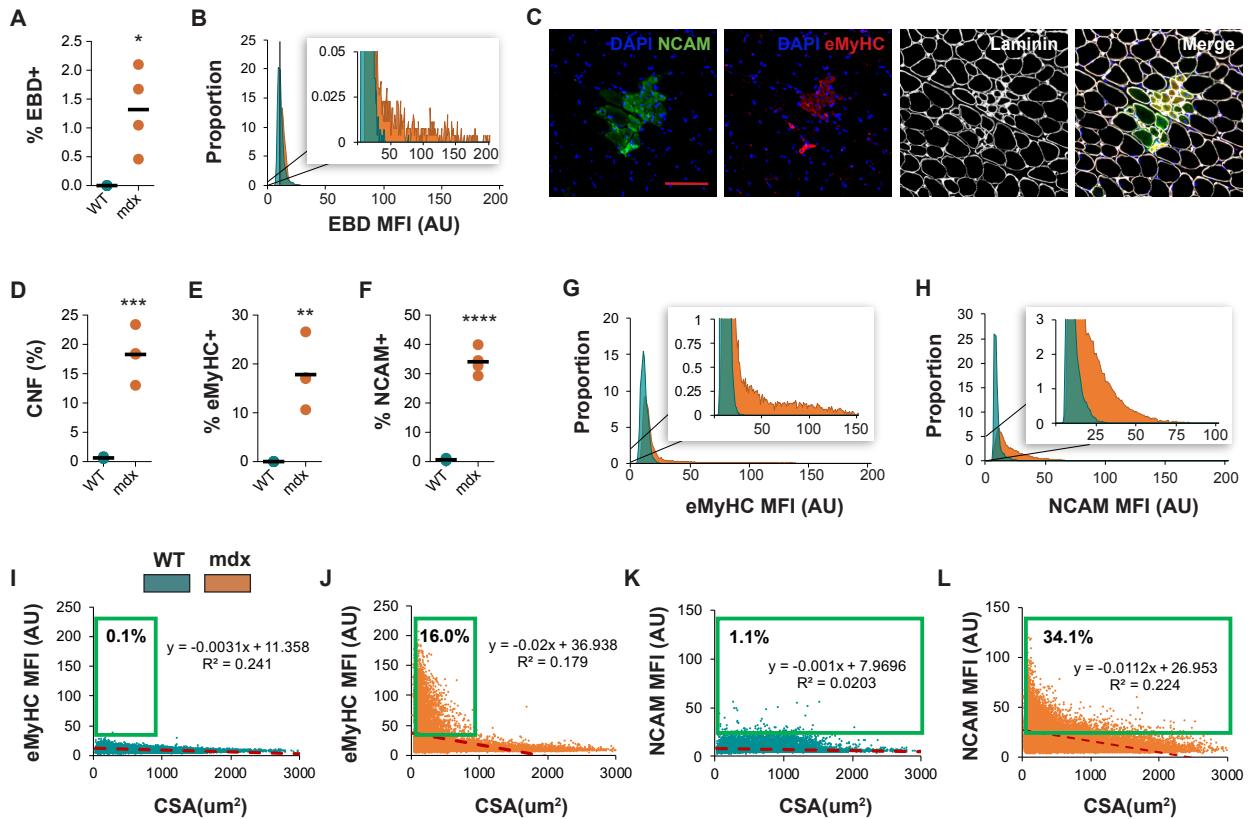


**Figure 2.10. Morphometric analysis of dystrophic pathology in mdx mice.**

A) Frequency of injured fibers (% EBD<sup>+</sup>) in entire quadriceps cross-sections of WT and mdx mice. B) Histogram of muscle EBD expression showing individual myofiber EBD expression displayed as mean fluorescence intensity (MFI). n= 4 for each group. C) Representative images of mdx mouse quadriceps cross-sections stained with DAPI (Blue), NCAM (Green), eMyHC (Red), and laminin (White). The percentage of centrally-nucleated (CNF, D), eMyHC<sup>+</sup> (E) and NCAM<sup>+</sup> (F) fibers (of all fibers) in entire WT and mdx quadriceps cross-sections. G-H) Histogram of eMyHC and NCAM expression showing individual myofiber expression displayed as MFI. Teal= WT; orange= mdx. I-L) Linear regression analysis comparing eMyHC or NCAM MFI and myofiber CSA (μm<sup>2</sup>) in WT and mdx mice. Each dot represents a single myofiber. Red-dashed line corresponds to the equation generated by the linear regression analysis. n=4 for each group. The boxed regions reflect data points that were above the background signal. Scale bar= 100 μm. AU= Arbitrary units. 4-week-old mice were used. \* p<0.05, \*\* p<0.01, \*\*\* p<0.001 and \*\*\*\* p<0.0001 using an unpaired two-tailed t-test with Welch's correction.



## CHAPTER 3

### **Muscle injury activates group 2 innate lymphoid cells to induce muscle eosinophilia**

Jenna M. Kastenschmidt, Gerald Coulis, Philip Pham, Rodolfo Rios, Ali H. Manna, Rachel Ayer, Rayan Yahia, Adam K. Savage, Richard M. Locksley, Jeffery A. Bluestone, Steven A. Moore, Tahseen Mozaffar, Carlee R. Giesige, Scott Q. Harper, S. Armando Villalta

## **ABSTRACT**

Type II innate immunity, characterized by muscle eosinophilia and M2-like macrophages, is required for efficient muscle regeneration. However, chronic activation and dysregulation of this response is a signature of the mdx mouse model of Duchenne muscular dystrophy (DMD). Sustained eosinophilia and activation of M2-like macrophages promote myofiber injury and fibrosis, respectively, but the mechanism underlying this response in dystrophic muscle is unknown. In the current study, we found that ST2-expressing ILC2s are present in healthy skeletal muscle and are expanded following acute muscle injury and during muscular dystrophy. IL-33 was upregulated in dystrophic muscle and was predominantly expressed by fibro/adipogenic progenitors (FAPs). Treatment of mdx mice with exogenous IL-2 and IL-33 expanded muscle ILC2s and significantly increased dystrophic muscle eosinophilia in an ILC2-dependent fashion. Interestingly, macrophage activation was unaffected in these studies. Skeletal muscle eosinophils expressed CCR3 and IL-5R and muscle ILC2s were shown to produce ligands for these receptors, CCL5 and IL-5, respectively. Thus, we discovered a novel ST2-mediated ILC2 and FAP interaction, leading to increased expression of IL-5 and CCL5 that promotes eosinophilia during muscular dystrophy.

## **INTRODUCTION**

Type II immunity is characterized by the production of cytokines, including IL-4, IL-5, IL-9, and IL-13, as well as the activation of cells such as T-helper 2 T cells, eosinophils, and alternatively activated macrophages (M2-like). These cellular responses are traditionally associated with allergy and host protection against helminth infection but are also critical for the initiation and promotion of tissues repair and remodeling following injury (Gieseck et al., 2018). In skeletal muscle, type II immune responses are essential for efficient and complete regeneration. For example, studies have shown that M2-like macrophages promote the differentiation of muscle progenitor cells (S Armando Villalta et al., 2009), and the prevention of their activation impairs

regeneration following acute injury (Arnold et al., 2007). Eosinophils have also been shown to promote regeneration in acute muscle injury models through the secretion of IL-4, which promotes fibro/adipogenic progenitors to support muscle regeneration (Heredia et al., 2013). In muscle disease such as Duchene muscular dystrophy (DMD), type II immunity is still essential for regeneration. However, asynchronous bouts of injury and repair lead to persistent activation of these responses that can further promote fibrosis and exacerbate disease. Although type II immunity plays an important role in regulating tissue homeostasis, its regulation is not completely understood.

The recent identification and characterization of group 2 innate lymphoid cells have revealed new regulatory networks of type II inflammation. ILC2s are tissue-resident lymphocytes that lack antigen receptors, are activated by tissues alarmins (i.e., IL-33, IL-25, TSLP) and are potent secretors of type II cytokines including IL-5 and IL-13 (Moro et al., 2010; Neill et al., 2010; April E. Price et al., 2010). Group 2 innate lymphoid cells (ILC2s) also promote eosinophil homeostasis and tissue eosinophilia (Molofsky et al., 2013; Nussbaum et al., 2013; Van Gool et al., 2014) and have been shown to promote the alternative activation of macrophages (Molofsky et al., 2013).

Here, we tested the hypotheses that ILC2s regulate type II immunity in skeletal muscle, specifically during chronic muscle disease. We report that ILC2s are increased following muscle damage and are activated to produce IL-5 and IL-13. The expansion of ILC2s using (IL-2/anti-IL-2 complex (IL-2c) together with IL-33 or the genetic deletion of ILC2s caused an increase or decrease in dystrophic muscle eosinophils, respectively. We found that muscle eosinophils expressed CCR3 and the production of CCR3 chemokines by ILC2s (including CCL5 and CCL9) were elevated in mdx muscle. We also provide evidence for a novel interaction between muscle ST2-expressing ILC2s and FAPs, which were an abundant source of IL-33. Our findings highlight a role for ILC2s in regulating the immunopathogenesis of muscular dystrophy by promoting muscle eosinophilia.

## **MATERIALS AND METHODS**

### **Mice**

Mdx mice (C57BL/10ScSn-Dmdmdx/J, The Jackson Laboratory stock #001801) were purchased from the Jackson Laboratory and bred in our colony. New mdx breeders were purchased after the 5th generation of breeding to avoid genetic drift. Mdx mice lacking ILC2s were generated by crossing mdx mice with the YetCre13.DTA mouse (April E. Price et al., 2010) in which the endogenous IL-13 promoter drives the expression of a yellow fluorescent protein (YFP)-Cre recombinase fusion protein. YetCre13 mice were subsequently crossed with transgenic mice in which a DTA transgene carrying a flox-stop-flox cassette was knocked into the ROSA26 locus (B6.129P2-Gt(ROSA)26Sortm1(DTA)Lky/J, The Jackson Laboratory #009669) (Voehringer et al., 2008). Cre expression in IL-13-producing cells leads to the excision of the stop cassette and subsequent expression of DTA, resulting in the ablation of IL-13-producing cells, including ILC2s. The mdx.ILC2 reporter mouse was generated by crossing mdx mice with Red5 transgenic mice, in which the endogenous IL-5 promoter drives the expression of tdTomato (B6(C)-Il5tm1.1(icre)Lky/J; The Jackson Laboratory stock # 030926) (Molofsky et al., 2013). Mdx.dblGATA mice were generated by crossing mdx mice with dblGATA mice that lack eosinophils due to a deletion of the GATA-1 locus (C.129S1(B6)-Gata1tm6Sho/J; Jackson Laboratory stock #005653) (Yu et al., 2002). Mdx mice that lack T cells were generated by crossing the mdx and TCR $\alpha$  knock out mice (B6.129S2-Tcratm1Mom/J; Jackson Laboratory stock #002116). C57BL/6J mice used for cardiotoxin (CTX)-induced injury were purchased from the Jackson Laboratory (stock # 000664).

Unless otherwise noted, mice used in this study were analyzed at four weeks of age. Both male and female mice were assessed and analyzed separately (data not shown) and together. In compliance with federal regulations, the use of mice in our study was approved by the University of California Irvine Institutional Animal Care and Use Committee.



### **Acute muscle injury**

Acute muscle injury was induced by injecting a total of 200  $\mu$ l of 10 $\mu$ m (in 1X PBS) Cardiotoxin (CTX; Latoxen laboratory; France) into the hindlimb muscles (30  $\mu$ l quadriceps, 50 $\mu$ l hamstring, 20  $\mu$ l gastrocnemius) of 8-wk-old C57BL/6J mice. Both limbs were injected with CTX, and muscles were pooled then interrogated by flow cytometry as described below.

### **Cell isolation and flow cytometry analysis**

Single-cell suspensions from hindlimb muscles were prepared as previously described (Kastenschmidt et al., 2018). Briefly, mice were first euthanized with carbon dioxide using a gradual fill method per American Veterinary Medical Association guidelines and were perfused with 1X PBS. The popliteal lymph node was removed, and all hindlimb muscles were excised then mechanically and enzymatically digested, filtered through 40 and 70  $\mu$ m mesh and cells were purified using gradient centrifugation. Cells were stained with Zombie NIR fixable viability dye (Biolegend), and the FC receptor was blocked by incubating cells for 15 minutes in TruStain FcX anti-mouse CD16/32 antibody (Biolegend). Anti-mouse antibodies used in this study are listed in **Table 3.1**. Intracellular staining of transcription factors was performed using the Foxp3/Transcription factor staining buffer set (eBioscience) per manufacturer directions. Surface and intracellular stains were incubated for 30 minutes while on ice and protected from light. Single-cell suspensions were analyzed or sorted using a FACS Aria Fusion (BD Biosciences) equipped with 405, 488, 561, and 640 lasers. Data were analyzed, and plots were generated using FlowJo software (FlowJo, LLC, Version 10.4).

### ***In vivo* cytokine treatment**

Mice were treated with IL-2/anti-IL-2 complex (IL-2c) as previously described (Villalta et al., 2014). Briefly, IL-2c was prepared by combining 0.5  $\mu$ g recombinant mouse IL-2 (eBioscience)

with 5 µg anti-mouse-IL2 antibody (clone JES6-1A12, eBioscience) and incubating at 37°C for 15 minutes. Mice were treated with Isotype control, IL-2c, 0.5 µg recombinant mouse IL-33 (Life Technologies), IL-2c in combination with IL-33, 0.5 µg recombinant mouse IL-25 (R and D systems), or IL-2c+IL-25. Mice in all treatment groups were administered agents intraperitoneally starting at two weeks of age. Animals were injected every other day for a total of 3 injections and were analyzed at four weeks of age.

### **Examination of gene expression using quantitative reverse transcription PCR (RT-qPCR)**

Liquid nitrogen-frozen muscle samples were homogenized, and RNA was extracted using TRIsure (Bioline) and the Quick-RNA Miniprep kit (Zymo Research) per manufacturer instructions. Cell populations were isolated using fluorescence-activated cell sorting (FACS), and RNA was isolated using the Quick-RNA Microkit (Zymo Research). Cells were FACS sorted directly into lysis buffer. Complementary DNA (cDNA) was synthesized from 150 ng (sorted cells) or 2000 ng (whole muscle) of RNA using the SensiFAST cDNA synthesis kit (Bioline). Gene expression was quantified using TaqMan expression assay probes (Applied Biosystems, **Table 3.2**) and 2x SensiFAST probe No-ROX mix (Bioline). All gene expression was normalized to 18s expression.

### **Histological analysis**

Mouse muscles were excised, frozen in liquid nitrogen-cooled isopentane and stored at -80°C. Eight-micron cross-sections were prepared on a Leica CM1950 cryostat, mounted on positively charged microscope slides (Fisher), and stored at -80°C until the time of staining. Cross-sections were removed from -80°C and were stained with Harris modified hematoxylin (Fisher) and eosin (Richard-Allen Scientific).

*FAP analysis:* For the immunofluorescence staining of IL-33 and PDGFR $\alpha$ , slides were first fixed in 2% paraformaldehyde (PFA) and endogenous peroxidases were blocked with 3%

H<sub>2</sub>O<sub>2</sub>. Sections were blocked for 1 hour with 5% normal donkey serum and 3% bovine serum albumin in 1X tris-buffered saline with 0.1% Tween 20. Sections were incubated with primary antibodies (**Table 3.3**) for 3 hours, washed with 1X PBS, and stained with secondary antibodies. A Tyramide SuperBoost kit (Invitrogen) was used for the detection of PDGFR $\alpha$  per manufacturer instructions.

*Fibrosis:* Muscle sections were fixed in 2% PFA, blocked for 1 hour with 5% normal donkey serum and 3% bovine serum albumin in 1X tris-buffered saline with 0.05% Tween 20, and stained with antibodies against collagen 1 alpha (**Table 3.3**) for 1 hour. Secondary antibodies used to detect collagen were added to sections and allowed to incubate for 1 hour at room temperature while protected from light. Nuclei were visualized by staining with 4',6-Diamidino-2-Phenylindole Dihydrochloride (DAPI) for 10 minutes while protected from light.

*Myofiber typing:* Myofiber typing of mouse soleus was performed as previously described (Kastenschmidt et al., 2019a). Briefly, sections were allowed to thaw and air dry then blocked using MOM blocking reagent. Sections were incubated with primary and secondary antibodies listed in **Table 3.3** hour each at room temperature and protected from light.

Stained sections were imaged using a Keyence BZ-X700 inverted fluorescence microscope (Keyence). The analysis of the positive collagen area was conducted using FIGI. Single-channel images of collagen 1 $\alpha$ -stained sections were thresholded to define the positive signal of collagen 1 $\alpha$  which was divided by the total muscle cross-sectional area to define % area positive. The quantification of myofiber type distribution was conducted using QuantiMus as previously described (Kastenschmidt et al., 2019a).

## **Treadmill running**

*Chronic exercise protocol:* As previously described, mdx.dblGATA<sup>-</sup> knock out mice and littermate controls (mdx.dbl.GATA<sup>+</sup>) were exercised three times per week on an Exer-3/6

(Columbus Instruments) treadmill at an inclination of 0 for 30 minutes at a speed of 12 meters per minute as previously described (Pessina et al., 2014). Mice were allowed to rest for 5 minutes for every 10 minutes of exercise. Mice were run for a total of 4 weeks and were allowed to rest one week before analysis.

*Exhaustion treadmill test:* Mice ran on an Exer-3/6 at an inclination of 0 and speed of 5 meters per minute for minutes. At 5 minutes of running, the speed was increased by 1 meter per minute until exhaustion. Mice were considered fatigued, and the test was stopped when the animal remained on the shocker plate for 20 seconds without attempting to reengage the treadmill.

### **Mouse activity monitoring**

During the fourth week of the chronic exercise protocol, mdx.dbIGATA<sup>-</sup> and mdx.dbIGATA<sup>+</sup> littermate controls were placed in PhenoMaster (TSE systems) metabolic cages immediately following the running protocol. Mouse activity was monitored for 48 hours following exercise. Movement was determined by the total number of beam breaks in all directions within specified time intervals.

### ***In situ* muscle force production measurements**

Mice were anesthetized for the entire procedure using an isoflurane apparatus with supplemental oxygen continuously delivered to the animal. Mice were also placed on a heating pad to maintain body temperature. The tibialis anterior (TA) muscle was exposed, and the tendon was tied to a muscle lever system motor (Aurora Scientific) using silk ligature. The sciatic nerve was cut, and an electric stimulus was delivered using a nerve cuff that was fabricated in-house. The optimal muscle length was determined by manipulating the length until the maximum twitch force was generated. The tetanic force was measured at the optimal length following an electric stimulus at a rate of 650 pulses per second for a 350-millisecond duration with a 4-minute rest

between stimuli. Mice were euthanized with CO<sub>2</sub> and cervical dislocation following the procedure. Force is displayed as Newtons (N) per gram of TA.

## Statistics

All statistical analysis was performed with GraphPad Prism software (Version 8.0, Graphpad Software Inc. San Diego, CA). The analysis includes a Student's t-test with Welch correction or a One-way ANOVA with Bonferroni correction where indicated. Error bars indicate standard error of the mean.

## RESULTS

### Injury promotes the expansion of innate lymphoid cells in acutely-damaged muscle

We used the cardiotoxin (CTX)-induced model of acute muscle injury to determine the temporal regulation of innate lymphoid cells (ILCs) following injury. This model provides a highly reproducible and synchronous model of muscle injury and regeneration, characterized by widespread myofiber necrosis during the first two days following CTX injury, extensive mononuclear infiltration by day 4, and complete clearance of cellular debris and active muscle regeneration by day 7 (**Figure 3.1A**) (Hardy et al., 2016; Lukjanenko et al., 2013). The hindlimb muscles of 8-wk-old, C57BL/6 mice were harvested before injection (uninjured) and 1, 4 and 7 days after injection with CTX and interrogated by flow cytometry to quantify the number of innate lymphocyte subsets in the tissue. Representative contour plots demonstrate the gating strategy used to identify subsets of CD45<sup>+</sup>Thy1<sup>+</sup> lymphocytes, including NK1.1<sup>+</sup> (ILC1, NK cells) and lineage negative (Lin<sup>-</sup>: CD3, CD19, TCR $\beta$ , CD11c, CD11b negative) KLRG1<sup>+</sup> (ILC2) and ROR $\gamma$ t<sup>+</sup> (ILC3) cells (**Figure 3.1B and Supplemental Figure 3.1A**). We also identified a temporal increase in the frequency and number of CD45<sup>+</sup>Thy1<sup>+</sup>NK1.1<sup>+</sup> (NK/ILC1 cells, **Figure 3.1C**) and CD45<sup>+</sup>Thy1<sup>+</sup>Lin<sup>-</sup>KLRG1<sup>+</sup> cells (ILC2, **Figure 3.1D**), with a proportionally greater increase in NK1.1<sup>+</sup> cells compared to KLRG1<sup>+</sup> cells (**Supplemental Figure 3.1B and 3.1C**). There was no

significant increase in the number and frequency of CD45<sup>+</sup>Thy1<sup>+</sup>Lin<sup>-</sup>RORγt<sup>+</sup> (ILC3) cells in acutely injured muscle at day 7 (**Figure 3.1E and Supplemental Figure 3.1D**). Noteworthy, the number of KLRG1<sup>+</sup> and NK1.1<sup>+</sup> cells were elevated during the stage of muscle regeneration in mdx mice (day 7, **Figure 3.1C and 3.1D**).

## **Group 2 Innate lymphoid cells are increased in diseased muscle**

Next, we determined the regulation of innate lymphoid cells in mdx mice, a mouse model of chronic muscle degeneration. We prepared single-cell suspensions of 4-wk-old, wildtype (WT) and mdx hindlimb muscle, and interrogated ILCs by flow cytometry (**Figure 3.1F**). Similar to acutely-injured muscle, CD45<sup>+</sup>Thy1<sup>+</sup>NK1.1<sup>+</sup> and CD45<sup>+</sup>Thy1<sup>+</sup>Lin<sup>-</sup>KLRG1<sup>+</sup> innate lymphoid cells were increased in number (**Figure 3.1G and 3.1H**) and frequency (**Supplemental Figure 3.1E and 3.1F**). A negligible number of CD45<sup>+</sup>Thy1<sup>+</sup>Lin<sup>-</sup>RORγt<sup>+</sup> cells were detected in dystrophic muscle (**Figure 3.1I and Supplemental Figure 3.1G**). Given the previous observation that type II innate immunity facilitates muscle regeneration, and that ILC2s are critical regulators of type II innate immunity, we further examined CD45<sup>+</sup>Thy1<sup>+</sup>Lin<sup>-</sup>KLRG1<sup>+</sup> cells. We used flow cytometry to quantify the expression of prototypical markers of ILC2s, including GATA3, CD25, CD127, KLRG1, IL-17RB (IL-25 receptor) and ST2 (IL-33 receptor) in CD45<sup>+</sup>Thy1<sup>+</sup>Lin<sup>-</sup> cells (**Figure 3.1J and Supplemental Figure 3.1H**). We found that 70-90% of CD45<sup>+</sup>Thy1<sup>+</sup>Lin<sup>-</sup> cells expressed these ILC2 markers (**Supplemental Figure 3.1I**), and their numbers were significantly increased in mdx mice (**Supplemental Figure 3.1J**).

We then quantified CD45<sup>+</sup>Thy1<sup>+</sup>Lin<sup>-</sup>KLRG1<sup>+</sup>CD127<sup>+</sup> ILC2 cells (**Supplemental Figure 3.1H**) during acute (4 wk) and chronic (12 wk) stages of disease in mdx mice. We found that ILC2s are present in WT muscle (~200-600 cell/g of muscle) at 4 and 12 wk of age (**Supplemental Figure 3.1K and 3.1L**). However, the number of ILC2s was significantly increased in 4-wk-old mdx mice (~4000 cell/g), and although they declined by 12 weeks, they were still significantly

elevated compared to WT, age-matched control mice. We also found that the number of KLRG1<sup>+</sup>CD127<sup>+</sup> ILC2s was increased by ~10-fold in an inducible mouse model of facioscapulohumeral muscular dystrophy (FSDH) (**Supplemental Figure 3.1M**). These data reveal that ILC2s are activated in response to multiple causes of muscle damage.

Upon activation, ILC2s have been shown to be potent producers of type II cytokines, including IL-13 (Monticelli et al., 2011; April E. Price et al., 2010). We next used flow cytometry to evaluate the production of IL-13 by skeletal muscle ILC2s in 4-wk-old WT and mdx mice. We found that the proportion of ILC2s producing IL-13 was increased in mdx (48.2%) mouse muscle compared to healthy WT (22.6%) controls (**Figure 3.1K and 3.1L**). Furthermore, the number of IL-13<sup>+</sup> ILC2s was also higher in dystrophic muscle (**Figure 3.1M**). The IL-13 mean fluorescence intensity (MFI) of ILC2s was also increased in mdx muscle, indicating that dystrophic muscle ILC2s produce more IL-13 than their WT counterparts (**Figure 3.1N**). Together these data indicated injury effectively induces the activation of ILC2s in skeletal muscle.

### **Interleukin-33 is predominantly expressed by fibro/adipogenic progenitors and activates muscle ILC2s**

To characterize the signal/s that activate ILC2s in dystrophic muscle, we used RT-qPCR to measure expression levels of the known ILC2-activating cytokines IL-25, IL-33 and TSLP. We found that IL-25, IL-33 and TSLP were upregulated in 4-wk-old dystrophic hamstring muscle compared to WT controls (**Figure 3.2A**). Importantly, lower quantitation cycle (Cq) values, indicating a higher copy number, revealed that IL-33 is the most abundantly expressed ILC2-activating cytokine in muscle (**Figure 3.2B**). We next sought to determine the cellular source of IL-33. We fractionated whole muscle by preparing single-cell suspensions, and FACS-purified key cellular populations, including CD45<sup>+</sup> immune cells (I), CD31<sup>+</sup> vascular endothelial cells (II), PDGFR $\alpha$ <sup>+</sup> fibro/adipogenic progenitors (FAPS, III), ITG $\alpha$ 7<sup>+</sup> satellite cells (SC, V) and PDGFR $\alpha$ <sup>-</sup> and ITG $\alpha$ 7<sup>-</sup> double-negative cells (IV) (**Figure 3.2C**). RT-qPCR analysis of the FACS-purified

populations revealed that IL-33 mRNA was most abundantly-expressed by FAPs (**Figure 3.2D**). We next confirmed the expression of IL-33 protein in PDGFR $\alpha$ <sup>+</sup> FAPs by immunofluorescent staining of 4-wk-old mdx quadriceps, which revealed that a proportion of PDGFR $\alpha$ <sup>+</sup> FAPs expressed nuclear-localized IL-33 (**Figure 2E**) (Moussion et al., 2008). Further analysis using flow cytometry also revealed that live PDGFR $\alpha$ <sup>+</sup> cells express Sca-1 but not CD45, CD31, or ITG $\alpha$ 7, indicating these are bona fide FAPs (**Figure 3.2E**, Lower).

Given the observation that IL-33 is the most abundantly expressed ILC2-activating cytokine (**Figure 3.2A and 3.2B**) and muscle ILC2 express the IL-33 receptor (ST2, **Figure 3.1J and Supplemental Figure 3.1I-J**), we examined the responsiveness of muscle ILC2 to expand to exogenous IL-33. Systemic administration of IL-33 in 2-wk-old mdx mice caused a significant increase in muscle ILC2s two weeks after the initial dose was provided (**Figure 3.2F**). As reported previously, IL-2 complex (IL-2c) also increased muscle ILC2 (Nussbaum et al., 2013; Roediger et al., 2013; Van Gool et al., 2014) and further potentiated muscle ILC2 expansion when used in combination with IL-33 (cIL-33, **Figure 3.2F**). Because muscle Tregs also express ST2 and expand in response to exogenously administered IL-33, we crossed mdx mice with T cell receptor alpha chain (TCR $\alpha$ )-deficient mice (mdx.TCR $\alpha$ <sup>-/-</sup>), which lack all  $\alpha\beta$  T cells, including Tregs, to eliminate any competitive mechanism that would obscure the effect of exogenous IL-33 on muscle ILC2s. Systemic administration of IL-2c as well as IL-33 in 2-wk-old mdx.TCR $\alpha$ <sup>-/-</sup> mice caused a significant increase in muscle ILC2s two weeks after the initial dose was provided (**Figure 3.2G**). Similar to mdx mice, we found treatment with IL-2c in combination with IL-33 further increased the number of ILC2s in skeletal muscle. These data show that IL-2 and IL-33 are potent activating signals for skeletal muscle ILC2s.

### **ILC2s promote eosinophilia in dystrophic muscle**



Eosinophilia is a feature of chronic muscle inflammation in mdx mice (Cai et al., 2000; Capote et al., 2016; Wehling-Henricks et al., 2010, 2008, 2004). Flow cytometry analysis of muscle single-cell suspensions showed that the frequency and absolute number of eosinophils were significantly elevated in mdx mice (**Supplemental Figure 3.2A-B**). Eosinophil numbers were greatest at 4 weeks of age when myofiber necrosis is most prominent in mdx mice, and although they declined in number by 12 weeks, eosinophils remained significantly higher than age-matched controls (**Supplemental Figure 3.3B**). Given that ILC2s are known to regulate eosinophils, we tested the hypothesis that the expansion of muscle eosinophilia in dystrophic mice is regulated by ILC2s. Mdx mice were crossed with the YetCre13-DTA<sup>+</sup> mouse model (April E. Price et al., 2010), in which the IL-13-mediated expression of diphtheria toxin A (DTA gene) causes the deletion of IL-13-producing cells, including ILC2s (**Figure 3.1K-N**). Muscle ILC2s were reduced by ~85% in 4-wk-old, mdx.YetCre13-DTA<sup>+</sup> compared to DTA<sup>-</sup> littermate mdx mice (**Figure 3.3A-B**). The reduction in ILC2s was accompanied by a significant decrease in the frequency and absolute number of muscle eosinophils (**Figure 3.3C-D**). Further, we also find that treatment of DTA<sup>-</sup> animals with cIL-33 lead to an expansion of the frequency and number of ILC2s (**Figure 3.3E-F**) as well as eosinophils (**Figure 3.3G-H**). However, there was no expansion of eosinophils in the muscle of mice lacking ILC2s (DTA<sup>+</sup>) (**Figure 3.3H**), demonstrating that ILC2s play a significant role in promoting skeletal muscle eosinophilia.

### **Muscle ILC2 are a source of eosinophilia-promoting factors**

Activated ILC2s have been shown to promote eosinophilia in other tissues, in part by their production of IL-13 that induces the expression of eosinophilia promoting chemokines (Nussbaum et al., 2013; April E. Price et al., 2010). Next, we wanted to further understand the mechanism in which ILC2s regulate dystrophic muscle eosinophilia by first testing the hypothesis that ILC2s promote eosinophil chemotaxis. We used flow cytometry to evaluate the expression of chemokine receptors known to be expressed on eosinophils (Lee et al., 2012). We found that the main

receptors on 4-wk-old mdx skeletal muscle eosinophils were CCR3 and IL5r (**Supplemental Figure 3.2C**). To elucidate what factors were promoting muscle eosinophilia, we evaluated the expression of CCR3 ligands (Larose et al., 2017; Zlotnik and Yoshie, 2012) in 4-wk-old WT and mdx skeletal muscle (**Supplemental Figure 3.2D**). Our assessment revealed that CCL9, CCL7, CCL5, and IL5 are all upregulated in diseased muscle compared to WT. We further aimed to elucidate the cellular source of CCL5, CCL7, CCL9, by evaluating their expression in FACS-isolated CD45<sup>-</sup> (Non-immune cells), CD11b<sup>+</sup> (Myeloid) and ILC2s (Lin<sup>-</sup>KLRG1<sup>+</sup>) cells from 4-wk-old mdx skeletal muscle (**Figure 3.2I**). We found that muscle ILC2s produced both CCL5 and CCL9 but were not significant producers of CCL7. Further, although ILC2s were a source of these factors, the myeloid cell compartment (CD11b<sup>+</sup> cells) also produced almost the same or higher levels of CCL5 and CCL9, respectively.

To further understand how ILC2s contribute to the chemotaxis of eosinophils to skeletal muscle, we used RT-qPCR to measure CCL5, CCL7, CCL9, and IL-5 in the muscle of mdx.YetCre13 DTA<sup>+</sup> and DTA<sup>-</sup> littermate control mice following treatment with cIL-33 (**Supplemental Figure 3.2E**). Our analysis showed that the skeletal muscle expression of CCL5 was slightly increased in mice lacking ILC2s. Further, we found that treated DTA<sup>+</sup> mice had decreased expression of skeletal muscle IL-5 (**Supplemental Figure 3.2E**). Since IL-5 is an important mediator of eosinophil development, survival, migration, and proliferation (Rothenberg and Hogan, 2006; Yamaguchi et al., 1988), we next evaluated its production by skeletal muscle ILC2s using the mdx.ILC2 reporter mice, where an endogenous IL-5 promoter drives tdTomato expression. We found that compared to WT, dystrophic muscle ILC2s expressed more IL-5 at both 4 and 12 weeks, as displayed by an increased MFI (**Figure 3.2J**). Together these data suggest that muscle ILC2s contribute to the promotion of muscle eosinophilia through both the production of eosinophil survival factors (IL-5) and chemokines (CCL5, CCL9).

### **Eosinophils in dystrophic muscle pathology**

We next aimed to further reveal the role of eosinophils in mdx pathology. Although eosinophils have been shown to promote regeneration in acute settings, their role in dystrophic muscle has been more elusive. Eosinophil derived factors promote myofibrillar degradation (Sugihara et al., 2001) and myofiber lysis (Wehling-Henricks et al., 2008) in dystrophin-deficient mice and eosinophils contain granule proteins (Noguchi et al., 1992; Wehling-Henricks et al., 2008) that promote fibrosis, a secondary pathogenic feature of DMD patients (Kharraz et al., 2014). In contrast, more recent studies have demonstrated that eosinophils do not promote muscle injury in mdx mice (Sek et al., 2019). To further define the role of eosinophils in DMD pathology, we histologically assessed the colocalization of eosinophils with regenerating or injured myofibers in WT and mdx muscle. To evaluate regenerating myofibers, 4-wk-old WT and mdx mouse quadriceps cross-sections were stained with antibodies against embryonic myosin heavy chain (eMyHC), a developmentally restricted gene expressed in newly regenerated fibers (Schiaffino et al., 2015). Cross-sections were also stained with Siglec-F to identify eosinophils (Zhang et al., 2004). Compared to WT mice, mdx cross-sections displayed a larger degree of regeneration, and more eosinophils were observed in these areas (**Figure 3.4A**). To assess muscle injury, mice were injected with Evans blue dye (EBD), a serum albumin binding dye that is taken up by injured fibers (Hamer et al., 2002). WT cross-sections displayed no injured fibers as well as very few eosinophils (**Figure 3.4B**). Although mdx sections had more injury present, very few eosinophils were found near these injured fibers (**Figure 3.4B**). More eosinophils were observed in regenerating versus injured areas of mdx muscle, suggesting that eosinophils are associated with regenerative responses and not those that promote injury during muscular dystrophy.

Since eosinophils have been shown to promote fibrosis in other chronic diseases, we further aimed to evaluate their potential role in regulating fibrosis during muscular dystrophy. Since mdx mice do not show extensive amounts of fibrosis until very late stages of disease, we adopted previously described protocols that utilize chronic exercise to accelerate the fibrotic

phenotype (Pessina et al., 2014). Adult mdx mice lacking eosinophils, mdx.dbIGATA<sup>+</sup>, as well as littermate controls (mdx.dbIGATA<sup>-</sup>), were ran on a treadmill three times per week for a total of 1 month then analyzed following seven days of rest (see Materials and Methods). To assess fibrosis, diaphragm cross-sections were stained with antibodies against collagen 1 $\alpha$  and the percent area that was collagen positive was calculated. We found that compared to mdx mice that have eosinophils, those lacking these cells had a similar amount of collagen present (**Figure 3.4C-D**). These data suggest that eosinophils may not regulate fibrosis in dystrophic muscle.

We also aimed to assess whether eosinophils play a further role in regulating muscle function. Voluntary mouse movement assessed by open field activity monitoring is a method to evaluate muscle function, and mdx mice display decreased activity compared to their wildtype counterparts. This effect is even more pronounced following exercise (Gibbs and Crosbie-Watson, 2017). In the fourth week of the chronic exercise regimen, mouse activity was monitored immediately following the treadmill run using metabolic cages. We observed that for the first 3 hours following exercise, mdx.dbIGATA<sup>-</sup> mice displayed less activity than mdx.dbIGATA<sup>+</sup> littermate controls. Interestingly, this difference was decreased by 12 hours post-run, and mice in both groups displayed the same amount of activity by 24 hours post-run (**Figure 3.4E**). Although not significant, we also found that the area under the curve of the movement for 24 hours post-run was also decreased (**Figure 3.4F**). These data suggest that dystrophic mice without eosinophils have greater fatigue following exercise. We further assessed muscle function by measuring the tetanic force generated by the tibialis anterior (TA) muscle in vivo. We found that there was no difference in force production between mdx.dbIGATA<sup>+</sup> and mdx.dbIGATA<sup>-</sup> mice, indicating that the observed decreased activity following exercise was not due to altered strength of the muscle.

As mice in these experiments were exercised for weeks, we predicted that the myofibers had been stimulated to adopt a more pro-endurance phenotype. Myofibers associated with increased endurance are fast-twitch, type 2 fibers, which can be further categorized based on

their energy metabolism (e.g., oxidative vs. glycolytic). To test this, we evaluated the myofiber type distribution in the soleus of mdx.dbIGATA<sup>+</sup> and mdx.dbIGATA<sup>-</sup> mice following chronic exercise. The soleus, which is primarily composed of slow-twitch type 1 fibers, was evaluated to better observe transitions to fast-twitch type 2 fibers (Talbot and Maves, 2016). Solei cross-sections were stained with antibodies against isoform-specific myosin heavy chains to detect type 1 (slow, oxidative), type IIa (Fast, oxidative), and type IIb (fast, glycolytic) fibers (Talbot and Maves, 2016). Myofibers negative for these myosin heavy chain isoforms are classified as type 2x fibers (**Figure 3.4H**). Our analysis revealed no difference in the myofiber type distribution regardless of the presence of eosinophils (**Figure 3.4I**). To further understand if eosinophils contribute to metabolic changes that may not result in changes to myofiber type distribution, we used RT-qPCR to evaluate the expression of metabolic genes in the soleus of these animals following chronic exercise (**Figure 3.4J**). Genes associated with glycolysis, including the glucose transporter Glut4, as well as hexokinase 2 (Hk2) and phosphofructokinase (Pfk), which are involved in glucose metabolism, were evaluated (Richter and Hargreaves, 2013). We also measured the expression of genes associated with oxidative metabolism, including carnitine palmitoyltransferase 1A (Cpt1a) and Peroxisome proliferator-activated receptor- $\gamma$  coactivator-1  $\alpha$  (PGC1 $\alpha$ ). Our analysis revealed however, that the presence or absence of eosinophils did not regulate the expression of these genes following chronic exercise (**Figure 3.4J**). All together, these data suggest that eosinophils do not regulate myofiber type or energy metabolism in dystrophic muscle.

### **Muscle ILC2s do not regulate muscle macrophages**

Recent studies have also implicated ILC2s in promoting the alternative activation of macrophages (Molofsky et al., 2013). As different activation states of macrophages can promote muscle injury or promote efficient regeneration, we assessed whether ILC2s play a role in

regulating their activation in dystrophic muscle. We used flow cytometry to evaluate the number and phenotype of macrophages in dystrophic muscle deficient in ILC2s (mdx.YetCre13-DTA<sup>+</sup> mice) compared to WT littermate controls (DTA<sup>-</sup>). We found that the proportion and number of skeletal muscle macrophages were not altered in DTA<sup>+</sup> mice compared to littermate controls (DTA<sup>-</sup>) (**Supplemental Figure 3.3A and 3.3B**). We also evaluated various subpopulations of macrophages to assess classically activated, m1-like (Ly6c<sup>+</sup>) cells associated with injury and M2-like cells (CD206<sup>+</sup>) shown to promote repair and regeneration. Macrophages are heterogeneous and highly plastic cells, and these traditional markers don't always completely describe all populations in muscle. To globally characterize all macrophage populations, we also quantified macrophages negative for both markers, which were designated double negative (DN). Our analysis showed that the number of cells composing each macrophage population was not affected by the presence or absence of ILC2s in dystrophic muscle (**Supplemental Figure 3.3C-E**).

We used an alternative strategy to evaluate the ILC2-mediated regulation of skeletal muscle macrophages by measuring them following treatment with exogenous cytokines that preferentially expand ILC2s *in vivo*. To delineate between ILC2- and T cell-mediated macrophage regulation, mdx.TCR $\alpha$ <sup>-/-</sup> mice were treated with IL-2c, IL-33, cIL-33 and isotype control antibodies. Cells from dissociated skeletal muscle were then assessed using flow cytometry. Although ILC2s were increased following treatment with IL-2c and to an even higher degree, cIL-33 (**Figure 3.2**), there was no change in the proportion or number of macrophages (**Supplemental Figure 3.3F and 3.4G**). Interestingly, the proportion, but not the number of total macrophages, were decreased in mice treated only with IL-33 (**Supplemental Figure 3.3F and 3.3G**). Further, there was no change in the number of cells comprising macrophage subpopulations in any treatment combination. Taken together, these data suggest that ILC2s do not regulate macrophage activation in dystrophic muscle.

## DISCUSSION

A common feature of muscle injury is the induction of type II innate immunity that shapes the quality and timing of skeletal muscle regeneration. Type II innate immunity in injured tissue is characterized by preferential expression of Th2-associated cytokines, IL-4, IL-5 and IL-13, and recruitment of M2-like macrophages and eosinophils. Although it is known that eosinophilia is a feature of in inflamed muscle in mdx mice, the mechanism regulating eosinophil recruitment to dystrophic muscle has not been elucidated. Here, we report that ST2-expressing ILC2s are present in healthy muscle and expand upon injury, indicating that they are a constituent of the muscle-resident immune cell niche, poised to respond to muscle injury. We also found that FAPs were the predominant source of IL-33, and exogenous IL-33 and IL-2c robustly expanded muscle ILC2s, which subsequently increased muscle eosinophils in dystrophic mice. Moreover, the deletion of ILC2s in mdx mice abrogated the IL-33-mediated expansion of eosinophils, showing that ILC2s are key regulators of muscle eosinophilia. The current study significantly advances our understanding of how type II innate immunity during muscle injury and regeneration is regulated by revealing that ILC2s are the principal regulators of muscle eosinophilia. Our findings highlight a novel FAP and ILC2 interaction, mediated by the ST2:IL-33 signaling axis, that promotes muscle eosinophilia during muscular dystrophy.

ILC2s are tissue-resident, innate lymphocytes activated by perturbations in tissue homeostasis and regulate type II innate immunity. We found that ILC2s are resident in skeletal muscle that expand following injury, and this expansion was associated with a concurrent increase in muscle eosinophilia. Muscle ILC2s did not express the IL-25 receptor (IL-17RB), nor did they expand in response to IL-25 treatment, suggesting that muscle ILC2s do not resemble the inflammatory ILC2s described in helminthic infection (Huang et al., 2015). Rather, muscle ILC2s expressed a canonical natural ILC2 phenotype (Huang and Paul, 2015), consistent with the notion that ILC2s regulate muscle homeostasis and regeneration. Exogenous IL-33 and IL-2

complex further increased the number of muscle ILC2s and the number of eosinophils in dystrophic muscle, and this expansion was lost when ILC2s were deleted in mdx mice. Notably, of the chemokine receptors interrogated in this study, CCR3 was the only receptor expressed by muscle eosinophils. CCR3 chemokines were elevated in dystrophic muscle compared to controls, implicating these factors, in conjunction with IL-5, as the pathophysiological regulators of eosinophilia in muscular dystrophy. Collectively, our findings indicate that muscle ILC2s promote type II innate immunity and muscle eosinophilia by producing IL-5 and eosinophil chemotactic factors to maintain skeletal muscle homeostasis.

Our findings contribute to the developing paradigm that type II innate immunity is activated during muscle regeneration by positioning ILC2s as key regulators of this response, namely by promoting eosinophilia. Given that type II innate immunity is required for muscle regeneration, our results also implicate an ILC2-eosinophil nexus that is critical in maintaining muscle homeostasis and promoting regeneration. In support of this hypothesis, muscle regeneration following cardio toxin-induced muscle injury was impaired in mice lacking eosinophils ( $\Delta$ dblGATA mice), owing to reduced FAP proliferation and their enhanced propensity to differentiate into adipocytes (Heredia et al., 2013). We also found that eosinophils preferentially localized to areas of active regeneration and were closely juxtaposed to eMyHC<sup>+</sup> regenerating myofibers (**Figure 3.3**). It is, however, important to consider the consequences of chronic activation of ILC2s and eosinophilia, in which case, these responses may become pathogenic. In this regard, chronic eosinophilia promotes muscle injury during muscular dystrophy; the depletion of eosinophils in mdx mice caused a reduction in myofiber injury (Wehling-Henricks et al., 2008). And although we did not observe a role for eosinophils in regulating fibrosis in these studies, additional experiments may be warranted since chronic eosinophilia promotes tissue fibrosis in other settings (Aceves, 2014). This is of the utmost importance as muscle fibrosis is a pathogenic feature of DMD.

ILC2s also promote the activation of M2-like macrophages, presumably through their production of IL-13, a potent type II cytokine that induces M2 macrophage activation (Molofsky et



al., 2013; April E. Price et al., 2010). Thus, we tested the hypothesis that muscle ILC2s promote M2 macrophage activation in dystrophic mice. Unexpectedly, we found that the expression of M2 macrophage markers or the number of M2-like macrophages were not affected in mdx mice lacking ILC2s. These results indicate that ILC2s or IL-13 do not regulate M2-like muscle macrophages in muscular dystrophy, and point at other type II cytokines as activators of M2 muscle macrophages. Eosinophils in acutely injured muscle expressed IL-4 and are required for regeneration, suggest that eosinophils similarly induce M2 macrophages in dystrophic muscle. However, our findings that the deletion of ILC2s caused a large decrease in muscle eosinophilia, but did affect M2 activation, argue against the hypothesis that eosinophils are a substantial source of IL-4 that promote M2-like macrophages during muscular dystrophy. Rather our data suggest that muscle macrophages acquire an M2-like program independent of type II innate immunity during muscular. An alternate mechanism guiding macrophage function in dystrophic muscle may center on the metabolic regulation of macrophage activation (Juban and Chazaud, 2017). Consistent with this postulate, studies performed in models of acute muscle injury have revealed that metabolism is a key determinant shaping macrophage activation and function during muscle injury and regeneration (Juban and Chazaud, 2017; Mounier et al., 2013).

Myeloid cell recruitment and activation of skeletal muscle-resident immune cells is a generalized response to various forms of muscle damage that is required for efficient muscle regeneration. However, continued and asynchronous muscle damage in muscular dystrophy dysregulates the inflammatory response, promoting chronic muscle inflammation that further exacerbates the severity and progression of muscular dystrophy. Our study reveals that ILC2s are a previously unappreciated facet of this response. The functional consequence of the muscle injury-induced regulation of ILC2s serves to induce type II innate immunity, specifically the recruitment of eosinophils, which is required for muscle regeneration. Our study also highlights a role for chemokines and IL-5 in the ILC2-mediated recruitment and/or local expansion of eosinophils in injured muscle. The preferential localization of eosinophils to sites enriched in

eMyHC<sup>+</sup> myofibers suggests that they preferentially promote regeneration. Further, our studies define an ILC2:eosinophil nexus that is regulated by FAPs, which induces a type II innate immune response to likely guide muscle regeneration. It will be equally important to determine the functional consequence of acute versus chronic activation of ILC2s and muscle eosinophilia on regeneration and the pathogenesis of muscular dystrophy. In summary, our studies highlight that ILC2s are the principal regulators of muscle eosinophilia following muscle damage, and reveal a potential therapeutic opportunity to target ILC2s and its eosinophil-tropic factors in muscle disorders.

**Table 3.1 Antibodies used for flow cytometry analysis.**

<b>Marker</b>	<b>Color</b>	<b>Vendor</b>	<b>Cat #</b>	<b>Clone</b>	<b>Final dilution</b>
Zombie	NIR	Biologend	423105	-	1:1000
IL-5R $\alpha$	APC	Biologend	153405	DIH37	1:100
CCR1	PE	Biologend	152507	S15040E	1:200
CCR3	APC-Fire750	Biologend	144521	J073E5	1:100
CCR5	A488	Biologend	107008	HM-CCR5	1:100
CCR2	BV605	Biologend	150615	SA203G11	1:100
Thy1	PerCP	Biologend	105322	30-H12	1:100
KLRG1	FITC	Biologend	138410	2F/KLRG1	1:100
CD45	APC	Biologend	103112	30-F11	1:800
CD4	BV605	Biologend	100548	RM4-5	1:500
ST2	PE	Biologend	145303	DIH9	1:200
IL17RB	PE	Biologend	146305	9B10	1:100
CD25	PE-Cy7	Biologend	102016	PC61	1:200
NK1.1	BV605	Biologend	108739	PK136	1:300
CD11b	PerCP-Cy5.5	Biologend	101228	M1/70	1:100
F4/80	PE	Biologend	123110	BMS	1:100
CD127	PE-Cy7	eBioscience	25-1271-82	A7R34	1:100
CD19	Pac-Blue	eBioscience	48-0193-82	eBio1D3	1:200
CD11b	Pac-Blue	eBioscience	48-0112-82	M1/70	1:200
CD11c	Pac-Blue	eBioscience	48-0114-82	N418	1:200
NK1.1	Pac-Blue	eBioscience	48-5941-82	PK136	1:100
CD3	Pac-Blue	eBioscience	48-0032-82	17A2	1:100
TCR $\beta$	Pac-Blue	eBioscience	48-5961-82	H57-597	1:100
GATA3	PE	eBioscience	12-9966-41	TWAJ	1:25
ROR $\gamma$ T	PE	eBioscience	12-69-81	B2D	1:300
IL-13	PE	eBioscience	25-7133-80	eBio13A	1:150
Siglec-F	BV421	BD	562681	E50-2440	1:150
CD11b	PerCP-Cy5.5	Biologend	101228	M1/70	1:100
F4/80	PE	Biologend	123110	BMS	1:100
Ly6C	FITC	eBioscience	128006	HK1.4	1:500
CD206	A647	Biologend	141712	C068C2	1:200

**Table 3.2 TaqMan probes used for gene expression analysis in mouse muscle.**

<b>Gene</b>	<b>Assay ID</b>
18s	Hs99999901_s1
IL-25	Mm00499822_m1
TSLP	Mm01157588_m1
IL-33	Mm00505403_m1
IL-5	Mm00439646_m1
IL-13	Mm00434204_m1
CCL3	Mm00441259_g1
CCL5	Mm01302427_m1
CCL7	Mm00443113_m1
CCL8	Mm01297183_m1
CCL9	Mm00441260_m1
CCL11	Mm00441238_m1
CCL24	Mm00444701_m1

**Table 3.3. Antibodies used for histology.**

<b>Antibody</b>	<b>Vendor</b>	<b>Cat #</b>	<b>Clone</b>	<b>Dilution</b>
<b>FAPs</b>				
Rat anti-mPDGFR $\alpha$	eBioscience	14-1401-81	APA5	1:300
Goat anti-mIL-33	R&D Systems	AF3626	Polyclonal	1:300
Donkey anti-rat-HRP	Jackson Immuno	712-035-153	N/A	1:100
Alexa Fluor 594 Tyramide	Invitrogen	B40957	N/A	1:100
Anti-goat Alexa Flour 488	Invitrogen	A-11055	N/A	1:200
<b>Fibrosis</b>				
Anti-rat Alexa Flour 488	Invitrogen	A21208	N/A	1:200
Sheep anti-Collagen 1 $\alpha$	R&D Systems	AF6220	Polyclonal	1:500
Anti-sheep Alexa Flour 594	Invitrogen	A11016	N/A	1:200
<b>Myofiber typing</b>				
Rabbit anti-Laminin	Sigma	L9393	Polyclonal	1:200
Anti-rabbit Alexa Flour 647	Invitrogen	A31573	N/A	1:200
Myosin Heavy Chain Type I	DSHB	BA-D5	BA-D5	1:200
Anti-Mouse IgG1 Cy2	Jackson Immuno	715-225-150	Polyclonal	1:400
Myosin Heavy Chain Type IIA	DSHB	SC-71	SC-71	1:200
Anti-Mouse IgG 2b DyLight 405	Jackson Immuno	115-475-207	Polyclonal	1:400
Myosin Heavy Chain Type IIB	DSHB	BF-F3	BF-F3	1:200
Anti-Mouse IgM DyLight 594	Jackson Immuno	115-516-020	Polyclonal	1:400

**Figure 3.1. Innate lymphoid responses in acutely-injured and mdx skeletal muscle.**

A) Experimental schematic of cardiotoxin (CTX)-injury in 8-week-old C57/BL6 mice (Top) and representative hematoxylin and eosin-stained tibialis anterior cross-sections (Bottom) in pre-injured (Pre Inj.) and days 1, 4 and 7 following injury. Scale bar= 100 $\mu$ m. n=5-6. B) Representative flow cytometry plots used to interrogate (from live, single cells) innate lymphoid cell populations in CTX-injured muscle. Numbers are frequencies are of the parent population. (C-E) Quantification of flow cytometry showing the number (per gram of muscle) of CD45<sup>+</sup>Thy1<sup>+</sup>NK1.1<sup>+</sup>, and CD45<sup>+</sup>Thy1<sup>+</sup>lineage<sup>-</sup>KLRG1<sup>+</sup> and CD45<sup>+</sup>Thy1<sup>+</sup>lineage<sup>-</sup>Roryt<sup>+</sup> cells in uninjured muscle and on day 1, 4, and 7 post-injury. Uninj= uninjured. Lineage dump= CD19,CD11b,CD11c,TCR $\beta$ ,CD3. F) Gating strategy and representative flow plots of innate lymphoid cells (from live, single cells) in 4-week WT and mdx skeletal muscle. Lineage dump= CD19,CD11b,CD11c,TCR $\beta$ ,CD3, NK1.1. G-I) Quantification of cells as in F normalized to mass. n= 4 for each group. J) Representative histogram of common ILC2 markers on muscle Lin<sup>-</sup> cells of WT and mdx mice. Iso= Isotype/FMO. Modal= normalized to mode. CD4<sup>+</sup> cells from mdx mice serve as a control. K) Representative flow plots of IL-13 expression in ILC2s of WT and mdx muscle. L) Percent of ILC2s that express IL-13. M) Number per gram of IL-13-expressing ILC2s. N) representative histogram (left) and quantification of MFI (right) of IL-13 expression in Lin<sup>-</sup> KLRG1<sup>+</sup> cells of WT (grey) and mdx (clear) mice. Light grey peak= Isotype control. n= 3-4. \*p<0.05, \*\*p<0.01, \*\*\*p<0.001, \*\*\*\*p<0.0001 using an unpaired t-test with Welch's correction or a one-way ANOVA with Bonferroni post hoc analysis. Asterisks indicate statistical analysis compared to control (A-I).

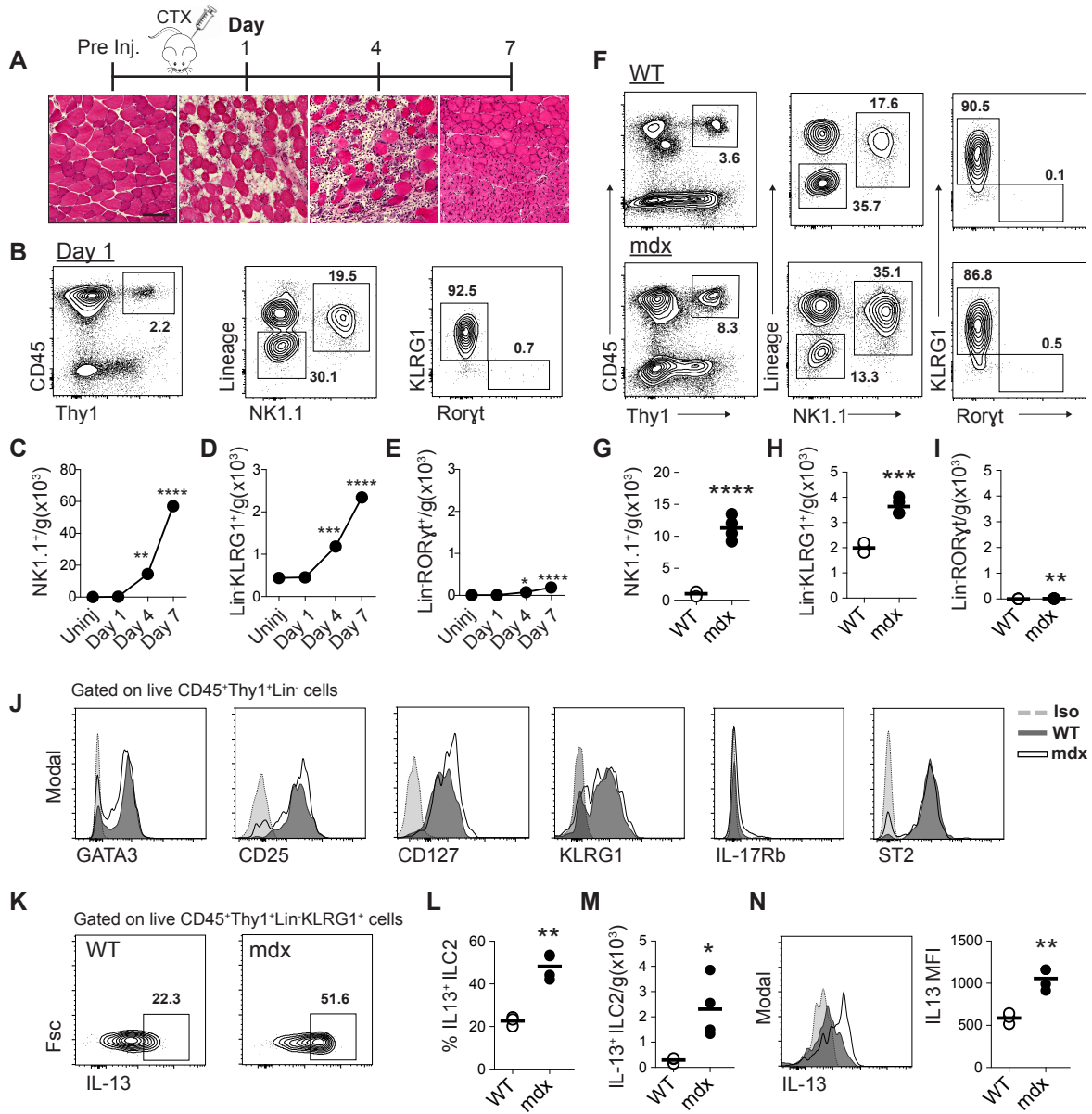


**Figure 3.2. Interleukin-33 is predominantly expressed by fibro/adipogenic progenitors and activates muscle ILC2s.**

A) Expression of known ILC2 activators in whole WT and mdx muscle at 4 weeks of age. AU= arbitrary units. B) Cq values associated with expression data in A. n= 8-10. C) Representative flow plot and gating strategy (from live, single cells) for populations sorted from mdx skeletal muscle at 4 weeks of age. D) IL-33 expression in cell populations as gated in C. E) PDGFR $\alpha$  and IL-33 immunofluorescence staining of mdx mouse quadriceps cross-sections at 4 weeks of age (Top) and flow cytometry histograms of marker expression on live PDGFR $\alpha$ <sup>+</sup> cells (Bottom) displayed as mean fluorescence intensity. modal= normalized to mode. F-G) ILC2 responses in mdx (F) and mdx.TCR $\alpha$ <sup>-/-</sup> (G) muscle following respective treatments shown as number per gram of muscle. n=6-11(F) and 3-5 (G). Iso= Isotype control, IL-2c= IL-2 complex, cIL-33= IL-2c + IL-33 and cIL-25= IL-25 + IL-2c. \*p<0.05, \*\*p<0.01 and \*\*\*\*p< 0.0001 using a one-way ANOVA with Bonferroni post hoc analysis.

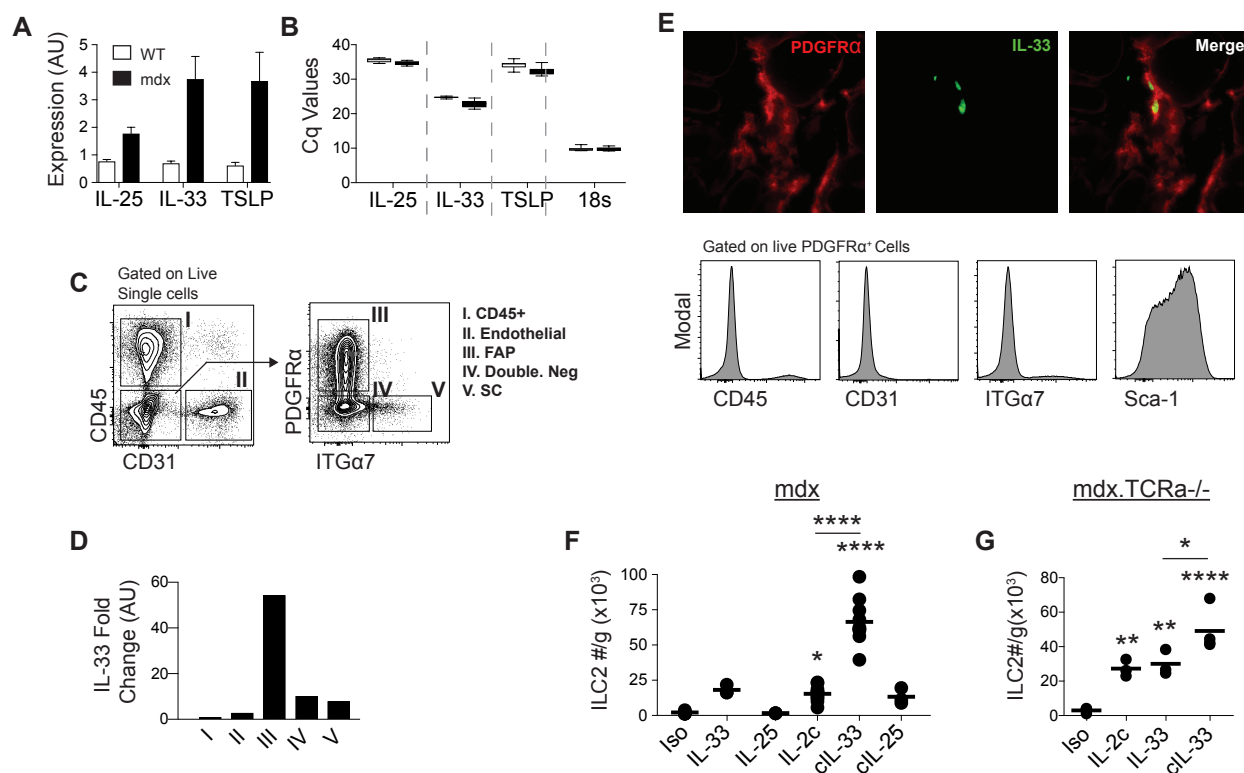




**Figure 3.3. ILC2s promote skeletal muscle eosinophilia.**

A) Tsnep plot showing 5000 Live, CD45<sup>+</sup>Thy1<sup>+</sup> cells from mdx.YetCre13 DTA<sup>-</sup> and DTA<sup>+</sup> mice. Grey= CD45<sup>+</sup>Thy1<sup>+</sup> cells, Red= ILC2s. B) Number per gram of muscle of ILC2s in DTA<sup>-</sup> (-) and DTA<sup>+</sup> (+) mice. C) Representative flow plots of cells from 4 week old mdx.Yetcre13 DTA<sup>+</sup> and DTA<sup>-</sup> mice (previously gated on live, single, CD11b<sup>+</sup>F4/80<sup>+</sup> cells) showing macrophages (F4/80+CD11b<sup>+</sup>Siglec-F<sup>-</sup>) and eosinophils (Eos; F4/80<sup>+</sup>CD11b<sup>+</sup>Siglec-F<sup>+</sup>). D) The number per gram of muscle of Eos in DTA<sup>-</sup> and DTA<sup>+</sup> mice. n= 3 (DTA-) and 4 (DTA+). Data representative of 1 experiment. E) Tsnep plot showing 5000 Live, CD45<sup>+</sup>Thy1<sup>+</sup> cells from mdx. YetCre13 DTA<sup>-</sup> and DTA<sup>+</sup> mice treated with IL-2c and IL-33 (cIL-33). F) Number per gram of muscle of ILC2s in - and + mice following treatment. G) Representative flow plots of cells from 4-week mdx.Yetcre13 DTA<sup>+</sup> and DTA<sup>-</sup> mice showing macrophages and eos as gated in C. H) The number per gram of muscle of eos in treated DTA<sup>-</sup> and DTA<sup>+</sup> mice. n= 4-10. I) Gene expression expressed as fold change of eosinophilia-promoting chemokines in CD45<sup>-</sup>, CD11b<sup>+</sup>, and ILC2s (Lin<sup>-</sup>KLRG1<sup>+</sup> cells) sorted from the skeletal muscle of 4-week mdx mice (n= 4 pooled mice). Data is normalized to CD45<sup>-</sup> cells. (J) Representative histogram and MFI quantification of ILC2s (CD45<sup>+</sup>Thy1<sup>+</sup>Lin<sup>+</sup>KLRG1<sup>+</sup>CD127<sup>+</sup> cells) from 4- and 12 wk-old WT and mdx Red5 reporter mice (TdTomato reporter driven by the IL-5 promoter) n= 11-12. \*p<0.05, \*\*\*p<0.001 and \*\*\*\*p<0.0001 using an unpaired t-test with Welch's correction or a one-way ANOVA with Bonferroni post hoc analysis. Asterisks indicate statistical analysis compared to control.

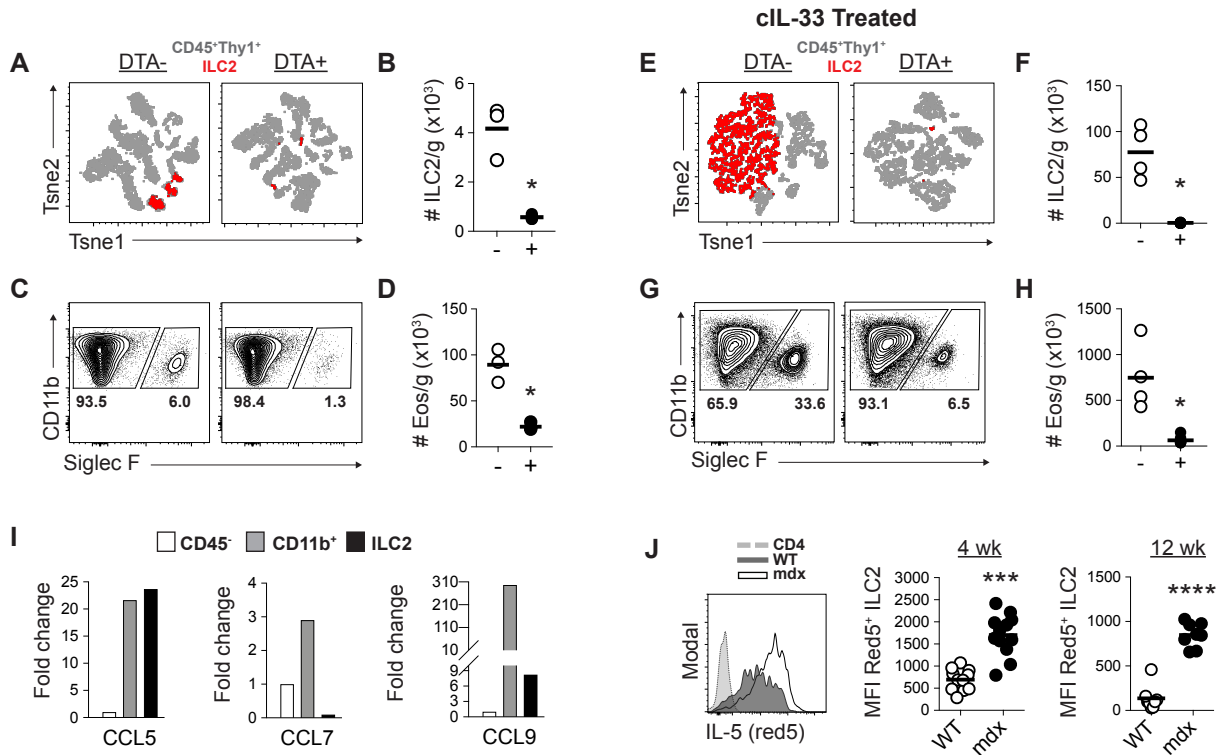
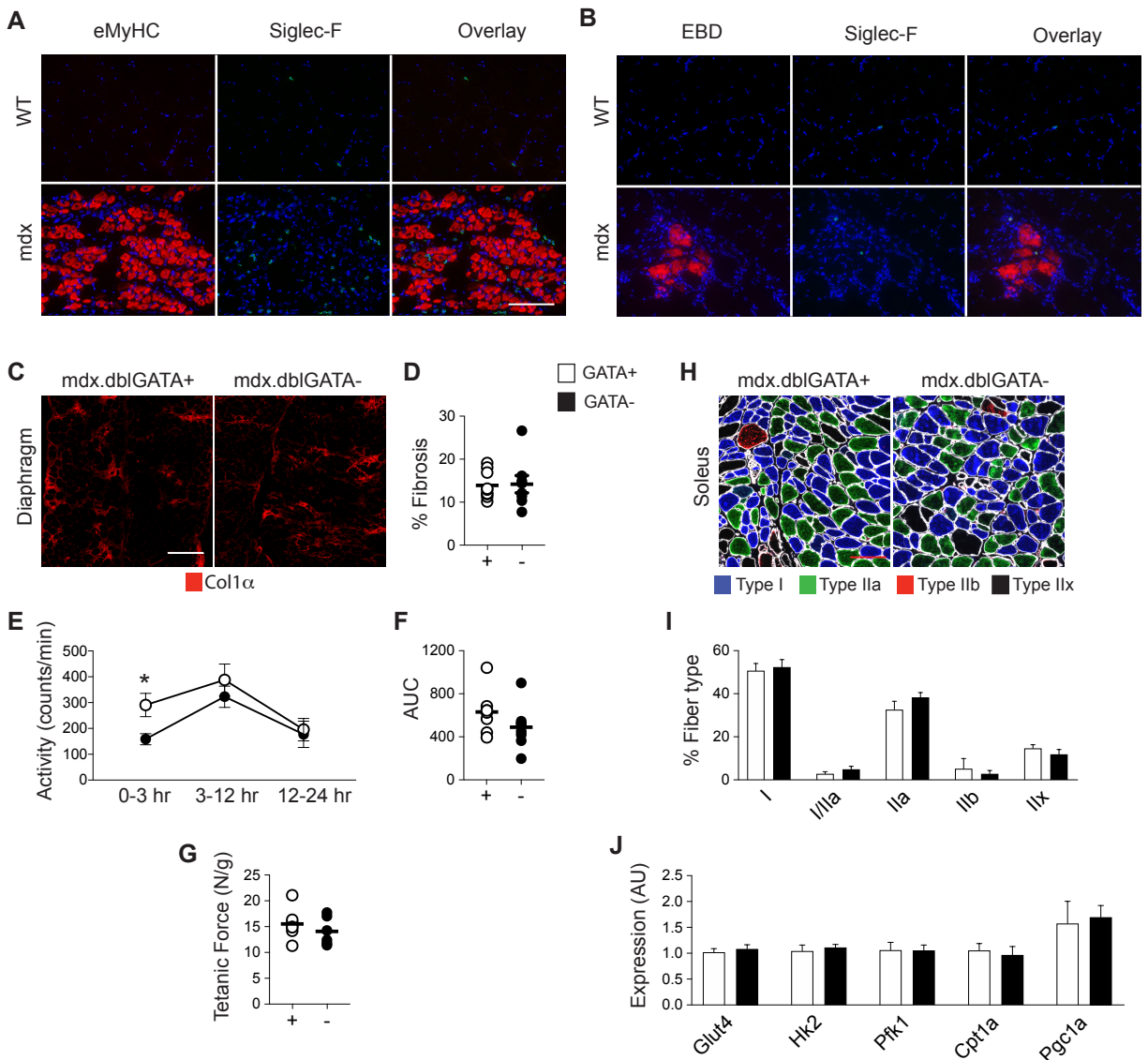


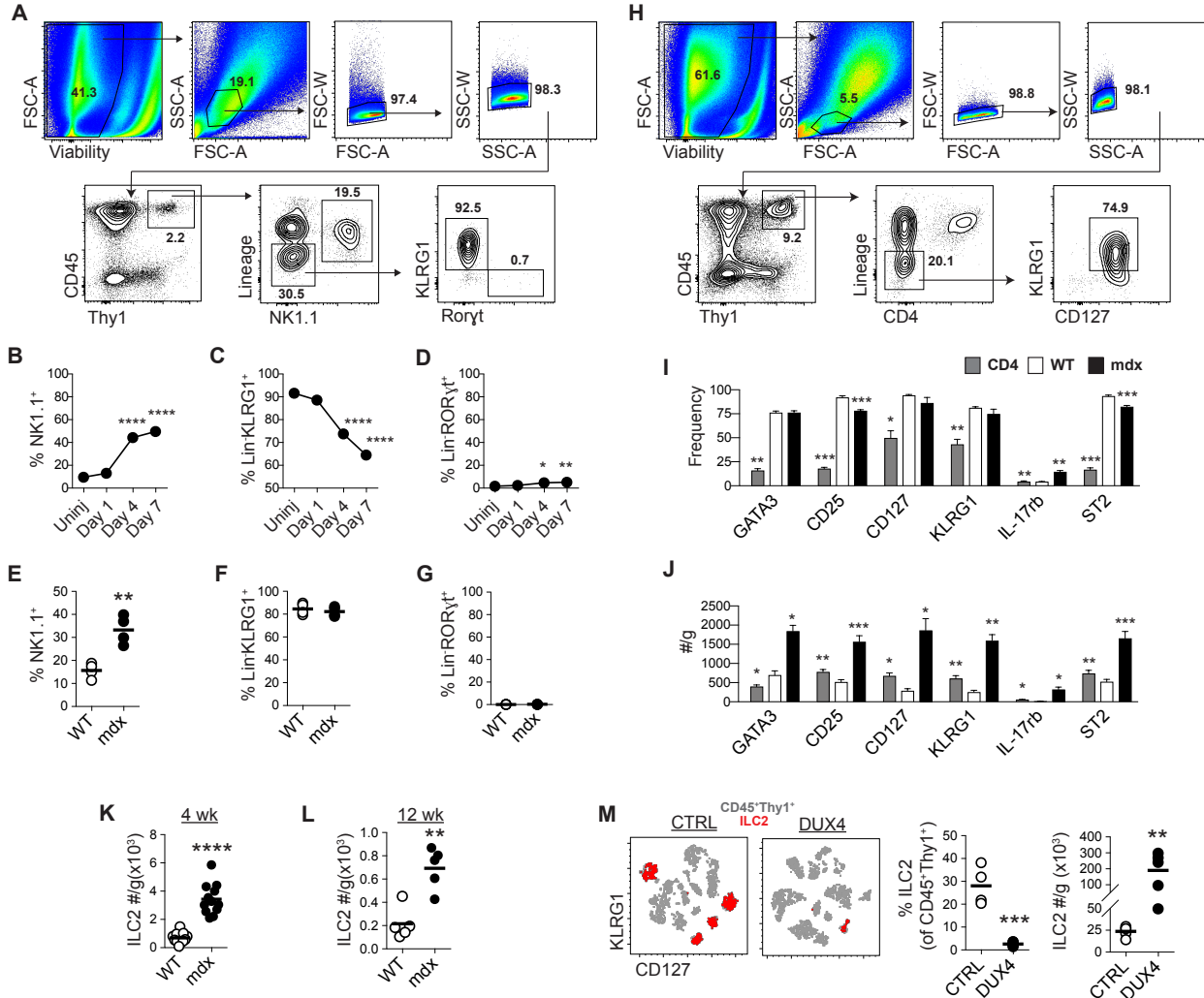
**Figure 3.4. Eosinophils during muscular dystrophy.**

A-B) Representative immunofluorescence staining of embryonic myosin heavy chain (eMyHC), Siglec-F, and Evans blue dye (EBD) in 4-week WT and mdx mouse quadriceps. C) Representative immunofluorescence staining of collagen 1 $\alpha$  (Col1 $\alpha$ ) in diaphragms of 6-7 month of mdx.dblGATA<sup>+</sup> (+) and mdx.dblGATA<sup>-</sup> (-) mice following 1 month running protocol. D) Quantification of percent area positive for Col1 $\alpha$  in diaphragms of mice in C. n=8. E) Activity of + (white) and - (black) mice in the 0-3, 3-12, and 12-24 hours (hr) immediately following running. F) Area under the curve (AUC) calculated for data in E. n=8. G) Maximum tetanic force produced by the tibialis anterior of + and - mice following running protocol. Values are Newtons (N) per gram (g) of muscle. n= 6-7. H) Representative immunofluorescence staining of isoform-specific myosin heavy chains in the soleus of mice following running protocol. I) Quantification of H showing the frequency of each myofiber type in the entire soleus. n=8. J) Fold expression in arbitrary units (AU) of metabolic genes in the contralateral soleus of mice in H-I. n= 8. \*p<0.05, using an unpaired t-test with Welch's correction.



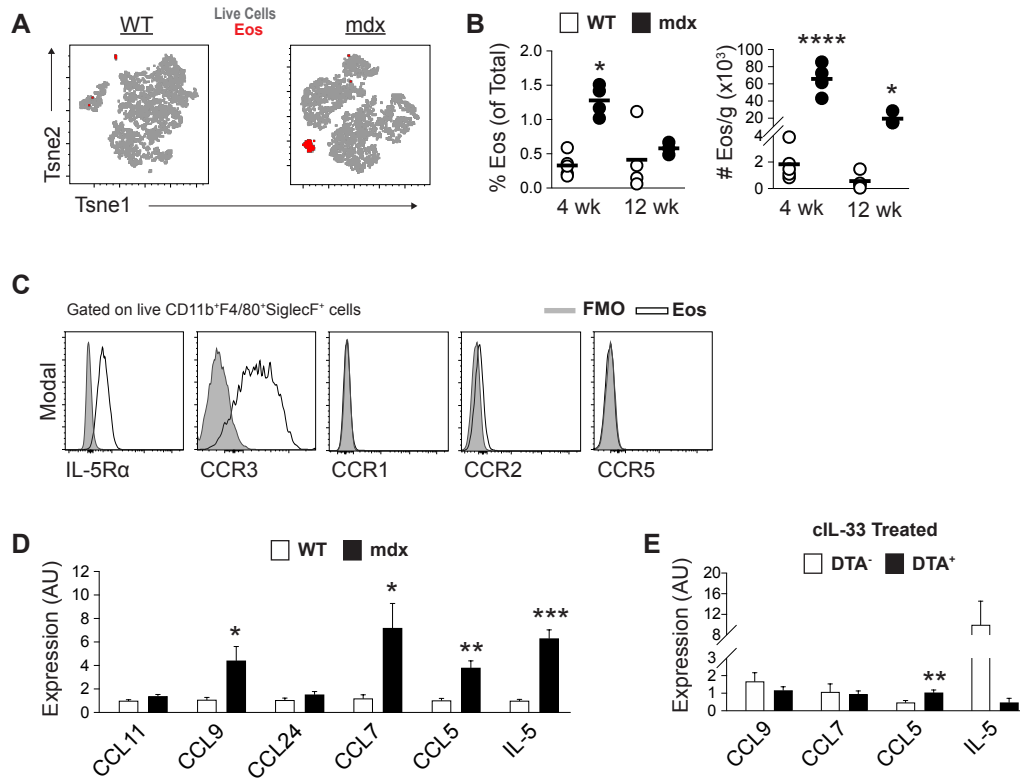
### Supplemental Figure 3.1. Evaluation of ILCs in skeletal muscle.

A) Gating strategy used to interrogate innate lymphoid cells in CTX-injured, WT, and mdx muscle at 4 weeks of age. Plots are representative of 4 pooled samples from CTX-injured muscle 1 day following injury. Numbers are frequencies of parent population. B-D) Percent (of parent populations) of innate lymphoid cells following CTX injury. E-G) Percent (of parent populations) of innate lymphoid cells in WT-injured and 4-week mdx skeletal muscle. H) Representative gating strategy for the interrogation of Lin<sup>-</sup> and ILC2s as quantified in I-L. I-J) Frequency (I) and number per gram (J) of Lin<sup>-</sup> or CD4<sup>+</sup> cells that express common ILC2 markers in WT and mdx mice at 4 weeks of age. CD4<sup>+</sup> cells from mdx mice serve as a control. K-L) Quantification of ILC2s in WT and mdx muscle at 4 and 12 weeks of age expressed as number of cells per gram. M) Tse plots showing 2000 live, CD45<sup>+</sup>Thy1<sup>+</sup> cells from control (CNTRL) and DUX4 overexpressing mice. Frequency (within live, CD45<sup>+</sup>Thy1<sup>+</sup> cells) and number per gram of muscle of ILC2s in control and DUX4 overexpressing muscle. n=4-5. Grey= CD45<sup>+</sup>Thy1<sup>+</sup> cells, Red= ILC2s. \*p<0.05, \*\*p<0.01, \*\*\*p<0.001, \*\*\*\*p<0.0001 using an unpaired t-test with Welch's correction or a one-way ANOVA with Bonferroni post hoc analysis.



**Supplemental Figure 3.2. Eosinophils and eosinophilia promoting factors in skeletal muscle.**

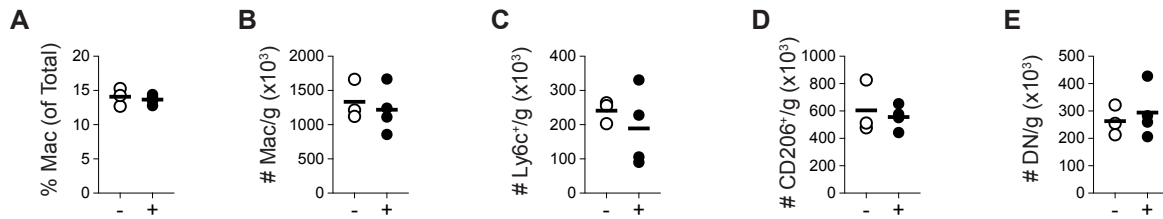
A) Tnsne plot showing 5000 live cells from WT and mdx mouse muscle at 4 weeks of age. Grey= all live cells, Red= eosinophils (Eos). B) The frequency (of total live cells) and number (per gram of muscle) of eos in the hind limb muscle of 4 and 12-wk-old WT and mdx mice. n= 3-5. C) Expression displayed as mean fluorescence intensity (MFI) for receptors on eosinophils (CD11b<sup>+</sup>F4/80<sup>+</sup>SiglecF<sup>+</sup> cells) from 4 week mdx muscle. n=5. D) Gene expression, in arbitrary units (AU), of CCR3 ligands expressed in WT or mdx muscle at 4 weeks of age. n= 6 for each group. E) Gene expression (AU) of chemokines in skeletal muscle from mdx.YetCre13 DTA<sup>-</sup> and DTA<sup>+</sup> mice treated with IL-2c and IL-33 (cIL-33).



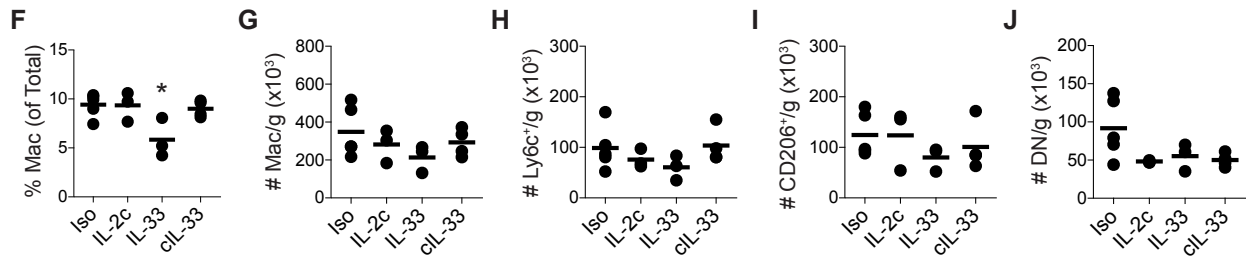
**Supplemental Figure 3.3. ILC2-mediated regulation of dystrophic muscle macrophages.**

A-E) Enumeration of flow cytometry data evaluating macrophages (Live single CD11b<sup>+</sup>F4/80<sup>+</sup>SiglecF<sup>-</sup>) cells from 4-wk-old mdx.YetCre13 DTA<sup>-</sup> (-) and DTA<sup>+</sup> (+) mice. A) Frequency of all macrophages (of live total cells). B) Number per gram of muscle macrophages. Number of Ly6c<sup>+</sup> macrophages (C), CD206<sup>+</sup> macrophages (D) and macrophages lacking both markers (double negative= DN) normalized to muscle mass. n= 3(-) and 4(+). F-J) Quantification of muscle macrophage form mdx.TCR $\alpha^{-/-}$  mice treated with exogenous cytokines. Iso= Isotype control, IL-2c= IL-2 complex and cIL-33= IL-2c + IL-33. Cells are defined as in A-E. n= 5 (Iso), 3 (IL-2c), 3 (IL-33), and 4 (cIL-33). Data pooled from 2 independent experiments. Statistics were performed using an unpaired t-test with Welch's correction or a one-way ANOVA with Bonferroni post hoc analysis; \*p<0.05.

mdx.Yetcre13



mdx.TCR $\alpha^{-/-}$  Cytokine Treatments



## CHAPTER 4: Summary and Conclusions

### Summary

The immune system has a well-established role in regulating the pathogenesis of DMD. Distinct facets of the immune system are shown to both exacerbate disease as well as promote regeneration. However, the regulation and exact mechanisms of these programs remain to be completely elucidated. This work was aimed at further understanding how type II immunity, which is classically associated with muscle regeneration, is regulated in dystrophic muscle by group 2 innate lymphoid cells (ILC2) (**Chapter 3**). ILC2s were increased and activated in dystrophic muscle and produced the type II cytokines IL-5 and IL-13. The regulation of these cells in muscle was also evaluated, and we found that IL-33 was the predominant alarmin expressed in skeletal muscle and is produced by FAPs. Importantly, we found that muscle ILC2s responded to exogenous IL-33, providing a method to expand these cells *in vivo* to further understand their role in DMD. Using exogenous cytokine treatment as well as ILC2-ablated mice, we found that ILC2s are potent regulators of skeletal muscle eosinophilia. Interestingly, the manipulation of ILC2s *in vivo* did not affect the number or phenotype of skeletal muscle macrophages, suggesting that ILC2s do not regulate dystrophic muscle macrophages.

We also aimed to understand the role that ILC2s play in regulating DMD pathology (**Chapter 3**). As we found that ILC2s are major drivers of muscle eosinophilia in mdx mice, we took the approach to evaluate skeletal muscle pathology in dystrophic mice with or without eosinophils. We also performed muscle function assays, and found that mice deficient in eosinophils became more exhausted following exercise compared to eosinophil-competent mice. However, the mechanism for this phenotype has yet to be determined. We further evaluated the force production, myofiber type distribution, and the muscle expression of metabolic genes in these experiments, but found no difference between mice with or without eosinophils. Further, we

also found that eosinophils were co-localized to areas of active regeneration, suggesting that these cells may play a role in promoting this response.

In addition to evaluating the ILC2-mediated regulation of type II immunity in dystrophic muscle, another arm of this dissertation focused on the generation of a method that allows for the accurate histological assessment of skeletal muscle morphology in a high-throughput manner (**Chapter 2**). QuantiMus is a software plugin for the histological analysis software, Flika, and it allows for the histological analysis of entire muscle cross-sections, a feature that is rare in other analysis software. QuantiMus uses machine learning algorithms to accurately and rapidly define myofibers in muscle cross-sections, which allows for further downstream analysis. QuantiMus is a complete tool that allows for the analysis of many morphometric features including, myofiber size, centrally-nucleated fibers, and the intracellular expression of any fluorescently-detected protein (e.g., Evan's blue dye to assess injury or embryonic myosin heavy chain to evaluate regeneration). QuantiMus has already been cited by 3 papers, indicating that this method is already having an impact in the field of muscle physiology.

### **ILC2s in muscle regeneration**

In this study, we found that ILC2s promote muscle eosinophilia, and our data show that eosinophils are enriched in regenerating areas of skeletal muscle, but are found in very low numbers in injured sites (**Figure 3.4A and 3.4B**). This is surprising and contradictory to other studies, which showed that eosinophils promote myofiber lysis (Wehling-Henricks et al., 2008). A more recent study suggested that eosinophils do not drive dystrophic muscle pathology in mdx mice (Sek et al., 2019), although the results of one study cannot fully evaluate the features of muscular dystrophy in its entirety. This study in combination with our findings indicate that the role of eosinophils, and the indirect role of ILC2s, in regulating dystrophic muscle pathology is likely redundant so that when absent from the muscle, other cell types can perform similar functions. This factor most likely explains the absence of a clear phenotype in eosinophil depleted muscle.

Our data showing the association of eosinophils with regeneration suggests that these cells may promote regeneration. This hypothesis requires further testing, but it provides another potential role for eosinophils in DMD. Further, this postulation is supported by studies conducted in acute injury models, which demonstrate that eosinophils promote muscle regeneration through an IL-4 mediated interaction with FAPs (Heredia et al., 2013).

We propose that ILC2s promote muscle regeneration indirectly by promoting eosinophilia, and that ILC2s have a direct role in promoting this response through interactions with muscle stem cells. ILC2s have been shown to produce amphiregulin (Areg), a growth factor that binds to epidermal growth factor receptor (EGFR) and promotes repair. Importantly, Areg has also been shown to promote myogenic differentiation of myofiber progenitors *in vitro* (Burzyn et al., 2013). However, the role of ILC2-derived Areg in skeletal muscle repair and regeneration is still under investigation. Taking into account the pro-regenerative effects from Treg-derived Areg, it can be postulated that these cells also play a pro-regenerative role following muscle injury. We found that ILC2s are a prominent source of Areg (**Figure 4.1A**) and that muscle progenitors (MSCs and FAPS) express EGFR (**Figure 4.1B**), suggesting a direct ILC2-muscle progenitor interaction. Further, we found that Areg was increased in mdx mice following treatment with cIL-33 (**Figure 4.1C**), which correlates with increased ILC2 numbers in the muscle (**Figure 3.2F**). Together these data indicate that ILC2s may also directly promote regeneration through interactions with muscle progenitors, and future studies will be aimed at testing this hypothesis.

### **ILC2s in skeletal muscle fibrosis**

In these functional studies, we found that dystrophic mice in which eosinophils were depleted had the same amount of collagen (i.e., fibrosis) in the diaphragm as control mice following a chronic exercise regimen that promotes fibrosis (**Figure 3.4C**) (Pessina et al., 2014). Since we showed that ILC2s promote skeletal muscle eosinophilia, we could conclude that ILC2s do not promote muscle fibrosis, at least in an eosinophil-dependent manner. Importantly, the



direct role of ILC2s in skeletal muscle fibrosis needs to be tested before we can draw further conclusions as to their role. This may be tested by evaluating collagen content (i.e., fibrosis) in the muscles of mdx.ILC2 deleter mice and littermate controls that have intact ILC2s. Previous studies show conflicting evidence as to the role of ILC2s in fibrosis, making it challenging to predict the role of these cells in muscle fibrosis. For example, a study by Gonzalez-Polo et al. showed that liver ILC2 numbers and activation are positively correlated with more severe liver fibrosis in patients, and that plasma levels of IL-33 are increased in cirrhotic patients (Gonzalez-Polo et al., 2019). Similarly, other studies conducted in mice have shown that the antibody-mediated depletion of ILC2s attenuates liver fibrosis (Mchedlidze et al., 2013). However, other reports have shown that IL-2c and IL-33 treatment, which caused the *in vivo* expansion of ILC2s and Tregs, was associated with decreased fibrosis in a mouse model of kidney injury (Sabapathy et al., 2019). Taken together, these studies indicate that the role of ILC2s in fibrosis is tissue and disease dependent, which needs to be considered when assessing dystrophic muscle.

### **ILC2-mediated regulation of dystrophic muscle macrophages**

One critical aspect of type II immunity is the activation of alternatively activated macrophages, which are polarized by signals including IL-4 and IL-13, which both bind the same receptor subunit. Since ILC2s are potent secretors of IL-13, we hypothesized that ILC2s promote the activation of M2-like macrophages. In support of this hypothesis, other studies have shown a role for ILC2s in promoting the alternative activation of macrophages. For example, adoptive transfer of ILC2s into mice with renal ischemic/reperfusion injury induced the activation of M2-like macrophages, which attenuated renal injury (Mchedlidze et al., 2013). In addition, ILC2s suppress IL-1 $\beta$  secretion in macrophages (Omata et al., 2018) and promote the skewing of bone marrow-derived macrophages to an M2-like phenotype *in vitro* (Besnard et al., 2015). However, our findings demonstrated that ILC2s do not regulate the number or phenotype of macrophages in dystrophic muscle (**Supplemental Figure 3.3**). Importantly, macrophage heterogeneity is more

complex than previously described, and the M1/M2 subsets only represent extreme phenotypes on a broad continuum of activation (Sica and Mantovani, 2012). Moreover, the absence of specific markers for distinct macrophage populations limits the sensitivity of flow cytometric analysis for further discrimination of these cell subsets.

To circumvent this limitation and better interrogate these cells, we used single-cell RNA sequencing as an unbiased approach to assess the transcriptional profiles of skeletal muscle macrophages (**Figure 4.2A**). Cells were grouped based on gene expression profiles, revealing six distinct populations of macrophages in the skeletal muscle (**Figure 4.2B**). Further, we found that some distinct clusters were found almost exclusively in mdx (clusters 0 and 2) or WT (cluster 1) muscle (**Figure 4.2B**), further suggesting distinct functions. Cluster 0 had high expression of genes that, when chronically activated, have been shown to promote fibrosis in skeletal muscle (**Figure 4.2C**). For example, osteopontin (*Spp1*) has been shown to promote muscle regeneration (Uaesoontrachoon et al., 2008), but in chronic injury setting like dystrophic muscle, may promote fibrosis (Vetrone et al., 2009). Similarly, galectin 3 (*Lgals3*) has been shown to promote fibrosis in several settings (Henderson et al., 2008; Nishi et al., 2007) and is highly expressed in macrophage cluster 0. Together, these data reveal dystrophic-muscle specific populations of macrophages that we predict may promote fibrosis in DMD. Future directions will next to test this hypothesis as well as further investigate the potential ILC2-mediated regulation of these distinct macrophage populations.

**Figure 4.1. Amphiregulin expression in dystrophic muscle.**

A) The gene expression of amphiregulin (Areg) and epidermal growth factor receptor (EGFR) in cells sorted from 4-wk-old mdx mouse muscle. Expression is normalized to CD45- (A) or mac (B). Mac= Macrophages, MSCs= muscle stem cells (i.e., Satellite cells), FAPS= Fibro/adipogenic progenitors. C) The expression of Areg in mdx mouse hamstring following treatment with isotype control (Iso), IL-2 complex (IL-2c), or IL-2c in combination with IL-33 (cIL-33). n= 6-9.

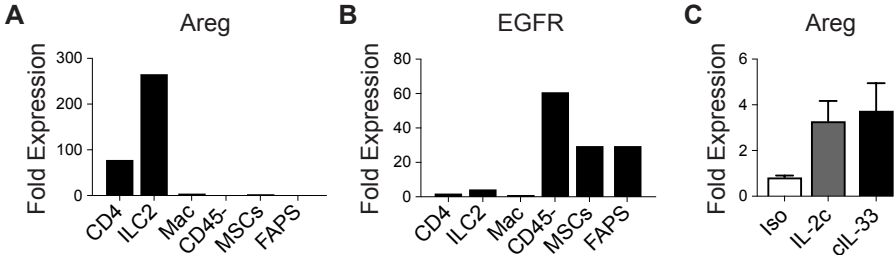
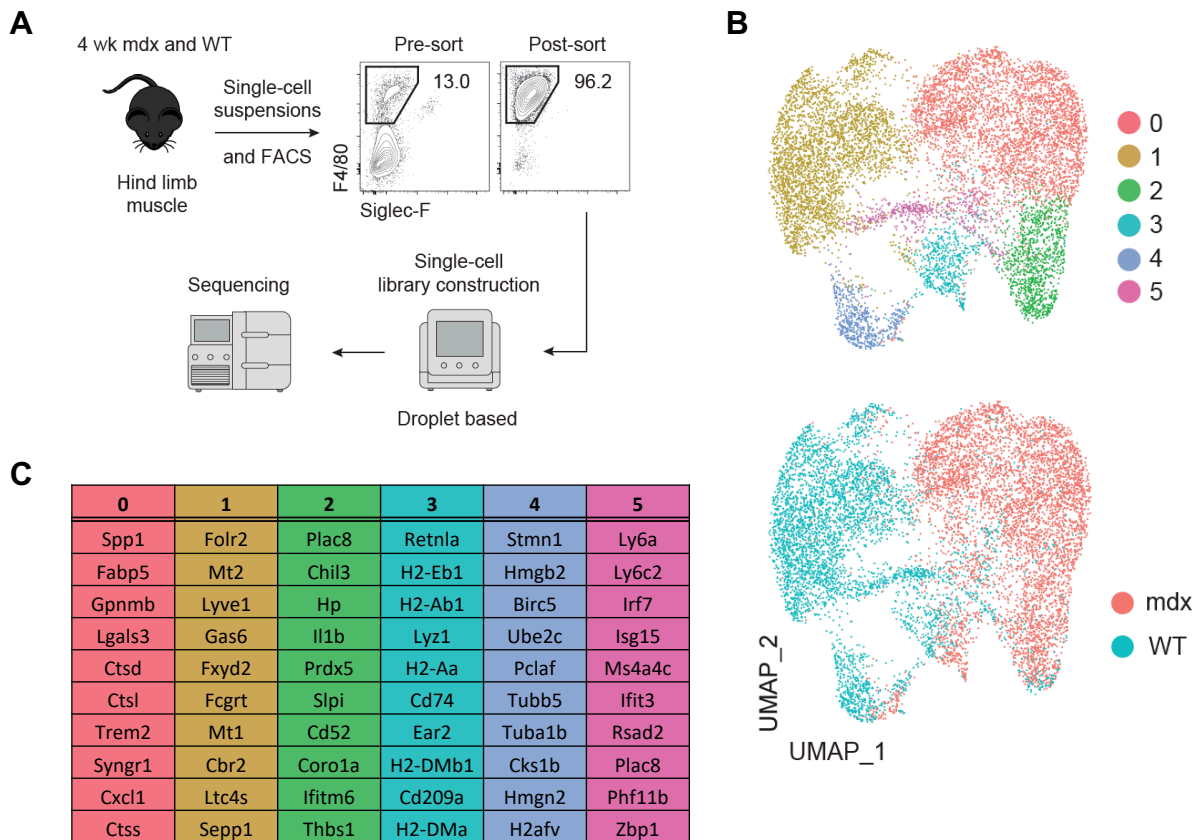


**Figure 4.2. Single-cell RNA sequencing of muscle macrophages.**

A) Experimental schematic of the single-cell sequencing of muscle macrophages. Skeletal muscle macrophages (Live, single, CD11b<sup>+</sup>F4/80<sup>+</sup>Siglec-F<sup>-</sup> cells) from WT and mdx mice were FACS-isolated and sequenced at a single-cell resolution using the 10x Genomics Chromium platform. B) UMAP plots were generated using a non-linear dimensionality reduction analysis algorithm (Seurat R package) to show macrophage (WT and mdx) populations grouped by gene expression (Top) or by genotype (Bottom). C) Top 10 differentially expressed genes in each cluster of B. Each dot represents one cell.



## REFERENCES:

- Aceves, S.S., 2014. Remodeling and fibrosis in chronic eosinophil inflammation. *Dig. Dis.* <https://doi.org/10.1159/000357004>
- Adamiak, K., Duch, P., Ślot, K., 2016. Object Classification Using Support Vector Machines with Kernel-based Data Preprocessing. *Image Process. Commun.* 21, 45–53. <https://doi.org/10.1515/ipc-2016-0015>
- Agbulut, O., Noirez, P., Beaumont, F., Butler-Browne, G., 2003. Myosin heavy chain isoforms in postnatal muscle development of mice. [https://doi.org/10.1016/S0248-4900\(03\)00087-X](https://doi.org/10.1016/S0248-4900(03)00087-X)
- Alam, R., Stafford, S., Forsythe, P., Harrison, R., Faubion, D., Lett-Brown, M.A., Grant, J.A., 1993. RANTES is a Chemotactic and Activating Factor for Human Eosinophils'. *J. Immunol.* 150, 3442–3448.
- Allsop, K.G., Ziter, F.A., 1981. Loss of Strength and Functional Decline in Duchenne's Dystrophy. *Arch. Neurol.* 38, 406–411. <https://doi.org/10.1001/archneur.1981.00510070040004>
- Antiga, E., Kretz, C.C., Klemmt, R., Massi, D., Ruland, V., Stumpf, C., Baroni, G., Hartmann, M., Hartschuh, W., Volpi, W., Del Bianco, E., Enk, A., Fabbri, P., Krammer, P.H., Caproni, M., Kuhn, A., 2010. Characterization of regulatory T cells in patients with dermatomyositis. *J Autoimmun* 35, 342–350. <https://doi.org/10.1016/j.jaut.2010.07.006>
- Arnold, L., Henry, A., Poron, F., Baba-Amer, Y., van Rooijen, N., Plonquet, A., Gherardi, R.K., Bénédicte Chazaud, 2007. Inflammatory monocytes recruited after skeletal muscle injury switch into antiinflammatory macrophages to support myogenesis. *J Exp Med* 204, 1057–1069. <https://doi.org/10.1084/jem.20070075>
- Artan, Y., 2011. Interactive Image Segmentation Using Machine Learning Techniques. 2011 *Can. Conf. Comput. Robot Vis.* 264–269. <https://doi.org/10.1109/CRV.2011.42>
- Banks, G.B., Combs, A.C., Odom, G.L., Bloch, R.J., Chamberlain, J.S., 2014. Muscle Structure Influences Utrophin Expression in mdx Mice. *PLoS Genet.* 10. <https://doi.org/10.1371/journal.pgen.1004431>
- Barlow, J.L., Bellosi, A., Hardman, C.S., Drynan, L.F., Heng Wong, S., Cruickshank, J.P., J McKenzie, A.N., 2012. Innate IL-13-producing nuocytes arise during allergic lung inflammation and contribute to airways hyperreactivity. *J. Allergy Clin. Immunol.* 129, 191-198.e4. <https://doi.org/10.1016/j.jaci.2011.09.041>
- Baumeister, S.K., Todorovic, S., Milić-Rašić, V., Dekomien, G., Lochmüller, H., Walter, M.C., 2009. Eosinophilic myositis as presenting symptom in  $\gamma$ -sarcoglycanopathy. *Neuromuscul. Disord.* 19, 167–171. <https://doi.org/10.1016/j.nmd.2008.11.010>
- Bell, C.D., Conen, P.E., 1968. Histopathological changes in Duchenne muscular dystrophy. *J. Neurol. Sci.* 7, 529–544. [https://doi.org/10.1016/0022-510X\(68\)90058-0](https://doi.org/10.1016/0022-510X(68)90058-0)
- Besnard, A.-G., Guabiraba, R., Niedbala, W., Palomo, J., Reverchon, F., Shaw, T.N., Couper, K.N., Ryffel, B., Liew, F.Y., 2015. IL-33-Mediated Protection against Experimental Cerebral Malaria Is Linked to Induction of Type 2 Innate Lymphoid Cells, M2 Macrophages and Regulatory T Cells. *PLOS Pathog.* 11, e1004607. <https://doi.org/10.1371/journal.ppat.1004607>
- Brenman, J.E., Chao, D.S., Xia, H., Aldape, K., Bredt, D.S., 1995. Nitric oxide synthase complexed with dystrophin and absent from skeletal muscle sarcolemma in Duchenne muscular dystrophy. *Cell* 82, 743–752. [https://doi.org/10.1016/0092-8674\(95\)90471-9](https://doi.org/10.1016/0092-8674(95)90471-9)
- Brigitte, M., Schilte, C., Plonquet, A., Baba-Amer, Y., Henri, A., Charlier, C., Tajbakhsh, S., Albert, M., Gherardi, R.K., Chrétien, F., 2010. Muscle resident macrophages control the immune cell reaction in a mouse model of notexin-induced myoinjury. *Arthritis Rheum.* 62, 268–279. <https://doi.org/10.1002/art.27183>
- Brooke, M.H., Fenichel, G.M., Griggs, R.C., Mendell, J.R., Moxley, R.T., Miller, J.P., Kaiser,

- K.K., Florence, J.M., Pandya, S., Signore, L., King, W., Robison, J., Head, R.A., Province, M.A., Seyfried, W., Mandel, S., 1987. Clinical Investigation of Duchenne Muscular Dystrophy. *Arch. Neurol.* 44, 812. <https://doi.org/10.1001/archneur.1987.00520200016010>
- Bulfield, G., Siller, W.G., Wight, P.A., Moore, K.J., 1984. X chromosome-linked muscular dystrophy (mdx) in the mouse. *Proc. Natl. Acad. Sci. U. S. A.* 81, 1189–92. <https://doi.org/10.1073/pnas.81.4.1189>
- Burzyn, D., Kuswanto, W., Kolodin, D., Shadrach, J.L., Cerletti, M., Jang, Y., Sefik, E., Tan, T.G., Wagers, A.J., Benoist, C., Mathis, D., 2013. A Special Population of regulatory T Cells Potentiates muscle repair. *Cell* 155, 1282–1295. <https://doi.org/10.1016/j.cell.2013.10.054>
- Bushby, K., Finkel, R., Birnkrant, D.J., Case, L.E., Clemens, P.R., Cripe, L., Kaul, A., Kinnett, K., McDonald, C., Pandya, S., Poysky, J., Shapiro, F., Tomezsko, J., Constantin, C., 2010. Diagnosis and management of Duchenne muscular dystrophy, part 1: diagnosis, and pharmacological and psychosocial management. *Lancet Neurol.* 9, 77–93. [https://doi.org/10.1016/S1474-4422\(09\)70271-6](https://doi.org/10.1016/S1474-4422(09)70271-6)
- Cai, B., Spencer, M.J., Nakamura, G., Tseng-Ong, L., Tidball, J.G., 2000. Eosinophilia of Dystrophin-Deficient Muscle Is Promoted by Perforin-Mediated Cytotoxicity by T Cell Effectors Baiyuan. *Am. J. Pathol.* 156, 1789–1796. [https://doi.org/10.1016/S0002-9440\(10\)65050-X](https://doi.org/10.1016/S0002-9440(10)65050-X)
- Cantarini, L., Volpi, N., Carbotti, P., Greco, G., Aglianò, M., Bellisai, F., Giannini, F., Alessandrini, C., Grasso, G., Galeazzi, M., 2009. Eosinophilia-associated muscle disorders: an immunohistological study with tissue localisation of major basic protein in distinct clinicopathological forms. *J Clin Pathol* 62, 442–447. <https://doi.org/10.1136/jcp.2008.060616>
- Capkovic, K.L., Stevenson, S., Johnson, M.C., Thelen, J.J., Cornelison, D.D.W., 2008. Neural cell adhesion molecule (NCAM) marks adult myogenic cells committed to differentiation. *Exp. Cell Res.* 314, 1553–1565. <https://doi.org/10.1016/j.yexcr.2008.01.021>
- Capote, J., Kramerova, I., Martinez, L., Vetrone, S., Barton, E.R., Sweeney, H.L., Miceli, M.C., Spencer, M.J., 2016. Osteopontin ablation ameliorates muscular dystrophy by shifting macrophages to a proregenerative phenotype. *J. Cell Biol.* 213, 275–288. <https://doi.org/10.1083/jcb.201510086>
- Castiglioni, A., Corna, G., Rigamonti, E., Basso, V., Vezzoli, M., Monno, A., Almada, A.E., Mondino, A., Wagers, A.J., Manfredi, A.A., Rovere-Querini, P., 2015. FOXP3<sup>+</sup> T cells recruited to sites of sterile skeletal muscle injury regulate the fate of satellite cells and guide effective tissue regeneration. *PLoS One* 10, 1–18. <https://doi.org/10.1371/journal.pone.0128094>
- Cella, M., Miller, H., Song, C., 2014. Beyond NK Cells: The Expanding Universe of Innate Lymphoid Cells. *Front. Immunol.* 5, 282. <https://doi.org/10.3389/fimmu.2014.00282>
- Chang, Y.J., Kim, H.Y., Albacker, L.A., Baumgarth, N., McKenzie, A.N.J., Smith, D.E., Dekruyff, R.H., Umetsu, D.T., 2011. Innate lymphoid cells mediate influenza-induced airway hyper-reactivity independently of adaptive immunity. *Nat. Immunol.* 12, 631–638. <https://doi.org/10.1038/ni.2045>
- Charleston, J.S., Schnell, F.J., Dworzak, J., Donoghue, C., Lewis, S., Chen, L., David Young, G., Milici, A.J., Voss, J., Dealwis, U., Wentworth, B., Rodino-Klapac, L.R., Sahenk, Z., Frank, D., Mendell, J.R., 2018. Eteplirsen treatment for Duchenne muscular dystrophy. *Neurology* 90, e2135–e2145. <https://doi.org/10.1212/WNL.0000000000005680>
- Charlton, C.A., Mohler, W.A., Blau, H.M., 2000. Neural cell adhesion molecule (NCAM) and myoblast fusion. *Dev. Biol.* 221, 112–119. <https://doi.org/10.1006/dbio.2000.9654>
- Chawla, A., Nguyen, K.D., Goh, Y.P.S., 2011. Macrophage-mediated inflammation in metabolic disease. *Nat. Rev. Immunol.* 11, 738–749. <https://doi.org/10.1038/nri3071>
- Cirak, S., Feng, L., Anthony, K., Arechavala-Gomez, V., Torelli, S., Sewry, C., Morgan, J.E.,

- Muntoni, F., 2012. Restoration of the dystrophin-associated glycoprotein complex after exon skipping therapy in Duchenne muscular dystrophy. *Mol. Ther.* 20, 462–7. <https://doi.org/10.1038/mt.2011.248>
- Cornelison, D.D.W., Wold, B.J., 1997. Single-Cell Analysis of Regulatory Gene Expression in Quiescent and Activated Mouse Skeletal Muscle Satellite Cells, *Developmental Biology*.
- Coutinho, A.E., Chapman, K.E., 2011. The anti-inflammatory and immunosuppressive effects of glucocorticoids, recent developments and mechanistic insights. *Mol. Cell. Endocrinol.* 335, 2. <https://doi.org/10.1016/J.MCE.2010.04.005>
- Covault, J., Sanes, J.R., 1986. Distribution of N-CAM in synaptic and extrasynaptic portions of developing and adult skeletal muscle. *J. Cell Biol.* 102, 716–730. <https://doi.org/10.1083/jcb.102.3.716>
- Covault, J., Sanes, J.R., 1985. Neural cell adhesion molecule (N-CAM) accumulates in denervated and paralyzed skeletal muscles. *Proc. Natl. Acad. Sci. U. S. A.* 82, 4544–8. <https://doi.org/10.1073/pnas.82.13.4544>
- De Paepe, B., De Bleecker, J.L., 2013. Cytokines and chemokines as regulators of skeletal muscle inflammation: presenting the case of Duchenne muscular dystrophy. *Mediat. Inflamm* 2013, 540310–540370. <https://doi.org/10.1155/2013/540370>
- Deng, B., Wehling-Henricks, M., Villalta, S.A., Wang, Y., Tidball, J.G., 2012. IL-10 Triggers Changes in Macrophage Phenotype That Promote Muscle Growth and Regeneration. *J. Immunol.* 189, 3669–3680. <https://doi.org/10.4049/jimmunol.1103180>
- Desilva, S., Drachman, D.B., Mellits, D., Kuncl, R.W., 1987. Prednisone Treatment in Duchenne Muscular Dystrophy: Long-term Benefit. *Arch. Neurol.* 44, 818–822. <https://doi.org/10.1001/archneur.1987.00520200022012>
- Diefenbach, A., Colonna, M., Koyasu, S., 2014. Immunity Review Development, Differentiation, and Diversity of Innate Lymphoid Cells. *Immunity* 41, 354–365. <https://doi.org/10.1016/j.immuni.2014.09.005>
- DiMario, J.X., Uzman, A., Strohman, R.C., 1991. Fiber regeneration is not persistent in dystrophic (mdx) mouse skeletal muscle. *Dev. Biol.* 148, 314–321. [https://doi.org/10.1016/0012-1606\(91\)90340-9](https://doi.org/10.1016/0012-1606(91)90340-9)
- Dubach-Powell, J., 2011. Quantitative determination of muscle fiber diameter (minimal Feret's diameter) and percentage of centralized nuclei. *treat-NMD* 1–16.
- Duboc, D., Meune, C., Lerebours, G., Devaux, J.-Y., Vaxsmann, G., Bécane, H.-M., 2005. Effect of perindopril on the onset and progression of left ventricular dysfunction in Duchenne muscular dystrophy. *J. Am. Coll. Cardiol.* 45, 855–857. <https://doi.org/10.1016/J.JACC.2004.09.078>
- Dubois, C., Figarella-Branger, D., Pastoret, C., Rampini, C., Karpati, G., Rougon, G., 1994. Expression of NCAM and its polysialylated isoforms during mdx mouse muscle regeneration and in vitro myogenesis. *Neuromuscul. Disord.* 4, 171–182. [https://doi.org/10.1016/0960-8966\(94\)90018-3](https://doi.org/10.1016/0960-8966(94)90018-3)
- Dumont, N.A., Bentzinger, C.F., Sincennes, M.-C., Rudnicki, M.A., 2015. Satellite Cells and Skeletal Muscle Regeneration. *Compr. Physiol.* 5, 1027–59. <https://doi.org/10.1002/cphy.c140068>
- Eberl, G., Colonna, M., Di Santo, J.P., McKenzie, A.N.J., 2015. Innate lymphoid cells: A new paradigm in immunology. *Science (80- )*. 348, aaa6566–aaa6566. <https://doi.org/10.1126/science.aaa6566>
- Ellefsen, K.L., Settle, B., Parker, I., Smith, I.F., 2014. An algorithm for automated detection, localization and measurement of local calcium signals from camera-based imaging. *Cell Calcium* 56, 147–156. <https://doi.org/10.1016/j.ceca.2014.06.003>
- Fallon, P.G., Ballantyne, S.J., Mangan, N.E., Barlow, J.L., Dasvarma, A., Hewett, D.R., McIlgorm, A., Jolin, H.E., McKenzie, A.N.J., 2006. Identification of an interleukin (IL)-25-dependent cell population that provides IL-4, IL-5, and IL-13 at the onset of helminth

- expulsion. *J. Exp. Med.* 203, 1105–16. <https://doi.org/10.1084/jem.20051615>
- Forkel, M., Mjösberg, J., 2016. Dysregulation of Group 3 Innate Lymphoid Cells in the Pathogenesis of Inflammatory Bowel Disease. *Curr. Allergy Asthma Rep.* <https://doi.org/10.1007/s11882-016-0652-3>
- Furusawa, J., Moro, K., Motomura, Y., Okamoto, K., Zhu, J., Takayanagi, H., Kubo, M., Koyasu, S., 2013. Critical Role of p38 and GATA3 in Natural. *J. Immunol.* 191, 1818–1826. <https://doi.org/10.4049/jimmunol.1300379>
- Garbincius, J.F., Michele, D.E., 2015. Dystrophin-glycoprotein complex regulates muscle nitric oxide production through mechanoregulation of AMPK signaling. *Proc. Natl. Acad. Sci. U. S. A.* 112, 13663–13668. <https://doi.org/10.1073/pnas.1512991112>
- Gardner-Medwin, D., 1980. Clinical features and classification of the muscular dystrophies. *Br. Med. Bull.* 36, 109–115.
- Gasteiger, G., Fan, X., Dikiy, S., Lee, S.Y., Rudensky, A.Y., 2015. Tissue residency of innate lymphoid cells in lymphoid and nonlymphoid organs. *Science (80- )*. 350, 981–5. <https://doi.org/10.1126/science.aac9593>
- Gauvreau, G.M., O’Byrne, P.M., Boulet, L.-P., Wang, Y., Cockcroft, D., Bigler, J., FitzGerald, J.M., Boedigheimer, M., Davis, B.E., Dias, C., Gorski, K.S., Smith, L., Bautista, E., Comeau, M.R., Leigh, R., Parnes, J.R., 2014. Effects of an Anti-TSLP Antibody on Allergen-Induced Asthmatic Responses. *N. Engl. J. Med.* 370, 2102–2110. <https://doi.org/10.1056/NEJMoa1402895>
- Geissmann, F., Jung, S., Littman, D.R., 2003. Blood Monocytes Consist of Two Principal Subsets with Distinct Migratory Properties. *Immunity* 19, 71–82.
- Gibbs, E.M., Crosbie-Watson, R.H., 2017. A simple and low-cost assay for measuring ambulation in mouse models of muscular dystrophy. *J. Vis. Exp.* 2017. <https://doi.org/10.3791/56772>
- Gieseck, R.L., Wilson, M.S., Wynn, T.A., 2018. Type 2 immunity in tissue repair and fibrosis. *Nat. Rev. Immunol.* <https://doi.org/10.1038/nri.2017.90>
- Gold, M.J., Antignano, F., Halim, T.Y.F., Hirota, J.A., Blanchet, M.-R., Zaph, C., Takei, F., McNagny, K.M., 2014. Group 2 innate lymphoid cells facilitate sensitization to local, but not systemic, TH2-inducing allergen exposures. *J. Allergy Clin. Immunol.* 133, 1142–1148.e5. <https://doi.org/10.1016/J.JACI.2014.02.033>
- Gonçalves, M.A.F.V., Janssen, J.M., Nguyen, Q.G., Athanasopoulos, T., Hauschka, S.D., Dickson, G., De Vries, A.A.F., 2011. Transcription factor rational design improves directed differentiation of human mesenchymal stem cells into skeletal myocytes. *Mol. Ther.* 19, 1331–1341. <https://doi.org/10.1038/mt.2010.308>
- Gonzalez-Polo, V., Pucci-Molineris, M., Cervera, V., Gambaro, S., Yantorno, S.E., Descalzi, V., Tiribelli, C., Gondolesi, G.E., Meier, D., 2019. Group 2 innate lymphoid cells exhibit progressively higher levels of activation during worsening of liver fibrosis. *Ann. Hepatol.* 18, 366–372. <https://doi.org/10.1016/j.aohep.2018.12.001>
- Gordon, S., 2003. Alternative activation of macrophages. *Nat Rev Immunol* 3, 23–35.
- Guirado, R., Carceller, H., Castillo-Gómez, E., Castrén, E., Nacher, J., 2018. Automated analysis of images for molecular quantification in immunohistochemistry. *Heliyon* 4, e00669. <https://doi.org/10.1016/j.heliyon.2018.e00669>
- Guiraud, S., Edwards, B., Squire, S.E., Moir, L., Berg, A., Babbs, A., Ramadan, N., Wood, M.J., Davies, K.E., 2019. Embryonic myosin is a regeneration marker to monitor utrophin-based therapies for DMD. *Hum. Mol. Genet.* 28, 307–319. <https://doi.org/10.1093/hmg/ddy353>
- Halim, T.Y.F., Krauß, R.H., Sun, A.C., Takei, F., 2012. Lung Natural Helper Cells Are a Critical Source of Th2 Cell-Type Cytokines in Protease Allergen-Induced Airway Inflammation. *Immunity* 36, 451–463. <https://doi.org/10.1016/J.IMMUNI.2011.12.020>
- Hamer, P., McGeachie, J., Davies, M., Grounds, M., 2002. Evans Blue Dye as an in vivo marker of myofibre damage: optimising parameters for detecting initial myofibre membrane



- permeability. *J. Anat.* 200, 69. <https://doi.org/10.1046/J.0021-8782.2001.00008.X>
- Hammers, D.W., Rybalko, V., Merscham-Banda, M., Hsieh, P.-L., Suggs, L.J., Farrar, R.P., 2015. Anti-inflammatory macrophages improve skeletal muscle recovery from ischemia-reperfusion. *J. Appl. Physiol.* 118, 1067–74. <https://doi.org/10.1152/jappphysiol.00313.2014>
- Hardy, D., Besnard, A., Latil, M., Jouvion, G., Briand, D., Thépenier, C., Pascal, Q., Guguin, A., Gayraud-Morel, B., Cavaillon, J.M., Tajbakhsh, S., Rocheteau, P., Chrétien, F., 2016. Comparative Study of Injury Models for Studying Muscle Regeneration in Mice. *PLoS One* 11, e0147198. <https://doi.org/10.1371/journal.pone.0147198>
- Haslett, J.N., Sanoudou, D., Kho, A.T., Bennett, R.R., Greenberg, S.A., Kohane, I.S., Beggs, A.H., Kunkel, L.M., 2002. Gene expression comparison of biopsies from Duchenne muscular dystrophy (DMD) and normal skeletal muscle. *Proc. Natl. Acad. Sci. U. S. A.* 99, 15000–5. <https://doi.org/10.1073/pnas.192571199>
- Hawke, T.J., Garry, D.J., 2001. invited review Myogenic satellite cells: physiology to molecular biology. *J Appl Physiol* 91.
- Henderson, N.C., Mackinnon, A.C., Farnworth, S.L., Kipari, T., Haslett, C., Iredale, J.P., Liu, F.T., Hughes, J., Sethi, T., 2008. Galectin-3 expression and secretion links macrophages to the promotion of renal fibrosis. *Am. J. Pathol.* 172, 288–298. <https://doi.org/10.2353/ajpath.2008.070726>
- Herbert, D.R., Douglas, B., Zullo, K., 2019. Group 2 innate lymphoid cells (ILC2): Type 2 immunity and helminth immunity. *Int. J. Mol. Sci.* 20. <https://doi.org/10.3390/ijms20092276>
- Heredia, J.E., Mukundan, L., Chen, F.M., Mueller, A.A., Deo, R.C., Locksley, R.M., Rando, T.A., Chawla, A., 2013. Type 2 innate signals stimulate fibro/adipogenic progenitors to facilitate muscle regeneration. *Cell* 153, 376–388. <https://doi.org/10.1016/j.cell.2013.02.053>
- Hoeksema, M.A., De Winther, M.P.J., 2016. Epigenetic Regulation of Monocyte and Macrophage Function. *Antioxidants Redox Signal.* 25, 758–774. <https://doi.org/10.1089/ars.2016.6695>
- Hoffman, E.P., Brown, R.H., Kunkel, L.M., 1987. Dystrophin: The protein product of the duchenne muscular dystrophy locus. *Cell* 51, 919–928. [https://doi.org/10.1016/0092-8674\(87\)90579-4](https://doi.org/10.1016/0092-8674(87)90579-4)
- Hotamisligil, G.S., 2006. Inflammation and metabolic disorders. *Nature* 444, 860–867. <https://doi.org/10.1038/nature05485>
- Hoyler, T., Klose, C.S.N., Souabni, A., Turqueti-Neves, A., Pfeifer, D., Rawlins, E.L., Voehringer, D., Busslinger, M., Diefenbach, A., 2012. The Transcription Factor GATA-3 Controls Cell Fate and Maintenance of Type 2 Innate Lymphoid Cells. *Immunity* 37, 634–648. <https://doi.org/10.1016/J.IMMUNI.2012.06.020>
- Hsu, J.D., Quinlivan, R., 2013. Scoliosis in Duchenne muscular dystrophy (DMD). *Neuromuscul. Disord.* 611–617. <https://doi.org/10.1016/j.nmd.2013.05.003>
- Huang, Y., Guo, L., Qiu, J., Chen, X., Hu-Li, J., Siebenlist, U., Williamson, P.R., Urban, J.F., Paul, W.E., 2015. IL-25-responsive, lineage-negative KLRG1 hi cells are multipotential “inflammatory” type 2 innate lymphoid cells. *Nat. Immunol.* 16, 161–169. <https://doi.org/10.1038/ni.3078>
- Huang, Y., Paul, W.E., 2015. Inflammatory group 2 innate lymphoid cells. *Int. Immunol.* dxv044. <https://doi.org/10.1093/intimm/dxv044>
- Humbles, A.A., Lloyd, C.M., McMillan, S.J., Friend, D.S., Xanthou, G., McKenna, E.E., Ghiran, S., Gerard, N.P., Yu, C., Orkin, S.H., Gerard, C., 2004. A critical role for eosinophils in allergic airways remodeling. *Science (80- )*. 305, 1776–9. <https://doi.org/10.1126/science.1100283>
- Illa, I., Leon-Monzon, M., Dalakas, M., 1992. Regenerating and Denervated Human Muscle Fibers and Satellite Cells Express Neural Cell Adhesion Molecule Recognized by Monoclonal Antibodies to Natural Killer Cells. *Ann Neurol.* 31, 46–52.

- Iordanov, M.S., Sundholm, A.J., Simpson, E.L., Hanifin, J.M., Ryabinina, O.P., Choi, R.J., Korcheva, V.B., Schneider, P., Magun, B.E., 2005. Cell Death-Induced Activation of Epidermal Growth Factor Receptor in Keratinocytes: Implications for Restricting Epidermal Damage in Dermatitis. *J. Invest. Dermatol.* 125, 134–142. <https://doi.org/10.1111/j.0022-202X.2005.23804.x>
- Juban, G., Chazaud, B., 2017. Metabolic regulation of macrophages during tissue repair: insights from skeletal muscle regeneration. *FEBS Lett.* <https://doi.org/10.1002/1873-3468.12703>
- Kastenschmidt, J.M., Avetyan, I., Armando Villalta, S., 2018. Characterization of the Inflammatory Response in Dystrophic Muscle Using Flow Cytometry, in: Bernardini, C. (Ed.), *Duchenne Muscular Dystrophy: Methods and Protocols*. Springer New York, New York, NY, pp. 43–56. [https://doi.org/10.1007/978-1-4939-7374-3\\_4](https://doi.org/10.1007/978-1-4939-7374-3_4)
- Kastenschmidt, J.M., Ellefsen, K.L., Mannaa, A.H., Giebel, J.J., Yahia, R., Ayer, R.E., Pham, P., Rios, R., Vetrone, S.A., Mozaffar, T., Villalta, S.A., 2019a. QuantiMus: A Machine Learning-Based Approach for High Precision Analysis of Skeletal Muscle Morphology. *Front. Physiol.* 10, 1416. <https://doi.org/10.3389/fphys.2019.01416>
- Kastenschmidt, J.M., Mannaa, A.H., Muñoz, K.J., Villalta, S.A., 2019b. Immune System Regulation of Muscle Injury and Disease, in: *Muscle Gene Therapy*. Springer International Publishing, pp. 121–139. [https://doi.org/10.1007/978-3-030-03095-7\\_7](https://doi.org/10.1007/978-3-030-03095-7_7)
- Katz, B., 1961. The termination of the afferent nerve fibre in the muscle spindle of the frog, *Biological Sciences*.
- Khairallah, R.J., Shi, G., Sbrana, F., Prosser, B.L., Borroto, C., Mazaitis, M.J., Hoffman, E.P., Mahurkar, A., Sachs, F., Sun, Y., Chen, Y.-W., Raiteri, R., Lederer, W.J., Dorsey, S.G., Ward, C.W., 2012. Microtubules underlie dysfunction in duchenne muscular dystrophy. *Sci. Signal.* 5, ra56. <https://doi.org/10.1126/scisignal.2002829>
- Kharraz, Y., Guerra, J., Pessina, P., Serrano, A.L., Muñoz-Cánoves, P., 2014. Understanding the Process of Fibrosis in Duchenne Muscular Dystrophy. *Biomed Res. Int.* 2014, 965631. <https://doi.org/10.1155/2014/965631>
- Khoury, D.J., Szalay, E.A., 2007. Bone Mineral Density Correlation With Fractures in Nonambulatory Pediatric Patients. *J. Pediatr. Orthop.* 27, 562–566. <https://doi.org/10.1097/01.bpb.0000279021.04000.d3>
- Kim, B.S., Siracusa, M.C., Saenz, S.A., Noti, M., Monticelli, L.A., Sonnenberg, G.F., Hepworth, M.R., Van Voorhees, A.S., Comeau, M.R., Artis, D., 2013. TSLP elicits IL-33-independent innate lymphoid cell responses to promote skin inflammation. *Sci. Transl. Med.* 5, 170ra16. <https://doi.org/10.1126/scitranslmed.3005374>
- Koenig, M., Hoffman, E.P., Bertelson, C.J., Monaco, A.P., Feener, C., Kunkel, L.M., 1987. Complete cloning of the duchenne muscular dystrophy (DMD) cDNA and preliminary genomic organization of the DMD gene in normal and affected individuals. *Cell* 50, 509–517. [https://doi.org/10.1016/0092-8674\(87\)90504-6](https://doi.org/10.1016/0092-8674(87)90504-6)
- Kohno, S., Ueji, T., Abe, T., Nakao, R., Hirasaka, K., Oarada, M., Harada-Sukeno, A., Ohno, A., Higashibata, A., Mukai, R., Terao, J., Okumura, Y., Nikawa, T., 2011. Rantes secreted from macrophages disturbs skeletal muscle regeneration after cardiotoxin injection in Cbl-b-deficient mice. *Muscle and Nerve* 43, 223–229. <https://doi.org/10.1002/mus.21829>
- Kostrominova, T.Y., Reiner, D.S., Haas, R.H., Ingermanson, R., McDonough, P.M., 2013. Automated methods for the analysis of skeletal muscle fiber size and metabolic type, 1st ed, *International Review of Cell and Molecular Biology*. Elsevier Inc. <https://doi.org/10.1016/B978-0-12-407694-5.00007-9>
- Kuang, S., Kuroda, K., Le Grand, F., Rudnicki, M.A., 2007. Asymmetric self-renewal and commitment of satellite stem cells in muscle. *Cell* 129, 999–1010. <https://doi.org/10.1016/j.cell.2007.03.044>
- Lapidos, K.A., Kakkar, R., McNally, E.M., 2004. The Dystrophin Glycoprotein Complex Signaling

- Strength and Integrity for the Sarcolemma. *Circ. Res.* 94, 1023–1031. <https://doi.org/10.1161/01.RES.0000126574.61061.25>
- Larose, M.C., Archambault, A.S., Provost, V., Laviolette, M., Flamand, N., 2017. Regulation of eosinophil and group 2 innate lymphoid cell trafficking in asthma. *Front. Med.* 4. <https://doi.org/10.3389/fmed.2017.00136>
- Larson, C.M., Henderson, R.C., 1981. Bone Mineral Density and Fractures in Boys with Duchenne Muscular Dystrophy. *J. Pediatr. Orthop.* 20, 71.
- Lee, J.J., Jacobsen, E.A., Ochkur, S.I., McGarry, M.P., Condjella, R.M., Doyle, A.D., Luo, H., Zellner, K.R., Protheroe, C.A., Willetts, L., Lesuer, W.E., Colbert, D.C., Helmers, R.A., Lacy, P., Moqbel, R., Lee, N.A., 2012. Human versus mouse eosinophils: “That which we call an eosinophil, by any other name would stain as red.” *J. Allergy Clin. Immunol.* <https://doi.org/10.1016/j.jaci.2012.07.025>
- Lepper, C., Partridge, T.A., Fan, C.-M., Gruss, P., 2011. An absolute requirement for Pax7-positive satellite cells in acute injury-induced skeletal muscle regeneration. *Development* 138, 3639–46. <https://doi.org/10.1242/dev.067595>
- Li, L., Xia, Y., Nguyen, A., Lai, Y.H., Feng, L., Mosmann, T.R., Lo, D., 1999. Effects of Th2 cytokines on chemokine expression in the lung: IL-13 potently induces eotaxin expression by airway epithelial cells. *J. Immunol.* 162, 2477–87.
- Lim, K.R.Q., Maruyama, R., Yokota, T., 2017. Eteplirsen in the treatment of Duchenne muscular dystrophy. *Drug Des. Devel. Ther.* 11, 533–545. <https://doi.org/10.2147/DDDT.S97635>
- Liu, F., Structures, T., 2009. Automated image segmentation of haematoxylin and eosin stained skeletal muscle cross-sections. *J. Microsc.* 6, 247–253. <https://doi.org/10.1111/j.1743-6109.2008.01122.x> Endothelial
- Liu, Y.-C., Zou, X.-B., Chai, Y.-F., Yao, Y.-M., 2014. Macrophage Polarization in Inflammatory Diseases. *Int. J. Biol. Sci.* 10. <https://doi.org/10.7150/ijbs.8879>
- Lloyd, C.M., Snelgrove, R.J., 2018. Type 2 immunity: Expanding our view. *Sci. Immunol.* <https://doi.org/10.1126/sciimmunol.aat1604>
- Lo Mauro, A., D’Angelo, M.G., Aliverti, A., 2015. Assessment and management of respiratory function in patients with duchenne muscular dystrophy: Current and emerging options. *Ther. Clin. Risk Manag.* 11, 1475–1488. <https://doi.org/10.2147/TCRM.S55889>
- Lu, H., Huang, D., Ransohoff, R.M., Zhou, L., 2011. Acute skeletal muscle injury: CCL2 expression by both monocytes and injured muscle is required for repair. *FASEB J.* 25, 3344–3355. <https://doi.org/10.1096/fj.10-178939>
- Lu, Haiyan, Huang, D., Saederup, N., Charo, I.F., Ransohoff, R.M., Zhou, L., 2011. Macrophages recruited via CCR2 produce insulin-like growth factor-1 to repair acute skeletal muscle injury. *FASEB J.* 25, 358–369. <https://doi.org/10.1096/fj.10-171579>
- Lukjanenko, L., Brachat, S., Pierrel, E., Lach-Trifilieff, E., Feige, J.N., 2013. Genomic Profiling Reveals That Transient Adipogenic Activation Is a Hallmark of Mouse Models of Skeletal Muscle Regeneration. *PLoS One* 8. <https://doi.org/10.1371/journal.pone.0071084>
- Lundberg, I., Brengman, J.M., Engel, A.G., 1995. Analysis of cytokine expression in muscle in inflammatory myopathies, Duchenne dystrophy, and non-weak controls. *J. Neuroimmunol.* 63, 9–16. [https://doi.org/10.1016/0165-5728\(95\)00122-0](https://doi.org/10.1016/0165-5728(95)00122-0)
- Madaro, L., Bouche, M., Bouché, M., 2014. From innate to adaptive immune response in muscular dystrophies and skeletal muscle regeneration: the role of lymphocytes. *Biomed Res Int* 2014, 438612–438675. <https://doi.org/10.1155/2014/438675>
- Maesner, C.C., Almada, A.E., Wagers, A.J., 2016. Established cell surface markers efficiently isolate highly overlapping populations of skeletal muscle satellite cells by fluorescence-activated cell sorting. *Skelet. Muscle* 6, 35. <https://doi.org/10.1186/s13395-016-0106-6>
- Mariol, M.-C., Ségalat, L., 2001. Muscular degeneration in the absence of dystrophin is a calcium-dependent process. *Curr. Biol.* 11, 1691–1694. [https://doi.org/10.1016/S0960-9822\(01\)00528-0](https://doi.org/10.1016/S0960-9822(01)00528-0)

- Martinez, F.O., Helming, L., Gordon, S., 2009. Alternative Activation of Macrophages: An Immunologic Functional Perspective. *Annu. Rev. Immunol.* 27, 451–483. <https://doi.org/10.1146/annurev.immunol.021908.132532>
- Matsuura, T., Li, Y., Giacobino, J.-P., Fu, F.H., Huard, J., 2007. Skeletal muscle fiber type conversion during the repair of mouse soleus: Potential implications for muscle healing after injury. *J. Orthop. Res.* 25, 1534–1540. <https://doi.org/10.1002/jor.20451>
- Mauro, A., 1961. Satellite cell of skeletal muscle fibers. *J Biophys Biochem Cytol* 493–495.
- McCabe, A., Dolled-Filhart, M., Camp, R.L., Rimm, D.L., 2005. Automated Quantitative Analysis (AQUA) of In Situ Protein Expression, Antibody Concentration, and Prognosis. *JNCI J. Natl. Cancer Inst.* 97, 1808–1815. <https://doi.org/10.1093/jnci/dji427>
- McCarthy, J.J., Mula, J., Miyazaki, M., Erfani, R., Garrison, K., Farooqui, A.B., Srikuea, R., Lawson, B.A., Grimes, B., Keller, C., Van Zant, G., Campbell, K.S., Esser, K.A., Dupont-Versteegden, E.E., Peterson, C.A., 2011. Effective fiber hypertrophy in satellite cell-depleted skeletal muscle. *Development* 138, 3657–66. <https://doi.org/10.1242/dev.068858>
- McDonald, A.A., Hebert, S.L., Kunz, M.D., Ralles, S.J., McLoon, L.K., 2015. Disease course in mdx:utrophin+/- mice: comparison of three mouse models of Duchenne muscular dystrophy. *Physiol. Rep.* 3, e12391–e12391. <https://doi.org/10.14814/phy2.12391>
- McDonald, C.M., Henricson, E.K., Abresch, R.T., Duong, T., Joyce, N.C., Hu, F., Clemens, P.R., Hoffman, E.P., Cnaan, A., Gordish-Dressman, H., CINRG Investigators, V., Chidambaranathan, S., Biggar, W.D., McAdam, L.C., Mah, J.K., Tulinius, M., Cnaan, A., Morgenroth, L.P., Leshner, R., Tesi-Rocha, C., Thangarajh, M., Duong, T., Kornberg, A., Ryan, M., Nevo, Y., Dubrovsky, A., Clemens, P.R., Abdel-Hamid, H., Connolly, A.M., Pestronk, A., Teasley, J., Bertorin, T.E., Webster, R., Kolski, H., Kuntz, N., Driscoll, S., Bodensteiner, J.B., Carlo, J., Gorni, K., Lotze, T., Day, J.W., Karachunski, P., Henricson, E.K., Abresch, R.T., Joyce, N.C., McDonald, C.M., 2018. Long-term effects of glucocorticoids on function, quality of life, and survival in patients with Duchenne muscular dystrophy: a prospective cohort study. *Lancet* 391, 451–461. [https://doi.org/10.1016/S0140-6736\(17\)32160-8](https://doi.org/10.1016/S0140-6736(17)32160-8)
- McDouall, R.M., Dunn, M.J., Dubowitz, V., 1990. Nature of the mononuclear infiltrate and the mechanism of muscle damage in juvenile dermatomyositis and Duchenne muscular dystrophy. *J. Neurol. Sci.* 99, 199–217. [https://doi.org/10.1016/0022-510X\(90\)90156-H](https://doi.org/10.1016/0022-510X(90)90156-H)
- McGreevy, J.W., Hakim, C.H., McIntosh, M.A., Duan, D., 2015. Animal models of Duchenne muscular dystrophy: from basic mechanisms to gene therapy. *Dis. Model. Mech.* 8, 195–213. <https://doi.org/10.1242/dmm.018424>
- Mchedlidze, T., Waldner, M., Zopf, S., Walker, J., Rankin, A.L., Schuchmann, M., Voehringer, D., McKenzie, A.N.J., Neurath, M.F., Pflanz, S., Wirtz, S., 2013. Interleukin-33-Dependent Innate Lymphoid Cells Mediate Hepatic Fibrosis. *Immunity* 39, 357–371. <https://doi.org/10.1016/J.IMMUNI.2013.07.018>
- Mendell, J.R., Moxley, R.T., Griggs, R.C., Brooke, M.H., Fenichel, G.M., Miller, J.P., King, W., Signore, L., Pandya, S., Florence, J., Schierbecker, J., Robison, J., Kaiser, K., Mandel, S., Arfken, C., Gilder, B., 1989. Randomized, Double-Blind Six-Month Trial of Prednisone in Duchenne's Muscular Dystrophy. *N. Engl. J. Med.* 320, 1592–1597. <https://doi.org/10.1056/NEJM198906153202405>
- Mendell, J.R., Shilling, C., Leslie, N.D., Flanigan, K.M., al-Dahhak, R., Gastier-Foster, J., Kneile, K., Dunn, D.M., Duval, B., Aoyagi, A., Hamil, C., Mahmoud, M., Roush, K., Bird, L., Rankin, C., Lilly, H., Street, N., Chandrasekar, R., Weiss, R.B., 2012. Evidence-based path to newborn screening for duchenne muscular dystrophy. *Ann. Neurol.* 71, 304–313. <https://doi.org/10.1002/ana.23528>
- Mercuri, E., Muntoni, F., 2013. Muscular dystrophies. *Lancet* 381, 845–860. [https://doi.org/10.1016/S0140-6736\(12\)61897-2](https://doi.org/10.1016/S0140-6736(12)61897-2)
- Miljkovic, D., Bassiouni, A., Cooksley, C., Ou, J., Hauben, E., Wormald, P.J., Vreugde, S., 2014.

- Association between group 2 innate lymphoid cells enrichment, nasal polyps and allergy in chronic rhinosinusitis. *Allergy Eur. J. Allergy Clin. Immunol.* 69, 1154–1161.  
<https://doi.org/10.1111/all.12440>
- Mjösberg, J.M., Trifari, S., Crellin, N.K., Peters, C.P., van Drunen, C.M., Piet, B., Fokkens, W.J., Cupedo, T., Spits, H., 2011. Human IL-25- and IL-33-responsive type 2 innate lymphoid cells are defined by expression of CRTH2 and CD161. *Nat. Immunol.* 12, 1055–1062.  
<https://doi.org/10.1038/ni.2104>
- Moat, S.J., Bradley, D.M., Salmon, R., Clarke, A., Hartley, L., 2013. Newborn bloodspot screening for Duchenne Muscular Dystrophy: 21 years experience in Wales (UK). *Eur. J. Hum. Genet.* 21, 1049–1053. <https://doi.org/10.1038/ejhg.2012.301>
- Molofsky, A.B., Nussbaum, J.C., Liang, H.-E., Van Dyken, S.J., Cheng, L.E., Mohapatra, A., Chawla, A., Locksley, R.M., 2013. Innate lymphoid type 2 cells sustain visceral adipose tissue eosinophils and alternatively activated macrophages. *J. Exp. Med.* 210, 535–49.  
<https://doi.org/10.1084/jem.20121964>
- Molofsky, A.B., Van Gool, F., Liang, H.E., Van Dyken, S.J., Nussbaum, J.C., Lee, J., Bluestone, J.A., Locksley, R.M., 2015. Interleukin-33 And Interferon-gamma Counter-Regulate Group 2 Innate Lymphoid Cell Activation During Immune Perturbation. *Immunity* 43, 161–174.  
<https://doi.org/10.1016/j.immuni.2015.05.019>
- Monticelli, L.A., Osborne, L.C., Noti, M., Tran, S. V., Zaiss, D.M.W.W., Artis, D., 2015. IL-33 promotes an innate immune pathway of intestinal tissue protection dependent on amphiregulin-EGFR interactions. *Proc. Natl. Acad. Sci. U. S. A.* 112, 10762–7.  
<https://doi.org/10.1073/pnas.1509070112>
- Monticelli, L.A., Sonnenberg, G.F., Abt, M.C., Alenghat, T., Ziegler, C.G.K., Doering, T.A., Angelosanto, J.M., Laidlaw, B.J., Yang, C.Y., Sathaliyawala, T., Kubota, M., Turner, D., Diamond, J.M., Goldrath, A.W., Farber, D.L., Collman, R.G., Wherry, E.J., Artis, D., 2012. Innate lymphoid cells promote lung tissue homeostasis following acute influenza virus infection. *Nat. Immunol.* 12, 1045–1054. <https://doi.org/10.1031/ni.2131>
- Monticelli, L.A., Sonnenberg, G.F., Abt, M.C., Alenghat, T., Ziegler, C.G.K., Doering, T.A., Angelosanto, J.M., Laidlaw, B.J., Yang, C.Y., Sathaliyawala, T., Kubota, M., Turner, D., Diamond, J.M., Goldrath, A.W., Farber, D.L., Collman, R.G., Wherry, E.J., Artis, D., 2011. Innate lymphoid cells promote lung-tissue homeostasis after infection with influenza virus. *Nat. Immunol.* 12, 1045–1054. <https://doi.org/10.1038/ni.2131>
- Moro, K., Kabata, H., Tanabe, M., Koga, S., Takeno, N., Mochizuki, M., Fukunaga, K., Asano, K., Betsuyaku, T., Koyasu, S., 2016. Interferon and IL-27 antagonize the function of group 2 innate lymphoid cells and type 2 innate immune responses. *Nat. Immunol.* 17, 76–86.  
<https://doi.org/10.1038/ni.3309>
- Moro, K., Yamada, T., Tanabe, M., Takeuchi, T., Ikawa, T., Kawamoto, H., Furusawa, J.-I., Ohtani, M., Fujii, H., Koyasu, S., 2010. Innate production of TH2 cytokines by adipose tissue-associated c-Kit+Sca-1+ lymphoid cells. *Nature* 463.  
<https://doi.org/10.1038/nature08636>
- Mosser, D.M., Edwards, J.P., 2008. Exploring the full spectrum of macrophage activation. *Nat Rev Immunol* 8, 958–969.
- Mounier, R.R., Théret, M., Arnold, L., Cuvellier, S., Bultot, L., Göransson, O., Sanz, N., Ferry, A., Sakamoto, K., Foretz, M., Viollet, B., Chazaud, B.B., Theret, M., Arnold, L., Cuvellier, S., Bultot, L., Göransson, O., Sanz, N., Ferry, A., Sakamoto, K., Foretz, M., Viollet, B., Chazaud, B.B., 2013. AMPKa1 regulates macrophage skewing at the time of resolution of inflammation during skeletal muscle regeneration. *Cell Metab.* 18, 251–264.  
<https://doi.org/10.1016/j.cmet.2013.06.017>
- Moussion, C., Ortega, N., Girard, J.P., 2008. The IL-1-like cytokine IL-33 is constitutively expressed in the nucleus of endothelial cells and epithelial cells in vivo: A novel “Alarmin”? *PLoS One* 3. <https://doi.org/10.1371/journal.pone.0003331>

- Murphy, M.M., Lawson, J.A., Mathew, S.J., Hutcheson, D.A., Kardon, G., 2011. Satellite cells, connective tissue fibroblasts and their interactions are crucial for muscle regeneration. *J. Cell Sci.* 124, e1.2-e1. <https://doi.org/10.1242/jcs098228>
- Musarò, A., Giacinti, C., Borsellino, G., Dobrowolny, G., Pelosi, L., Cairns, L., Ottolenghi, S., Cossu, G., Bernardi, G., Battistini, L., Molinaro, M., Rosenthal, N., 2004. Stem cell-mediated muscle regeneration is enhanced by local isoform of insulin-like growth factor 1. *Proc. Natl. Acad. Sci. U. S. A.* 101, 1206–10. <https://doi.org/10.1073/pnas.0303792101>
- Nagaraju, K., Willmann, R., 2009. Developing standard procedures for murine and canine efficacy studies of DMD therapeutics. *Neuromuscul. Disord.* 6, 247–253. <https://doi.org/10.1111/j.1743-6109.2008.01122.x> Endothelial
- Nayak, J., Naik, B., Behera, H.S., 2015. A comprehensive survey on support vector machine in data mining tasks: Applications & challenges. *Int. J. Database Theory Appl.* 8, 169–186. <https://doi.org/10.14257/ijtda.2015.8.1.18>
- Neill, D.R., Wong, S.H., Bellosi, A., Flynn, R.J., Daly, M., Langford, T.K.A., Bucks, C., Kane, C.M., Fallon, P.G., Pannell, R., Jolin, H.E., McKenzie, A.N.J., 2010. Nuocytes represent a new innate effector leukocyte that mediates type-2 immunity. *Nat. Lett.* 464. <https://doi.org/10.1038/nature08900>
- Ng, R., Banks, G.B., Hall, J.K., Muir, L.A., Ramos, J.N., Wicki, J., Odom, G.L., Konieczny, P., Seto, J., Chamberlain, J.R., Chamberlain, J.S., 2012. Animal Models of Muscular Dystrophy. *Prog. Mol. Biol. Transl. Sci.* 105, 83–111. <https://doi.org/10.1016/B978-0-12-394596-9.00004-4>
- Nguyen, H.X., Tidball, J.G., 2003. Null Mutation of gp91<sup>phox</sup> Reduces Muscle Membrane Lysis During Muscle Inflammation in Mice. *J. Physiol.* 553, 833–841. <https://doi.org/10.1113/jphysiol.2003.051912>
- Nguyen, H.X., Tidball, J.G., 2002. Interactions between neutrophils and macrophages promote macrophage killing of rat muscle cells in vitro. *J. Physiol.* 547, 125–132. <https://doi.org/10.1113/jphysiol.2002.031450>
- Nishi, Y., Sano, H., Kawashima, T., Okada, T., Kuroda, T., Kikkawa, K., Kawashima, S., Tanabe, M., Goto, T., Matsuzawa, Y., Matsumura, R., Tomioka, H., Liu, F.T., Shirai, K., 2007. Role of galectin-3 in human pulmonary fibrosis. *Allergol. Int.* 56, 57–65. <https://doi.org/10.2332/allergolint.O-06-449>
- Nitahara-Kasahara, Y., Hayashita-Kinoh, H., Chiyo, T., Nishiyama, A., Okada, H., Takeda, S., Okada, T., 2014. Dystrophic mdx mice develop severe cardiac and respiratory dysfunction following genetic ablation of the anti-inflammatory cytokine IL-10. *Hum Mol Genet* 23, 3990–4000. <https://doi.org/10.1093/hmg/ddu113>
- Noguchi, H., Kephart, G.M., Colby, T. V., Gleich, G.J., 1992. Tissue Eosinophilia and Eosinophil Degranulation in Syndromes Associated with Fibrosis. *Am. Journal Pathol.* 140, 521–528.
- Nowak, K.J., Davies, K.E., 2004. Duchenne muscular dystrophy and dystrophin: Pathogenesis and opportunities for treatment: Third in molecular medicine review series. *EMBO Rep.* <https://doi.org/10.1038/sj.embor.7400221>
- Nussbaum, J.C., Van Dyken, S.J., Von Moltke, J., Cheng, L.E., Mohapatra, A., Molofsky, A.B., Thornton, E.E., Krummel, M.F., Chawla, A., Liang, H.-E.E., Locksley, R.M., 2013. Type 2 innate lymphoid cells control eosinophil homeostasis. *Nature* 502, 245–8. <https://doi.org/10.1038/nature12526>
- Omairi, S., Hau, K.-L., Collin-Hooper, H., Montanaro, F., Goyenvalle, A., Garcia, L., Patel, K., 2017. Link between MHC Fiber Type and Restoration of Dystrophin Expression and Key Components of the DAPC by Tricyclo-DNA-Mediated Exon Skipping. *Mol. Ther. Nucleic Acids* 9, 409–418. <https://doi.org/10.1016/j.omtn.2017.10.014>
- Omata, Y., Frech, M., Primbs, T., Wirtz, S., Schett, G., Zaiss Correspondence, M.M., 2018. Group 2 Innate Lymphoid Cells Attenuate Inflammatory Arthritis and Protect from Bone Destruction in Mice. *Cell Rep.* 24, 169–180. <https://doi.org/10.1016/j.celrep.2018.06.005>

- Passamano, L., Taglia, A., Palladino, A., Viggiano, E., D'Ambrosio, P., Scutifero, M., Rosaria Cecio, M., Torre, V., DE Luca, F., Picillo, E., Paciello, O., Piluso, G., Nigro, G., Politano, L., 2012. Improvement of survival in Duchenne Muscular Dystrophy: retrospective analysis of 835 patients. *Acta Myol.* 31, 121–5.
- Pedregosa, F., Varoquaux, G., Gramfort, A., Michel, V., Thirion, B., Grisel, O., Blondel, M., Prettenhofer, P., Weiss, R., Dubourg, V., Vanderplas, J., Passos, A., Cournapeau, D., Brucher, M., Perrot, M., Duchesnay, É., 2012. Scikit-learn: Machine Learning in Python. *J. Mach. Learn. Res.* 12, 2825–2830. <https://doi.org/10.1007/s13398-014-0173-7.2>
- Pelly, V.S., Kannan, Y., Coomes, S.M., Entwistle, L.J., Rückerl, D., Seddon, B., Macdonald, A.S., Mckenzie, A., Wilson, M.S., 2016. IL-4-producing ILC2s are required for the differentiation of TH2 cells following *Heligmosomoides polygyrus* infection. *Mucosal Immunol.* 9, 1407–1417. <https://doi.org/10.1038/mi.2016.4>
- Peng, H., Jiang, X., Chen, Y., Sojka, D.K., Wei, H., Gao, X., Sun, R., Yokoyama, W.M., Tian, Z., 2013. Liver-resident NK cells confer adaptive immunity in skin-contact inflammation. *J. Clin. Invest.* 123, 1444–1456. <https://doi.org/10.1172/JCI66381>
- Pescatori, M., Broccolini, A., Minetti, C., Bertini, E., Bruno, C., Bernardini, C., Mirabella, M., Silvestri, G., Giglio, V., Modoni, A., Pedemonte, M., Tasca, G., Galluzzi, G., Mercuri, E., Tonali, P.A., Ricci, E., Gnocchi, D., Gene, E., 2007. Gene expression profiling in the early phases of DMD: a constant molecular signature characterizes DMD muscle from early postnatal life throughout disease progression. *FASEB J. • Res. Commun.* 21, 1210–1226. <https://doi.org/10.1096/fj.06-7285com>
- Pessina, P., Cabrera, D., Morales, M.G., Riquelme, C.A., Gutiérrez, J., Serrano, A.L., Brandan, E., Muñoz-Cánoves, P., 2014. Novel and optimized strategies for inducing fibrosis in vivo: focus on Duchenne Muscular Dystrophy. *Skelet. Muscle* 4. <https://doi.org/10.1186/2044-5040-4-7>
- Petrof, B.J., Shrager, J.B., Stedman, H.H., Kelly, A.M., Sweeney, H.L., 1993. Dystrophin protects the sarcolemma from stresses developed during muscle contraction. *Proc. Natl. Acad. Sci. U. S. A.* 90, 3710–4. <https://doi.org/10.1073/PNAS.90.8.3710>
- Pizza, F.X., Peterson, J.M., Baas, J.H., Koh, T.J., 2005. Neutrophils contribute to muscle injury and impair its resolution after lengthening contractions in mice. *J. Physiol.* 562, 899–913. <https://doi.org/10.1113/jphysiol.2004.073965>
- Pope, S.M., Brandt, E.B., Mishra, A., Hogan, S.P., Zimmermann, N., Rothenberg, M.E., Pope, S.M., Hogan, S.P., Matthaei, K.I., Foster, P.S., 2001. IL-13 induces eosinophil recruitment into the lung by an IL-5- and eotaxin-dependent mechanism. *J. Allergy Clin. Immunol.* 108, 594–601. <https://doi.org/10.1067/mai.2001.118600>
- Poposki, J.A., Klingler, A.I., Tan, B.K., Soroosh, P., Banie, H., Lewis, G., Hulse, K.E., Stevens, W.W., Peters, A.T., Grammer, L.C., Schleimer, R.P., Welch, K.C., Smith, S.S., Conley, D.B., Raviv, J.R., Karras, J.G., Akbari, O., Kern, R.C., Kato, A., 2017. Group 2 innate lymphoid cells are elevated and activated in chronic rhinosinusitis with nasal polyps. *Immunity, Inflamm. Dis.* 5, 233–243. <https://doi.org/10.1002/iid3.161>
- Price, April E., Liang, H.-E., Sullivan, B.M., Reinhardt, R.L., Eisle, C.J., Erle, D.J., Locksley, R.M., Weiss, A., 2010. Systemically dispersed innate IL-13-expressing cells in type 2 immunity. *Proc. Natl. Acad. Sci. U. S. A.* 107, 11489–11494. <https://doi.org/10.1073/pnas.1003988107>
- Price, April E., Liang, H.E., Sullivan, B.M., Reinhardt, R.L., Eisle, C.J., Erle, D.J., Locksley, R.M., 2010. Systemically dispersed innate IL-13-expressing cells in type 2 immunity. *Proc. Natl. Acad. Sci. U. S. A.* 107, 11489–11494. <https://doi.org/10.1073/pnas.1003988107>
- Pulendran, B., Artis, D., 2012. New Paradigms in Type 2 Immunity. *Science (80- )*. 337, 431–435.
- Rando, T.A., Crowley, R.S., Carlson, E.J., Epstein, C.J., Mohapatra, P.K., 1998. Overexpression of copper/zinc superoxide dismutase: A novel cause of murine muscular

- dystrophy. *Ann. Neurol.* 44, 381–386. <https://doi.org/10.1002/ana.410440315>
- Rasic, M. V., Vojinovic, D., Pesovic, J., Mijalkovic, G., Lukic, V., Mladenovic, J., Kosac, A., Novakovic, I., Maksimovic, N., Romac, S., Todorovic, S., Pavicevic, S.D., 2014. Intellectual ability in the duchenne muscular dystrophy and dystrophin gene mutation location. *Balk. J. Med. Genet.* 17, 25–36. <https://doi.org/10.2478/bjmg-2014-0071>
- Rayavarapu, S., Coley, W., Kinder, T.B., Nagaraju, K., 2013. Idiopathic inflammatory myopathies: Pathogenic mechanisms of muscle weakness. *Skelet. Muscle* 3, 13. <https://doi.org/10.1186/2044-5040-3-13>
- Rederstorff, M., Castets, P., Arbogast, S., Lainé, J., Vassilopoulos, S., Beuvin, M., Dubourg, O., Vignaud, A., Ferry, A., Krol, A., Allamand, V., Guicheney, P., Ferreiro, A., Lescure, A., 2011. Increased Muscle Stress-Sensitivity Induced by Selenoprotein N Inactivation in Mouse: A Mammalian Model for SEPN1-Related Myopathy. *PLoS One* 6, e23094. <https://doi.org/10.1371/journal.pone.0023094>
- Reyes-Fernandez, P.C., Periou, B., Decrouy, X., Relaix, F., Authier, F.J., 2019. Automated image-analysis method for the quantification of fiber morphometry and fiber type population in human skeletal muscle. *Skelet. Muscle* 9, 15. <https://doi.org/10.1186/s13395-019-0200-7>
- Richter, E.A., Hargreaves, M., 2013. Exercise, GLUT4, and skeletal muscle glucose uptake. *Physiol. Rev.* 93, 993–1017. <https://doi.org/10.1152/physrev.00038.2012>
- Rifai, Z., Welle, S., Moxley, R.T., Lorenson, M., Griggs, R.C., 1995. Effect of prednisone on protein metabolism in Duchenne dystrophy. *Am. J. Physiol. - Endocrinol. Metab.* 268. <https://doi.org/10.1152/ajpendo.1995.268.1.e67>
- Rigamonti, E., Zordan, P., Sciorati, C., Rovere-Querini, P., Brunelli, S., Rigamonti, E., Zordan, P., Sciorati, C., Rovere-Querini, P., Brunelli, S., 2014. Macrophage Plasticity in Skeletal Muscle Repair, Macrophage Plasticity in Skeletal Muscle Repair. *BioMed Res. Int. BioMed Res. Int.* 2014, 2014, e560629. <https://doi.org/10.1155/2014/560629>
- Rochlin, K., Yu, S., Roy, S., Baylies, M.K., 2010. Myoblast fusion: When it takes more to make one. *Dev. Biol.* 341, 66–83. <https://doi.org/10.1016/j.ydbio.2009.10.024>
- Roediger, B., Kyle, R., Yip, K.H., Sumaria, N., Guy, T. V., Kim, B.S., Mitchell, A.J., Tay, S.S., Jain, R., Forbes-Blom, E., Chen, X., Tong, P.L., Bolton, H.A., Artis, D., Paul, W.E., De St Groth, B.F., Grimbaldston, M.A., Le Gros, G., Weninger, W., Fazekas de St Groth, B., Grimbaldston, M.A., Le Gros, G., Weninger, W., 2013. Cutaneous immunosurveillance and regulation of inflammation by group 2 innate lymphoid cells. *Nat. Immunol.* 14, 564–573. <https://doi.org/10.1038/ni.2584>
- Rosenberg, A.S., Puig, M., Nagaraju, K., Hoffman, E.P., Villalta, S.A., Rao, V.A., Wakefield, L.M., Woodcock, J., 2015. Immune-mediated pathology in Duchenne muscular dystrophy. *Sci. Transl. Med.* 7, 299rv4-299rv4. <https://doi.org/10.1126/scitranslmed.aaa7322>
- Rothenberg, M.E., Hogan, S.P., 2006. The Eosinophil. *Annu. Rev. Immunol.* 24, 147–174. <https://doi.org/10.1146/annurev.immunol.24.021605.090720>
- Sabapathy, V., Cheru, N.T., Corey, R., Mohammad, S., Sharma, R., 2019. A Novel Hybrid Cytokine IL233 Mediates regeneration following Doxorubicin-Induced Nephrotoxic Injury. *Sci. Rep.* 9, 3215. <https://doi.org/10.1038/s41598-019-39886-9>
- Salimi, M., Barlow, J.L., Saunders, S.P., Xue, L., Gutowska-Owsiak, D., Wang, X., Huang, L.-C., Johnson, D., Scanlon, S.T., McKenzie, A.N.J., Fallon, P.G., Ogg, G.S., 2013. A role for IL-25 and IL-33-driven type-2 innate lymphoid cells in atopic dermatitis. *J. Exp. Med.* 210, 2939–2950. <https://doi.org/10.1084/JEM.20130351>
- Schakman, O., Kalista, S., Barbé, C., Loumaye, A., Thissen, J.P., 2013. Glucocorticoid-induced skeletal muscle atrophy. *Int. J. Biochem. Cell Biol.* <https://doi.org/10.1016/j.biocel.2013.05.036>
- Schiaffino, S., Gorza, L., Sartore, S., Saggin, L., Carli, M., 1986. Embryonic myosin heavy chain as a differentiation marker of developing human skeletal muscle and rhabdomyosarcoma.



- A monoclonal antibody study. *Exp. Cell Res.* 163, 211–220. [https://doi.org/10.1016/0014-4827\(86\)90574-4](https://doi.org/10.1016/0014-4827(86)90574-4)
- Schiaffino, S., Rossi, A.C., Smerdu, V., Leinwand, L.A., Reggiani, C., 2015. Developmental myosins: expression patterns and functional significance. *Skelet. Muscle* 5, 22. <https://doi.org/10.1186/s13395-015-0046-6>
- Schröder, T., Fuchss, J., Schneider, I., Stoltenburg-Didinger, G., Hanisch, F., 2013. Eosinophils in hereditary and inflammatory myopathies. *Acta Myol.* 32, 148–153.
- Seale, P., Sabourin, L.A., Girgis-Gabardo, A., Mansouri, A., Gruss, P., Rudnicki, M.A., 2000. Pax7 Is Required for the Specification of Myogenic Satellite Cells. *Cell* 102, 777–786. [https://doi.org/10.1016/S0092-8674\(00\)00066-0](https://doi.org/10.1016/S0092-8674(00)00066-0)
- Sek, A.C., Moore, I.N., Smelkinson, M.G., Pak, K., Minai, M., Smith, R., Ma, M., Percopo, C.M., Rosenberg, H.F., 2019. Eosinophils Do Not Drive Acute Muscle Pathology in the mdx Mouse Model of Duchenne Muscular Dystrophy. *J. Immunol.* 203, 476–484. <https://doi.org/10.4049/jimmunol.1900307>
- Sica, A., Mantovani, A., 2012. Macrophage plasticity and polarization: in vivo veritas. *J. Clin. Invest.* 122, 787–795. <https://doi.org/10.1172/JCI59643DS1>
- Silversides, C.K., Webb, G.D., Harris, V.A., Biggar, D.W., 2003. Effects of deflazacort on left ventricular function in patients with Duchenne muscular dystrophy. *Am. J. Cardiol.* 91, 769–772. [https://doi.org/10.1016/S0002-9149\(02\)03429-X](https://doi.org/10.1016/S0002-9149(02)03429-X)
- Smith, L.R., Barton, E.R., 2014. SMASH - semi-automatic muscle analysis using segmentation of histology: A MATLAB application. *Skelet. Muscle* 4. <https://doi.org/10.1186/2044-5040-4-21>
- Smith, S.G., Chen, R., Kjarsgaard, M., Huang, C., Oliveria, J.-P., O’Byrne, P.M., Gauvreau, G.M., Boulet, L.-P., Lemiere, C., Martin, J., Nair, P., Sehmi, R., 2016. Increased numbers of activated group 2 innate lymphoid cells in the airways of patients with severe asthma and persistent airway eosinophilia. *J. Allergy Clin. Immunol.* 137, 75-86.e8. <https://doi.org/10.1016/J.JACI.2015.05.037>
- Song, E., Ouyang, N., Hörbelt, M., Antus, B., Wang, M., Exton, M.S., 2000. Influence of Alternatively and Classically Activated Macrophages on Fibrogenic Activities of Human Fibroblasts. *Cell. Immunol.* 204.
- Spencer, M.J., Montecino-Rodriguez, E., Dorshkind, K., Tidball, J.G., 2001. Helper (CD4+) and cytotoxic (CD8+) T cells promote the pathology of dystrophin-deficient muscle. *Clin. Immunol.* 98, 235–243. <https://doi.org/10.1006/clim.2000.4966>
- Spencer, M.J., Tidball, J.G., 2001. Do immune cells promote the pathology of dystrophin-deficient myopathies? *Neuromuscul. Disord.* 11, 556–64.
- Spits, H., Artis, D., Colonna, M., Diefenbach, A., Di Santo, J.P., Eberl, G., Koyasu, S., Locksley, R.M., McKenzie, A.N.J., Mebius, R.E., Powrie, F., Vivier, E., 2013. Innate lymphoid cells—a proposal for uniform nomenclature. *Nat. Rev. Immunol.* 13, 145–149. <https://doi.org/10.1038/nri3365>
- Spits, H., Cupedo, T., 2012. Innate Lymphoid Cells: Emerging Insights in Development, Lineage Relationships, and Function. *Annu. Rev. Immunol.* 30, 647–675. <https://doi.org/10.1146/annurev-immunol-020711-075053>
- Spurney, C.F., 2011. Cardiomyopathy of duchenne muscular dystrophy: Current understanding and future directions. *Muscle and Nerve* 44, 8–19. <https://doi.org/10.1002/mus.22097>
- St.-Pierre, S.J.G., Chakkalakal, J. V., Kolodziejczyk, S.M., Knudson, J.C., Jasmin, B.J., Megeney, L.A., 2004. Glucocorticoid treatment alleviates dystrophic myofiber pathology by activation of the calcineurin/NF-AT pathway. *FASEB J.* 18, 1937–1939. <https://doi.org/10.1096/fj.04-1859fje>
- Straub, V., Rafael, J.A., Chamberlain, J.S., Campbell, K.P., 1997. Animal models for muscular dystrophy show different patterns of sarcolemmal disruption. *J. Cell Biol.* 139, 375–385. <https://doi.org/10.1083/jcb.139.2.375>

- Sugihara, R., Kumamoto, T., Ito, T., Ueyama, H., Toyoshima, I., Tsuda, T., 2001. Human muscle protein degradation in vitro by eosinophil cationic protein (ECP). *Muscle and Nerve* 24, 1627–1634. <https://doi.org/10.1002/mus.1198>
- Swirski, F.K., Nahrendorf, M., Etzrodt, M., Panizzi, P., Figueiredo, J., Kohler, R.H., Chudnovskiy, A., Waterman, P., Aikawa, E., Mempel, T.R., Libby, P., Weissleder, R., Pittet, M.J., 2010. Identification of Splenic Reservoir Monocytes and Their Deployment to Inflammatory Sites. *Science* (80-. ). 325, 612–616. <https://doi.org/10.1126/science.1175202>.Identification
- Talbot, J., Maves, L., 2016. Skeletal muscle fiber type: using insights from muscle developmental biology to dissect targets for susceptibility and resistance to muscle disease. *WIREs Dev Biol* 5, 518–534. <https://doi.org/10.1002/wdev.230>
- Tang, Q., Bluestone, J.A., 2008. The Foxp3+ regulatory T cell: a jack of all trades, master of regulation. *Nat Immunol* 9, 239–244.
- Tedesco, F.S., Dellavalle, A., Diaz-manera, J., Messina, G., Cossu, G., 2010. Review series Repairing skeletal muscle : regenerative potential of skeletal muscle stem cells. *J. Clin. Invest.* 120, 11–19. <https://doi.org/10.1172/JCI40373>.and
- Thomas, T.O., Morgan, T.M., Burnette, W.B., Markham, L.W., 2012. Correlation of heart rate and cardiac dysfunction in duchenne muscular dystrophy. *Pediatr. Cardiol.* 33, 1175–1179. <https://doi.org/10.1007/s00246-012-0281-0>
- Tidball, J.G., 2017. Regulation of muscle growth and regeneration by the immune system. *Nat. Publ. Gr.* 17, 165–178. <https://doi.org/10.1038/nri.2016.150>
- Tidball, J.G., 2005. Inflammatory processes in muscle injury and repair. *Am. J. Physiol. - Integr. Comp. Physiol.* 288, 345–353. <https://doi.org/10.1152/ajpregu.00454.2004>.
- Tidball, J.G., Wehling-Henricks, M., 2007. Macrophages promote muscle membrane repair and muscle fibre growth and regeneration during modified muscle loading in mice in vivo. *J. Physiol.* 578, 327–336. <https://doi.org/10.1113/jphysiol.2006.118265>
- Tiemessen, M.M., Jagger, A.L., Evans, H.G., van Herwijnen, M.J., John, S., Taams, L.S., 2007. CD4+CD25+Foxp3+ regulatory T cells induce alternative activation of human monocytes/macrophages. *Proc Natl Acad Sci U S A* 104, 19446–19451.
- Tonkin, J., Temmerman, L., Sampson, R.D., Gallego-colon, E., Barberi, L., Bilbao, D., Schneider, M.D., Musarò, A., Rosenthal, N., 2015. Monocyte/Macrophage-derived IGF-1 Orchestrates Murine Skeletal Muscle Regeneration and Modulates Autocrine Polarization. *Mol. Ther.* 23, 1189–1200. <https://doi.org/10.1038/mt.2015.66>
- Torres, L.F.B., Duchon, L.W., 1987. The mutant mdx: Inherited myopathy in the mouse: Morphological studies of nerves, muscles and end-plates. *Brain* 110, 269–299. <https://doi.org/10.1093/brain/110.2.269>
- Turner, J.-E., Morrison, P.J., Wilhelm, C., Wilson, M., Ahlfors, H., Renauld, J.-C., Panzer, U., Helmbj, H., Stockinger, B., 2013. IL-9-mediated survival of type 2 innate lymphoid cells promotes damage control in helminth-induced lung inflammation. *J. Exp. Med.* 210, 2951–65. <https://doi.org/10.1084/jem.20130071>
- Uaesoontrachoon, K., Yoo, H.J., Tudor, E.M., Pike, R.N., Mackie, E.J., Pagel, C.N., 2008. Osteopontin and skeletal muscle myoblasts: Association with muscle regeneration and regulation of myoblast function in vitro. *Int. J. Biochem. Cell Biol.* 40, 2303–2314. <https://doi.org/10.1016/j.biocel.2008.03.020>
- Van Battum, E.Y., Gunput, R.A.F., Lemstra, S., Groen, E.J.N., Yu, K. Lou, Adolfs, Y., Zhou, Y., Hoogenraad, C.C., Yoshida, Y., Schachner, M., Akhmanova, A., Pasterkamp, R.J., 2014. The intracellular redox protein MICAL-1 regulates the development of hippocampal mossy fibre connections. *Nat. Commun.* 5. <https://doi.org/10.1038/ncomms5317>
- Van Der Walt, S., Schönberger, J.L., Nunez-Iglesias, J., Boulogne, F., Warner, J.D., Yager, N., Guillard, E., Yu, T., 2014. scikit-image: image processing in Python. *PeerJ* 2, e453. <https://doi.org/10.7717/peerj.453>

- Van Gool, F., Molofsky, A.B., Morar, M.M., Rosenzweig, M., Liang, H.-E., Klatzmann, D., Locksley, R.M., Bluestone, J. a, 2014. Interleukin-5-producing group 2 innate lymphoid cells control eosinophilia induced by interleukin-2 therapy. *Blood* 124, 3572–3576. <https://doi.org/10.1182/blood-2014-07-587493>
- Varga, T., Mounier, R., Patsalos, A., Gogolak, P., Peloquin, M., Horvath, A., Pap, A., Daniel, B., Nagy, G., Pintye, E., Poliska, S., Cuvellier, S., Ben Larbi, S., Sansbury, B.E., Spite, M., Brown, C.W., Chazaud, B., Nagy, L., 2016. Macrophage PPARgamma, a Lipid Activated Transcription Factor Controls the Growth Factor GDF3 and Skeletal Muscle Regeneration. *Immunity* 45, 1038–1051. <https://doi.org/10.1016/j.immuni.2016.10.016>
- Vercoulen, Y., Bellutti Enders, F., Meerding, J., Plantinga, M., Elst, E.F., Varsani, H., van Schieveen, C., Bakker, M.H., Klein, M., Scholman, R.C., Spliet, W., Ricotti, V., Koenen, H.J.P.M., de Weger, R.A., Wedderburn, L.R., van Royen-Kerkhof, A., Prakken, B.J., 2014. Increased presence of FOXP3+ regulatory T cells in inflamed muscle of patients with active juvenile dermatomyositis compared to peripheral blood. *PLoS One* 9, e105353. <https://doi.org/10.1371/journal.pone.0105353>
- Vetrone, S.A., Montecino-Rodriguez, E., Kudryashova, E., Kramerova, I., Hoffman, E.P., Liu, S.D., Miceli, M.C., Spencer, M.J., 2009. Osteopontin promotes fibrosis in dystrophic mouse muscle by modulating immune cell subsets and intramuscular TGF-beta. *J Clin Invest* 119, 1583–1594. <https://doi.org/10.1172/JCI37662>
- Vignali, D.A., Collison, L.W., Workman, C.J., 2008. How regulatory T cells work. *Nat Rev Immunol* 8, 523–532.
- Villalta, S.A., Nguyen, H.X., Deng, B., Gotoh, T., Tidball, J.G., 2009. Shifts in macrophage phenotypes and macrophage competition for arginine metabolism affect the severity of muscle pathology in muscular dystrophy. *Hum Mol Genet* 18, 482–496. <https://doi.org/10.1093/hmg/ddn376>
- Villalta, S.A., Rinaldi, C., Deng, B., Liu, G., Fedor, B., Tidball, J.G., 2011. Interleukin-10 reduces the pathology of mdx muscular dystrophy by deactivating M1 macrophages and modulating macrophage phenotype. *Hum Mol Genet* 20, 790–805.
- Villalta, S.A., Rosenberg, A.S., Bluestone, J.A., 2015. The immune system in Duchenne muscular dystrophy: Friend or foe. *Rare Dis. (Austin, Tex.)* 3, e1010966. <https://doi.org/10.1080/21675511.2015.1010966>
- Villalta, S.A., Rosenthal, W., Martinez, L., Kaur, A., Sparwasser, T., Tidball, J.G., Margeta, M., Spencer, M.J., Bluestone, J.A., 2014. Regulatory T cells suppress muscle inflammation and injury in muscular dystrophy. *Sci Transl Med* 6, 258ra142. <https://doi.org/10.1126/scitranslmed.3009925>
- Voehringer, D., Liang, H.-E., Locksley, R.M., 2008. Homeostasis and Effector Function of Lymphopenia-Induced “Memory-Like” T Cells in Constitutively T Cell-Depleted Mice. *J. Immunol.* 180, 4742–4753. <https://doi.org/10.4049/jimmunol.180.7.4742>
- Walker, J.A., Mckenzie, A.N., 2013. Development and function of group 2 innate lymphoid cells. *Curr. Opin. Immunol.* 25, 148–155. <https://doi.org/10.1016/j.coi.2013.02.010>
- Wang, X.Y., Wang, T., Bu, J., 2011. Color image segmentation using pixel wise support vector machine classification. *Pattern Recognit.* 44, 777–787. <https://doi.org/10.1016/j.patcog.2010.08.008>
- Wang, X.Y., Zhang, X.J., Yang, H.Y., Bu, J., 2012. A pixel-based color image segmentation using support vector machine and fuzzy C-means. *Neural Networks* 33, 148–159. <https://doi.org/10.1016/j.neunet.2012.04.012>
- Wehling-Henricks, M., Jordan, M.C., Gotoh, T., Grody, W.W., Roos, K.P., Tidball, J.G., 2010. Arginine metabolism by macrophages promotes cardiac and muscle fibrosis in mdx muscular dystrophy. *PLoS One* 5. <https://doi.org/10.1371/journal.pone.0010763>
- Wehling-Henricks, M., Lee, J.J., Tidball, J.G., 2004. Prednisolone decreases cellular adhesion molecules required for inflammatory cell infiltration in dystrophin-deficient skeletal muscle.

- Neuromuscul. Disord. 14, 483–490. <https://doi.org/10.1016/j.nmd.2004.04.008>
- Wehling-Henricks, M., Sokolow, S., Lee, J.J., Myung, K.H., Villalta, S.A., Tidball, J.G., 2008. Major basic protein-1 promotes fibrosis of dystrophic muscle and attenuates the cellular immune response in muscular dystrophy. *Hum. Mol. Genet.* 17, 2280–2292. <https://doi.org/10.1093/hmg/ddn129>
- Wehling, M., Spencer, M.J., Tidball, J.G., 2001. A nitric oxide synthase transgene ameliorates muscular dystrophy in mdx mice. *J. Cell Biol.* 155, 123–131. <https://doi.org/10.1083/jcb.200105110>
- Weinstock, A., Green, C., Cohen, B.H., Prayson, R.A., 1997. Becker Muscular Dystrophy Presenting as Eosinophilic Inflammatory Myopathy in an Infant. *J Child Neurol* 12, 146–147.
- Wen, Y., Murach, K.A., Vechetti, I.J., Fry, C.S., Vickery, C.D., Peterson, C.A., McCarthy, J.J., Campbell, K.S., 2017. MyoVision: Software for Automated High-Content Analysis of Skeletal Muscle Immunohistochemistry. *J. Appl. Physiol.* jap.00762.2017. <https://doi.org/10.1152/jap.00762.2017>
- Wermuth, P.J., Jimenez, S.A., The significance of macrophage polarization subtypes for animal models of tissue fibrosis and human fibrotic diseases. *Clin. Transl. Med.* 4, 2. <https://doi.org/10.1186/s40169-015-0047-4>
- Wood, C.L., Straub, V., 2018. Bones and muscular dystrophies: what do we know? *Curr. Opin. Neurol.* 31, 583–591. <https://doi.org/10.1097/WCO.0000000000000603>
- Wu, D., Molofsky, A.B., Liang, H.-E., Ricardo-Gonzalez, R.R., Jouihan, H.A., Bando, J.K., Chawla, A., Locksley, R.M., 2011. Eosinophils sustain adipose alternatively activated macrophages associated with glucose homeostasis. *Science (80-. )*. 332, 243–7. <https://doi.org/10.1126/science.1201475>
- Yamaguchi, Y., Suda, T., Suda, J., Eguchi, M., Miura, Y., Harada, N., Tominaga, A., Takatsu, K., 1988. Purified interleukin 5 supports the terminal differentiation and proliferation of murine eosinophilic precursors. *J. Exp. Med.* 167, 43–56. <https://doi.org/10.1084/jem.167.1.43>
- Ying, S., Meng, Q., Zeibecoglou, K., Robinson, D.S., Macfarlane, A., Humbert, M., Kay, A.B., Robinson, K., Macfarlane, A., Humbert, M., Barry Sun Ying, A., Meng, Q., Zeibecoglou, K., 2016. Eosinophil Chemotactic Chemokines (Eotaxin, Eotaxin-2, RANTES, Monocyte Chemoattractant Protein-3 (MCP-3), and MCP-4), and C-C Chemokine Receptor 3 Expression in Bronchial Biopsies from Atopic and Nonatopic (Intrinsic) Asthmatics. *J. Immunol.* 163, 6321–6329. <https://doi.org/10.4049/jimmunol.1300235>
- Yu, C., Cantor, A.B., Yang, H., Browne, C., Wells, R.A., Fujiwara, Y., Orkin, S.H., 2002. Targeted deletion of a high-affinity GATA-binding site in the GATA-1 promoter leads to selective loss of the eosinophil lineage in vivo. *J. Exp. Med.* 195, 1387–1395. <https://doi.org/10.1084/jem.20020656>
- Zaitoun, N.M., Aqel, M.J., 2015. Survey on Image Segmentation Techniques. *Procedia Comput. Sci.* 65, 797–806. <https://doi.org/10.1016/j.procs.2015.09.027>
- Zhang, J.Q., Biedermann, B., Nitschke, L., Crocker, P.R., 2004. The murine inhibitory receptor mSiglec-E is expressed broadly on cells of the innate immune system whereas mSiglec-F is restricted to eosinophils. *Eur. J. Immunol.* 34, 1175–1184. <https://doi.org/10.1002/eji.200324723>
- Zhao, W., Lu, H., Wang, X., Ransohoff, R.M., Zhou, L., 2016. CX3CR1 deficiency delays acute skeletal muscle injury repair by impairing macrophage functions. *FASEB J.* 30, 380–393. <https://doi.org/10.1096/fj.14-270090>
- Zlotnik, A., Yoshie, O., 2012. The Chemokine Superfamily Revisited. *Immunity.* <https://doi.org/10.1016/j.immuni.2012.05.008>